Technical Report ECOM-0547-F

Reports Control Symbol
OSD-1366

April 1969

Azimuth and Elevation Direction Finder Techniques

Final Report

1 July 1967 through 31 December 1968

Report No. 6

Contract DAAB07-67-C0547
DA Project 5A6 79191 D902-05-11

Prepared by

J. E. Ferris, W. B. Henry, P. H. Wilcox and W. E. Zimmerman

The University of Michigan Radiation Laboratory
Department of Electrical Engineering
Ann Arbor, Michigan

For

United States Army Electronics Command, Fort Monmouth, N. J.

ABSTRACT

During the period covered by the final report the Radiation Laboratory of the University of Michigan has designed, developed and tested an Azimuth - Elevation Direction Finding system. The tests are not felt to be conclusive, however, they do demonstrate the capability of this system to perform azimuth and elevation direction finding of detected RF sources. The system has been tested in both the free space environment (employing an antenna range) and in a cluttered RF environment employing an aircraft from which azimuth and elevation data has been collected. The results of the free space tests suggest that the system has an accuracy of $\pm 5^{o}$ in both azimuth and elevation. However, it is difficult to assign an accuracy figure to the system on the basis of the fly-by tests due to the hostile environment in which the system was operated. This report presents a review of the system from its conception to its final testing phases with suggested recommendations for improvements.

FOREWORD

This report was prepared by The University of Michigan Radiation Laboratory of the Department of Electrical Engineering under Contract DAAB07-67-C0547. This contract was initiated under United States Army Project No. 5A6 79191 D902-05-11 "Azimuth and Elevation Direction Finder Techniques". The work is administered under the direction of the Electronics Warfare Division, Advanced Techniques Branch at Fort Monmouth, New Jersey. Mr. S. Stiber is the Project Manager and Mr. E. Ivone is the Contract Monitor. This report covers the period of 1 July 1967 through 31 December 1968.

The material reported herein represents the results of the preliminary investigation into the study of techniques for designing broadband circularly polarized azimuth - elevation direction finder systems.

The authors wish to express their thanks to Messrs. E. Bublitz, and E. Kuzyk for their efforts in the experimental work that has been performed during the final reporting period on the contract, and M. Gurney for his efforts in the mechanical design of components that are associated with the azimuth - elevation direction finding system, and to M. Wright for her help with the manuscript of the final report.

TABLE OF CONTENTS

LIST OF ILLUSTRATIONS

LIST OF ILLUSTRATIONS

Continued

LIST OF ILLUSTRATIONS

Continued

I

INTRODUCTION

During the period 1 July 1967 through 31 December 1968 the University of Michigan Radiation Laboratory has investigated the feasibility of designing, developing, and fabricating an Azimuth - Elevation Direction Finder (A-EDF) system. During the above period, an exploratory model has been assembled and partially evaluated. However, because of the limitation of time and funds a thorough evaluation of this system has not been possible. Sufficient experience with the system has shown that the proposed technique is feasible, and has provided the designers with additional insight as to improvements that should be made in future systems.

1.1 Azimuth - Elevation Direction Finder Requirements

As a part of the system requirements the A-EDF was to have a broadband frequency range capability (600 - 3000 MHz) employing a single antenna system. The antenna system was to consist of a minimum of 16 broadband cavity backed flat planar spirals mounted on a 6 foot diameter hemispherical surface. The gain of the individual antenna elements was to be no less than 5dB above a circularly polarized isotropic source over the frequency band of operation. The circularly polarized axial ratio of the antenna elements was to be less than 3dB over the above frequency range and the VSWR characteristics was to be less than 3:1 with respect to 50 Ω. The azimuth - elevation system was to provide 360° of azimuth coverage and 90° elevation coverage, and was to have an accuracy of $\pm 2^{\circ}$ in azimuth and $\pm 5^{\circ}$ in elevation at any specified frequency within its operating band.

In addition to the antenna system, an antenna scanning and control unit was to be provided which consisted of a computer or similar electronic device. This unit was to provide electronic scanning of the antenna elements and include the necessary logic circuitry for direction finding with the system. In its simplest form the system was to obtain the relative amplitude information from the elements of the antenna array, process it and present in a visual form the bearing indication of the direction of arrival of received signals. The antenna array was to be scanned by an electromechanical device with a variable scanning rate so as to optimize performance on pulsed, CW, AM, and FM type signals. The system was to be capable of operation from a nominal 115 volt, 50 to 60 Hz power source, and all power supplies required for the operation of the system were to be provided. The environmental conditions of the equipment were as follows: ambient temperature in the range of -10° F to $+120^{\circ}$ F; wind, wind velocity of up to 40 mph; rain, two inches of rainfall at varying rates of a period of 12 hours with

a windspeed as high as 25mph. The non-operating environmental conditions specified that the equipment was to be capable of withstanding the shock and vibration induced during transportation as loose cargo. For making standard laboratory bench tests on the equipment, the environmental conditions were to be: room temperature ambient $77^{o} \pm 10^{o}$, altitude - normal ground, vibration - none, and humidity - room ambient up to 90 percent relative humidity.

As a result of the analytical studies associated with the A-EDF, we have found that it is extremely important that the electrical characteristics of the antenna elements must be well behaved such that the radiation characteristics do not vary both as a function of angular orientation of a particular antenna as well as the frequency of operation. To ensure that the antennas will have the required consistency in radiation characteristics, both as a function of angular orientation and the frequency of operation, consideration has been given to the employment of conical spirals having a quadrafilar element being fed by a stripline balun configuration as noted in Chapter II of this report.

II

QUADRAFILAR SPIRAL ANTENNA INVESTIGATION

2.1 Quadrafilar Balun

Articles in the open literature on broadband coaxial couplers have stressed the need for extremely high mechanical tolerances to be associated with the center conductor width, overlap, and separation between the stripline and ground planes. Earlier experimental work (at this laboratory) with the stripline couplers and the 90^{o} phase shifter, required for the balun system, was conducted employing crude tolerances for the above item. Although the results were not outstanding, the components exhibited predictable responses. To evaluate the effect of tolerances, a stripline coupler was etched from a 4:1 scale drawing. The drawing was photo-reduced and a coupler was etched using the photo negative. This coupler was tested to determine the effect of employing tighter tolerances in printing and conducting filaments and assembly of the coupler. Preliminary data showed that the coupler's electrical characteristics were quite similar to the coupler employing crude tolerances and made from brass shim stock. The major difference appears to be in the isolation of port 4, which is a non-coupled port. But even here the two sets of data did not differ significantly. Time did not permit a detailed study of the effect of tolerances on the overall coupler performance but at present there is an indication that tolerances are not as critical as one might expect from reading reports in the literature.

Pictures of broadband couplers generally show them to have 45^{o} miter joints at the intersection of the quarter wavelength sections of the coupler. The reason given for using the 45^{o} miter bends is that it reduces the reflections from the junction and improves the overall coupler performance. In our work with these couplers, using both the sharp 90^{o} transition and the mitered 45^{o} transition, we have found the 45^{o} transition reduces the coupling of the stripline coupler. This reduction in coupling is believed to be due to the orthogonal component of currents in the mitered section. This reduction in coupling is especially evident in the center conductor which has a higher coupling coefficient. Therefore, the overlap that is required to give a particular coupling with a 90^{o} transition must be increased to give the same coupling when one is using 45^{o} mitered transitions. Reflectometer data and the coupling data do not show a great increase in performance by using the 45^{o} mitered joints over the 90^{o} transitions. Impedance discontinuities of the 90^{o} cross overs can be greatly reduced by staggering the cross over such that a more nearly constant line width is maintained through the transition. This means that the transition point on one side of the stripline is displaced from the transition point on the other side of the line to maintain a constant or more nearly uniform line width across the transition.

The phase shifter that is required in the balun network has been fabricated from Rexolite 2200 material and has been checked over the 5:1 operating band. The reference line for the phase shifter was constructed from 0.141 coaxial line instead of using a stripline section of 50 Ω stripline as was used in the final model.

Since the individual components of the balun were mounted in separate packages for individual testing, it was necessary to connect these components with coaxial cable for testing of the engineering model of the balun network. This is undesirable since the cabling involves extra connectors and loss that would not be present in the final version of the balun network. The average phase of the two tandem (8 and 10dB) couplers was 83^{o}, instead of 90^{o}. This difference was due to the total coupling coefficient of the tandem coupler being lower than the design value of -3.0dB.

Figure 2-1 is a graph of the phase of the 90^{o} hybrid formed by the tandem 8.3dB couplers. A total phase of the tandem 8.3dB couplers varies from a high of 94^{o} to a low of 65^{o} but has a majority of the values near the average of 83^{o}. Figure 2-2 is a graph of the phase shift through the total balun system consisting of the tandem couplers and the 90^{o} phase shifter. The maximum phase shift between the two arms of the output is 191^{o} with a minimum value being 156^{o}. Average value of the phase shifter across the band is 175^{o} which reflects the fact that the tandem couplers do not have a true 90^{o} phase shift. The phase in this case was measured by terminating the line with a 10dB precision load in front of the connection to a tee while the second terminal was connected to a 50 Ω load. Table 2-1 is a measure of the output power of the two balanced outputs from the balun system. In this measurement one of the balanced outputs was taken at a reference and the dB ratio was taken of the second output. In this case the average unbalance between the two ports is 0.34dB with a maximum deviation between the ports of 0.9dB.

A reflectometer was used to measure the reflection coefficient of the assembled balun with the matched outputs terminated in 50 Ω loads. The 50 Ω loads were then removed and the balun system outputs were coupled to the windings of a cavity backed bifilar spiral and the reflection coefficient was again measured across the band. The reflection coefficient did show an increase when coupled to the cavity backed spiral but it was not as severe as we had earlier expected as the VSWR remained well below 3:1. Oscillations of the reflection coefficient increased with frequency but did not show the erratic variations that were expected. Unfortunately the remaining time did not permit the checking of the phase and amplitude of the balun across the frequency band with mismatched

terminations such as found with the spiral antenna which typically has a balanced impedance of 150 Ω between elements. Feeding the antenna with 50 Ω stripline baluns would give a 1.5:1 mismatch at each terminal.

TABLE 2-1

Relative Power Division of Balun

Frequency (GHz)	Ratio of Terminal Voltages (Percent)	Ratio of Terminal Power (dB)
1.0	97.2	.24
1.1	95.2	.43
1.2	96.8	.28
1.3	95.2	.43
1.4	96.8	.28
1.5	95.2	.43
1.6	95.6	.39
1.7	90.0	.92
1.8	93.6	.58
1.9	92.4	.68
2.0	94.0	.54
2.2	96.4	.32
2.4	101.6	-.14
2.6	105.6	-.47
2.8	98.8	.10
3.0	94.8	.46

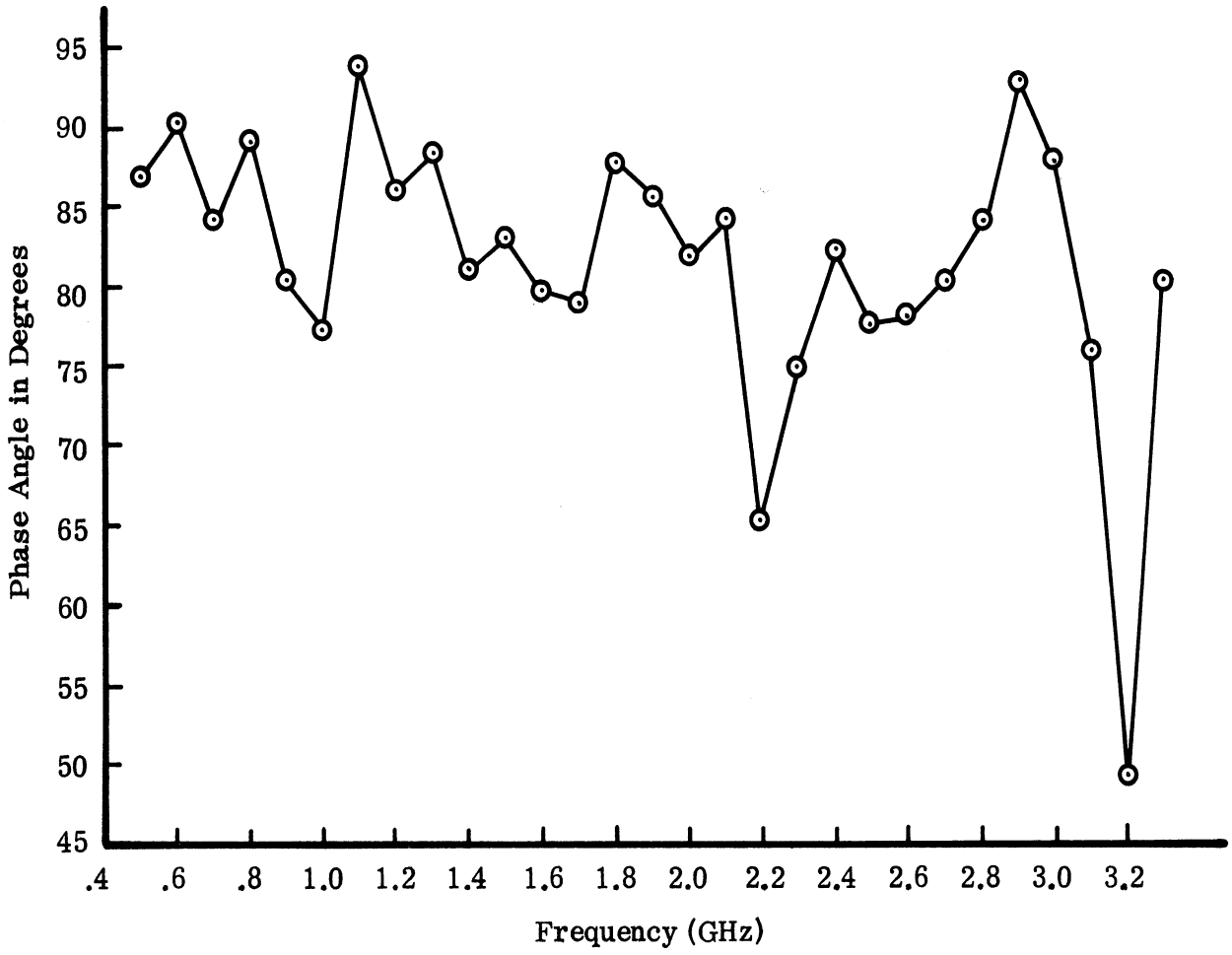

FIG. 2-1: PHASE ANGLE BETWEEN OUTPUT TERMINALS OF TANDEM 8.3dB COUPLERS.

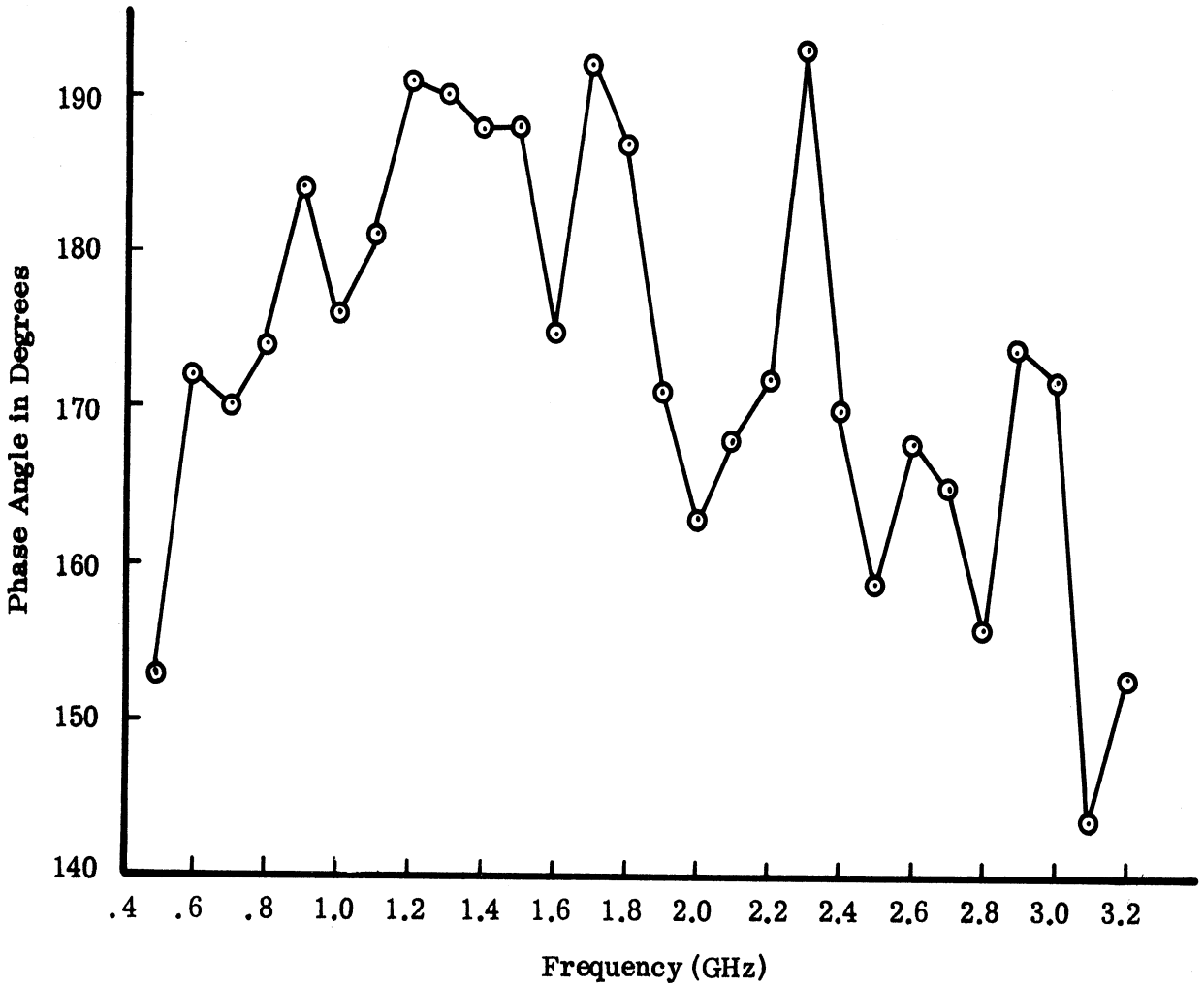

FIG. 2-2: PHASE ANGLE BETWEEN OUTPUT TERMINALS OF THE STRIPLINE BALUN.

2.2 Quadrafilar Balun Results

An engineering model of the quadrafilar balun exhibits amplitude and phase variations as shown respectively in Figs. 2-3 and 2-4. In Fig. 2-3 it is shown that the amplitude variation at the four ports is small. However, the phase data (Fig. 2-4) is not well behaved.

The quadrafilar balun is shown in Fig. 2-5. This balun consists of three broadband 3dB directional couplers and a broadband 90^{o} phase shifter. For the purposes of this program, broadband is defined to be a 5:1 frequency band that covers the range of 0.6 - 3.0 GHz. To minimize coupling between adjacent components, it was necessary to use screws throughout the balun network as can be seen in Fig. 2-6. For this particular balun configuration, a total of approximately 600 screws were required to minimize coupling between components. Spacing between the screws must be $\lambda/8$ or less at the highest frequency of interest. It has been found that the spacing between the screws and the stripline center conductor can be as small as $\lambda/8$ at the highest frequency of interest without affecting the impedance characteristics of the stripline.

The phase variations associated with port 2 relative to port 1 theoretically should have been 90^{o}, $\pm 10^{o}$, and the data of Fig. 2-4 shows that this phase variation over a major portion of the band was within these limits. However, at a frequency of 2.0 GHz the phase has a discrepancy of approximately $+30^{o}$. The cause of this variation is not understood and the problem requires further study. However, of greater concern is the data for ports 1-3 and 1-4 which have a larger discrepancy associated with them. It is of interest to note that the data for ports 1-3 relative to that for ports 1-4 shows phase differences of approximately 90^{o} over the 5:1 frequency band which is desirable. The fact that the data for ports 1-2 agrees well with the expected 90^{o} phase variation suggests that the three 3dB hybrids shown in Fig. 2-5 are operating as designed. This conclusion is further substantiated because the amplitude variations at the four ports are also well behaved as shown in Fig. 2-3. The linear slope associated with the curves of ports 1-3 and 1-4 relative to the data of 1-2 suggests that the broadband 90^{o} phase shifter is not functioning properly. Because the two curves for the ports 1-3 and 1-4 vary in a linear fashion suggests that the reference line of Fig. 2-5 is of the wrong length. It is assumed the broadband phase shifter was properly etched, for if it were not it is very probable that the curves of ports 1-3 and 1-4 relative to 1-2 would not have exhibited the linear phase discrepancy shown in Fig. 2-4.

Pattern data for the quadrafilar spiral antenna has not been encouraging. The cause for the poor pattern behavior is believed to result both from the poor phase response of the balun network and the inaccuracies associated with the winding of the quadrafilar spiral elements.

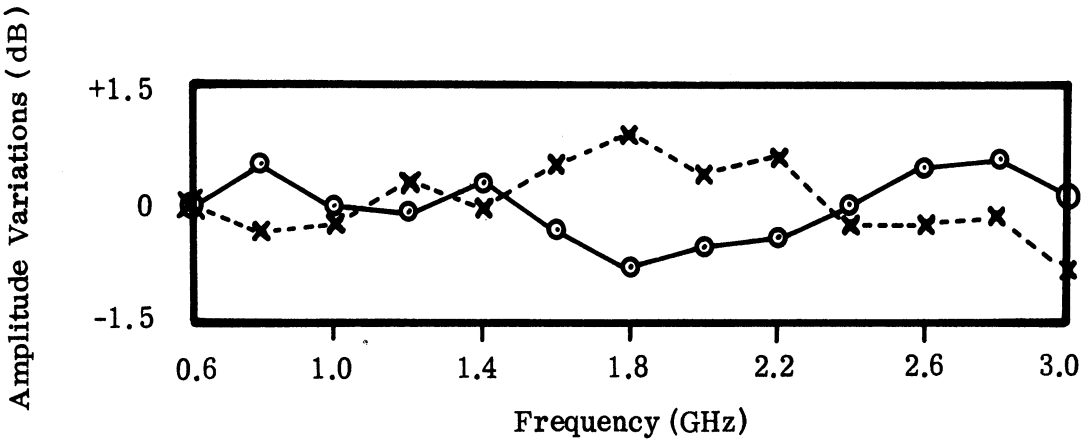

FIG. 2-3: QUADRAFILAR OUTPUT AMPLITUDE VARIATIONS.

⊙—⊙ Port 1 - 4 ✕--✕ Port 2 - 3

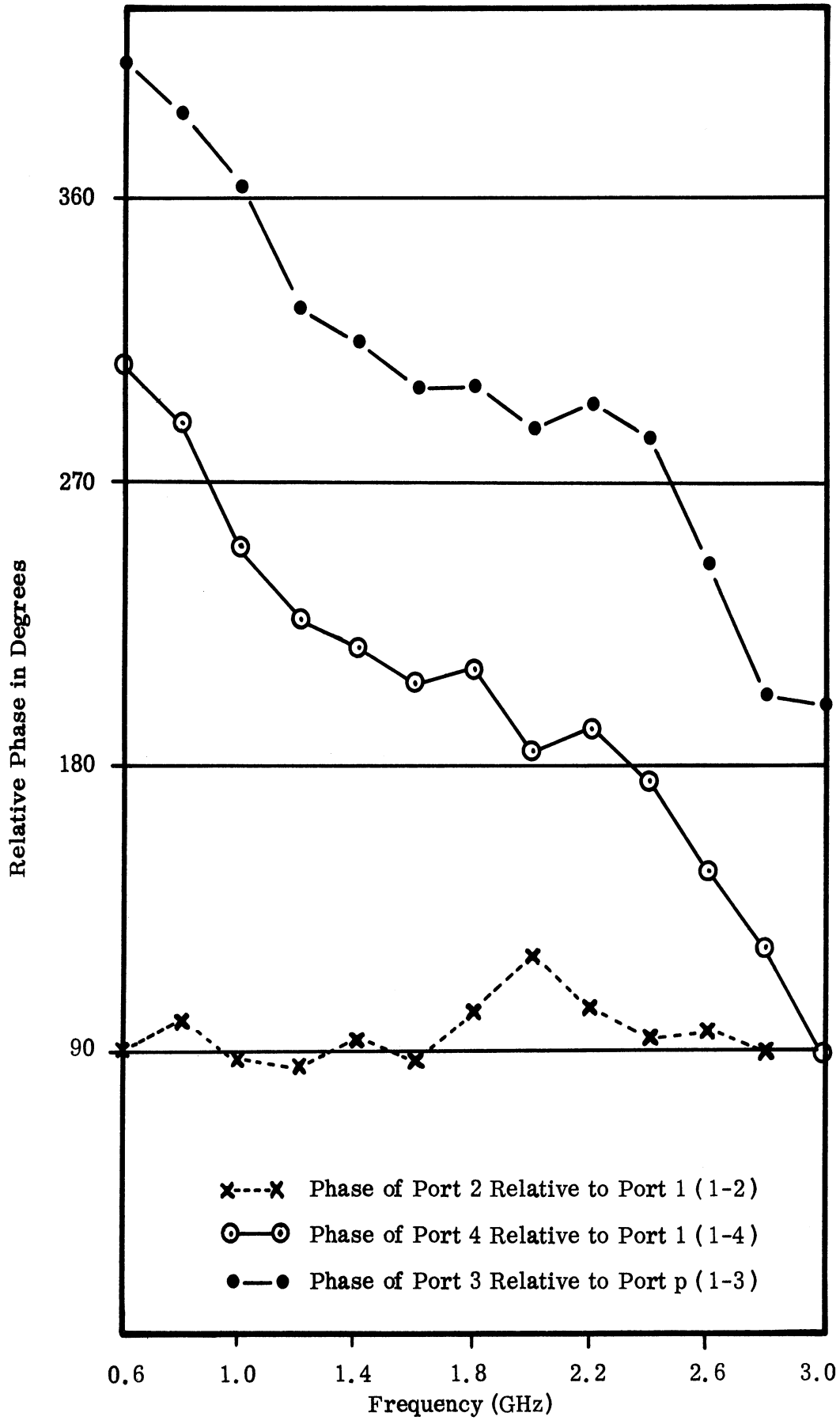

FIG. 2-4: PHASE RELATIONSHIP BETWEEN THE FOUR PORTS OF THE QUADRAFILAR BALUN versus FREQUENCY.

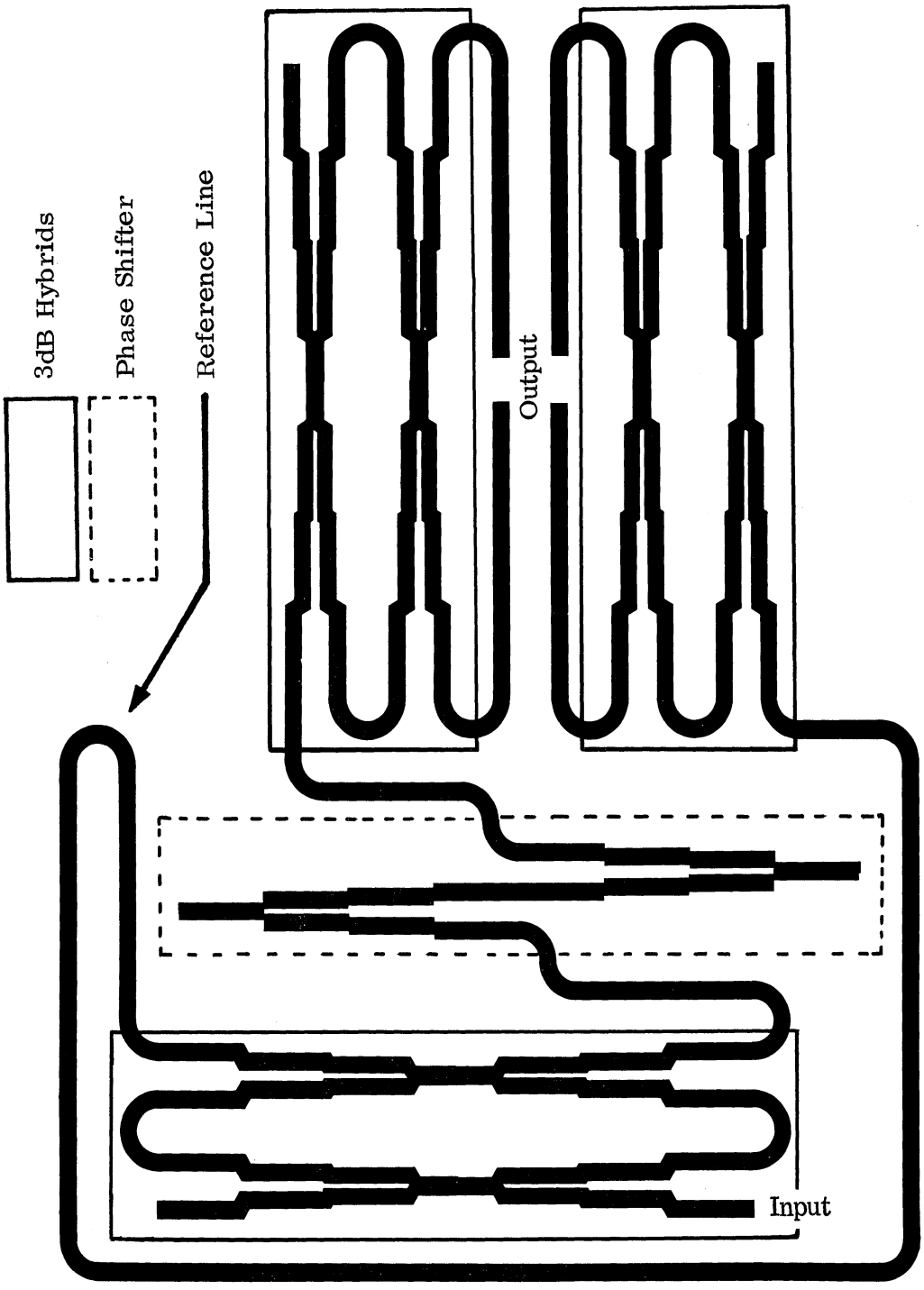

FIG. 2-5: QUADRAFILAR BALUN.

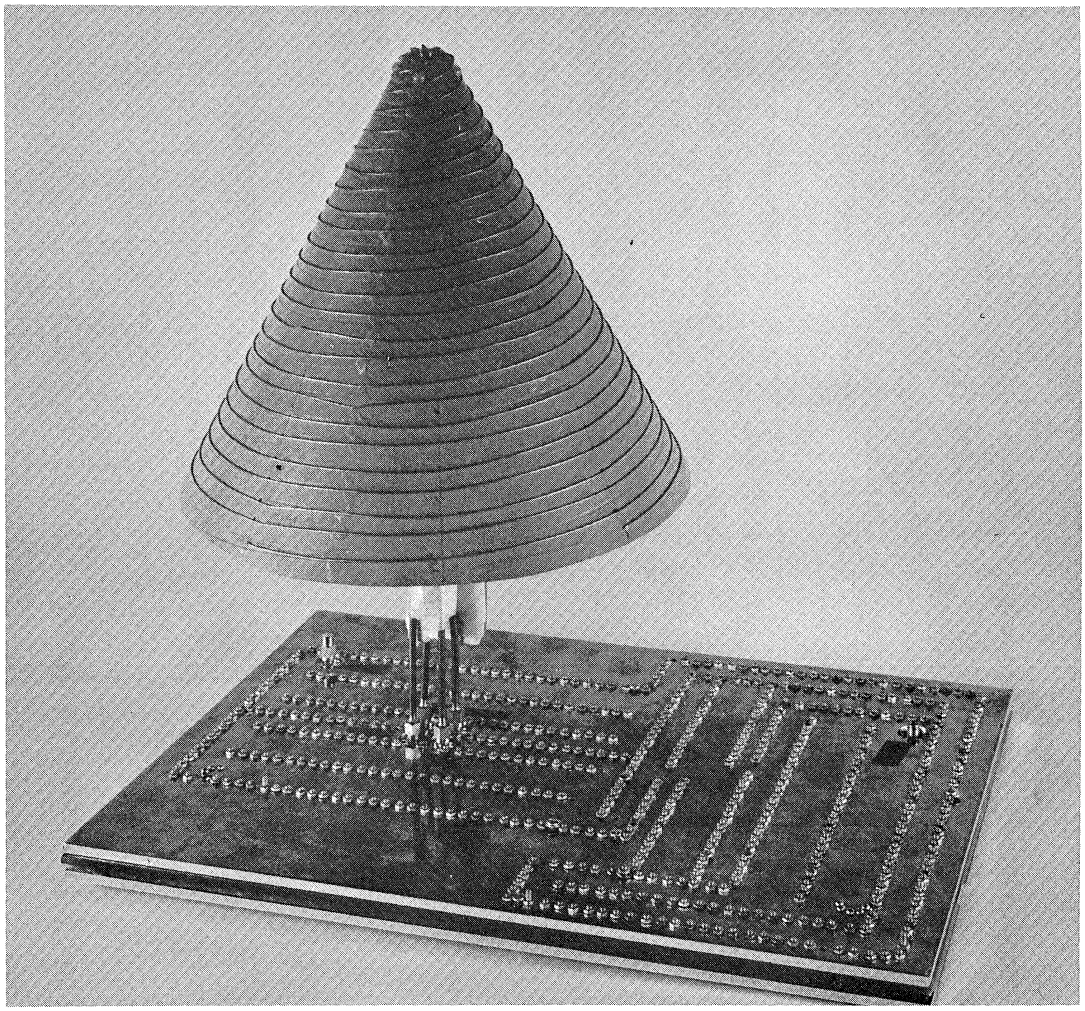

FIG. 2-6: QUADRAFILAR SPIRAL AND BALUN.

To provide some comparison as to the desirability of employing a well behaved (electrically) balun network, two sets of data are presented for a cavity backed spiral antenna, one fed with a modified Duncan - Minerva balun and the other by a broadband stripline balun network. Typical pattern data is shown in Figs. 2-7 and 2-8. The two sets of data noted above were recorded at several frequencies in the 0.6 - 3.0 GHz frequency range. It will be observed from this data that at several frequencies the Duncan - Minerva patterns show some deterioration in comparison with the data for the bifilar stripline case. There are some anomalies noted in the bifilar stripline data and this is felt to be caused by the higher order modes that may be radiated by the bifilar spiral configuration as noted in the first quarterly report (ECOM-0547-1) dated October, 1967.

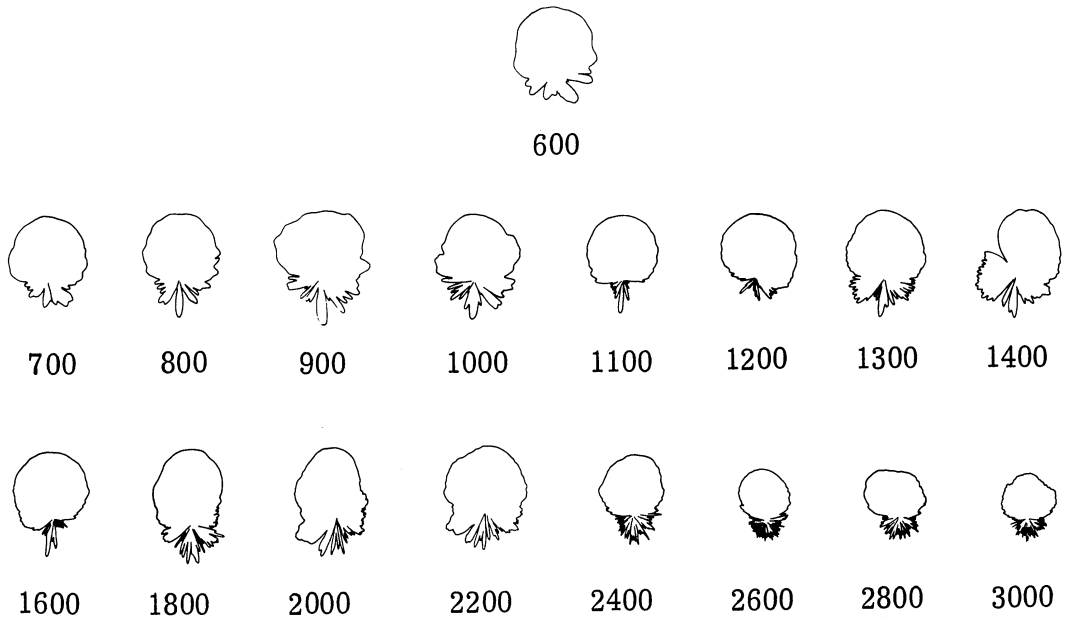

FIG. 2-7: 15 TURN CAVITY BACKED SPIRAL WITH A DUNCAN-MINERVA BALUN MOUNTED AT THE ZENITH OF A 6 FOOT HEMISPHERE (E-Plane Patterns for a 5:1 Frequency Band).

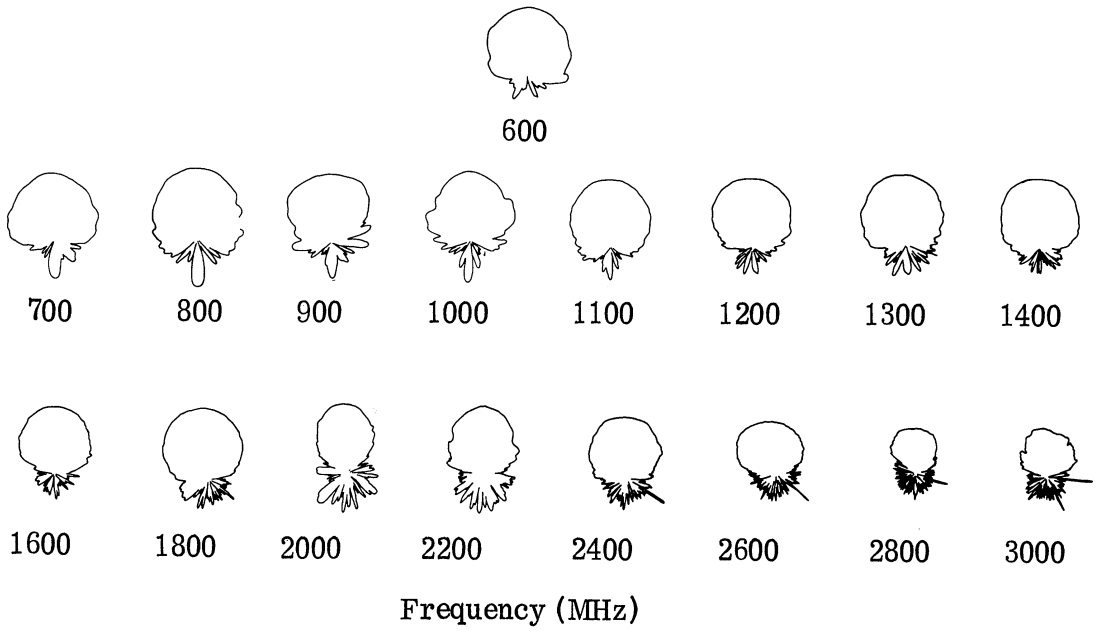

FIG. 2-8: 15 TURN CAVITY BACKED SPIRAL WITH A BROADBAND STRIPLINE BALUN MOUNTED AT THE ZENITH OF A 6 FOOT HEMISPHERE (E-Plane Patterns for a 5:1 Frequency Band).

III

TECHNICAL DISCUSSION OF AZIMUTH - ELEVATION DIRECTION FINDER

Below is presented three discussions as follows:

1) A general description of the A-EDF system.

2) The general theory associated with the system, and

3) Typical results that have been obtained from the exploratory model.

3.1 General Discussion of Azimuth - Elevation Direction Finder

The A-EDF, as designed and fabricated, is shown in the block diagram of Fig. 3-1. The system consists of an antenna, electromechanical switch, receiver, video amplifier, memory voltmeter, an A/D converter, computer, and a visual display.

The antenna system consists of a hemispherical surface with 17 antennas. Each antenna has associated with it a particular θ and ϕ coordinate of a standard spherical coordinate system. Direction finding is accomplished (employing data processing techniques) utilizing the relative amplitudes received by each of the 17 antennas. The antennas are interrogated by a rotating electromechanical switch, which has several rotational rates ranging from 1 - 1000 rpm. The operator is able to select the optimum switching rate to be compatible with the received signals of interest.

The switch consists of 17 input ports (each to be identified with a particular antenna). In addition to the signal input, two interrupt signals (Ref. Sig.) are available from the switch for the computer to identify the signal port being interrogated. The interrupt signals are generated by light beams. One of the interrupts provides information pertaining to each revolution of the switch while the other denotes when each antenna is being interrogated. The switch interrogates each of the antennas such that the information is collected and stored in the computer in a sequential format. For example, if the first antenna is associated with $\theta = 80^{\circ}$, $\phi = 0^{\circ}$, employing the spherical coordinate system of Fig. 3-2, the second antenna would be at $\theta = 80^{\circ}$, $\phi = 45^{\circ}$; the third at $\theta = 80^{\circ}$, $\phi = 90^{\circ}$, etc., through the 17th antenna. For the exploratory model, the 17 antennas were located as follows: one at the pole, a ring of 8 antennas at $\theta = 40^{\circ}$, and a second ring of 8 antennas at $\theta = 80^{\circ}$. The antennas for each of the rings are equally spaced in ϕ increments of 45°.

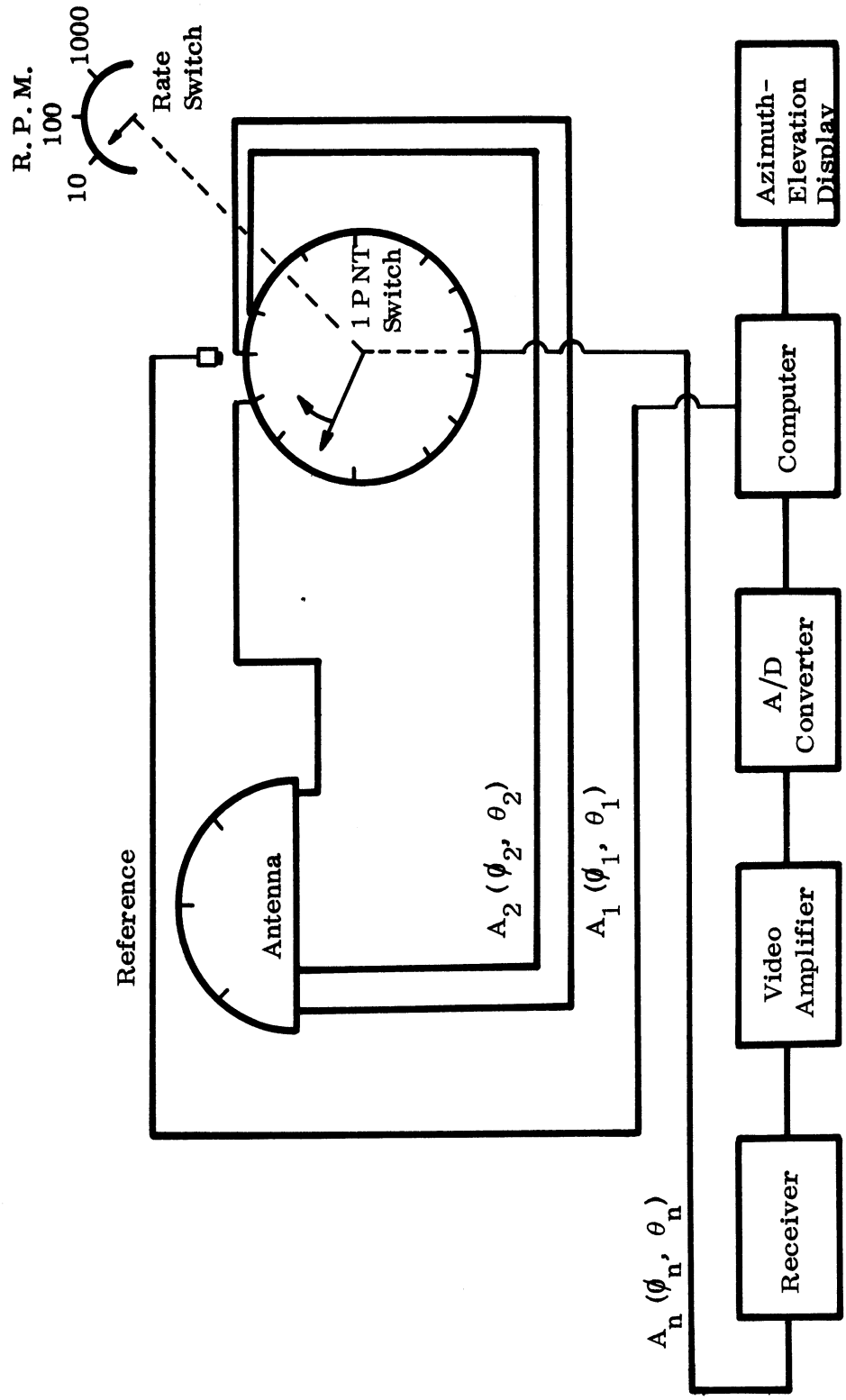

FIG. 3-1: AZIMUTH - ELEVATION DIRECTION FINDER.

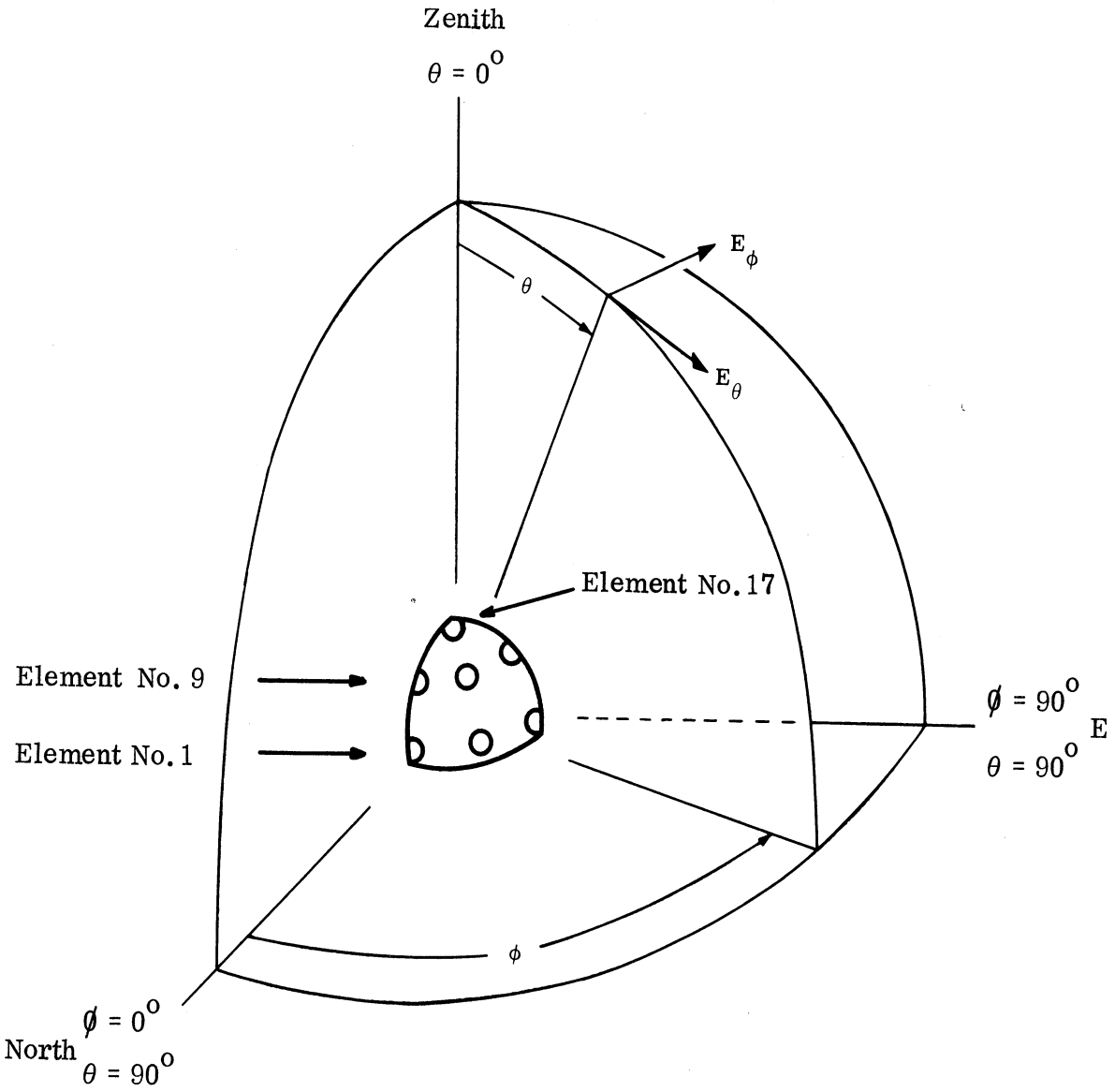

FIG. 3-2: AZIMUTH - ELEVATION COORDINATE SYSTEM.

The switch interrupts are transmitted from the switch directly to the computer to properly identify the signals being inserted in the computer. RF signals are first fed to the RF receiver to be amplified and detected. A video amplifier is required following the receiver to amplify the detected data to insure proper operation of the memory voltmeter. In the event more than one frequency is received (within the bandwidth of the receiver) an Automatic Signal Recognition Unit (ASRU) may be employed to resolve ambiguities, (this equipment is not a part of the A-EDF). The data from the memory voltmeter or ASRU is then transferred to the analog-to-digital converter, where it is digitalized in a format compatible with the computer.

In the computer data is stored sequentially as follows; the first storage compartment contains data for the pole antenna. The second storage compartment has data from the antenna located at $\theta = 40^{o}$, $\phi = 0^{o}$; and the third compartment has data for $\theta = 40^{o}$, $\phi = 45^{o}$, etc., through the 17 antennas.

Within the computer a vector evaluation of the data is performed from which directional information is obtained and displayed. Figure 3-3 is a simplified flow chart of the computer program employed to perform the direction finding analysis. In the first block, data is stored as noted above. Next, the data that has been collected and stored is scanned to determine the maximum signal (A_{max}); all of the remaining data is then normalized with respect to A_{max} as noted in Fig. 3-3. After normalization, the data for each antenna is separated into the three rectangular components (associated with the θ and ϕ coordinates of the particular antenna under consideration) as noted in the third block. The data for the pole antenna is separated into the A_{1x}, A_{1y}, and A_{1z} components as follows:

$$A_{1x} = A_1 \sin \theta_1 \cos \phi_1 \tag{3.1}$$

$$A_{1y} = A_1 \sin \theta_1 \sin \phi_1 \tag{3.2}$$

and

$$A_{1z} = A_1 \cos \theta_1 \tag{3.3}$$

A similar set of data will be obtained for each of the remaining antennas, (2 through 17). From this data a summation of all the sub x, y, and z components is performed as noted in the fourth block. From the summation,

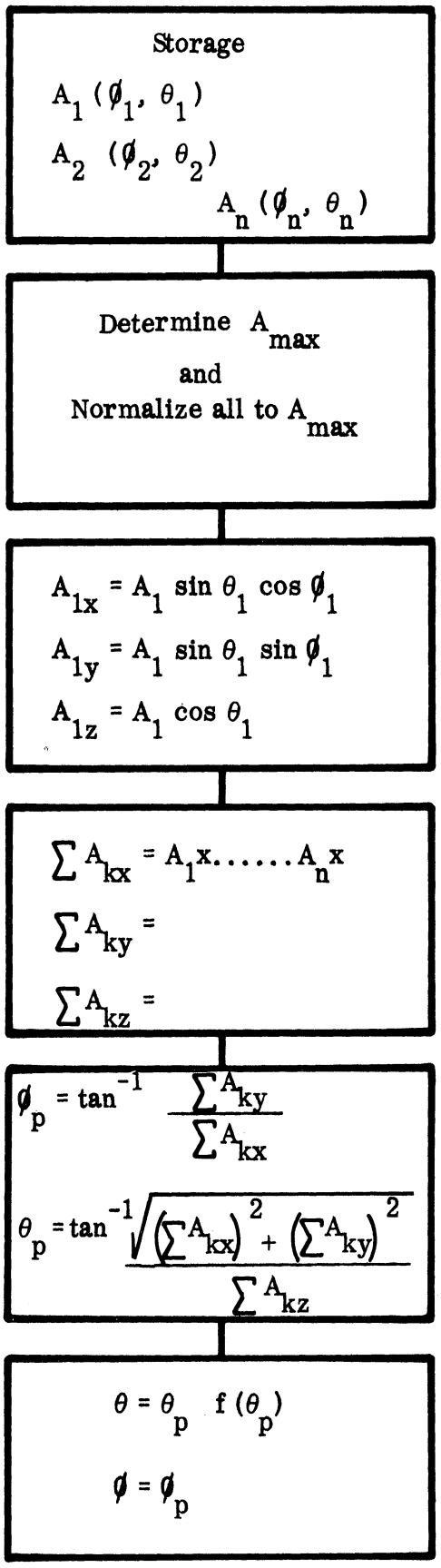

FIG. 3-3: AZIMUTH - ELEVATION DIRECTION FINDER SIMPLIFIED COMPUTER FLOW DESIGN.

the predicted angles (θ_p and ϕ_p) are determined employing the expressions,

$$\phi_p = \tan^{-1} \frac{\sum A_{ky}}{\sum A_{kx}} \tag{3.4}$$

and

$$\theta_p = \tan^{-1} \frac{\sqrt{\left(\sum A_{kx}\right)^2 + \left(\sum A_{ky}\right)^2}}{\sum A_{kz}} \tag{3.5}$$

Several analytical computer analyses have been performed which have shown that the θ_p differs from the actual angles (θ_A). However, these errors can easily be accounted for by the insertion of a correction factor in the computer. Therefore, the final operation of the computer is to correct θ_p to obtain the actual (θ_A) angles of the signal under interrogation as shown in the sixth block of the flow chart. The computer output is displayed in digital form by NIXIE tubes.

The antennas employed with the system are cavity backed spirals. The electromechanical switch operates over the 5:1 frequency band and exhibits a VSWR of less than 3:1 within the frequency range of 600 - 3000 MHz. The data processing equipment consists of a Hewlett-Packard wide band amplifier, a Micro-Instrument memory voltmeter, a Texas Instrument A/D converter, and a Varian 620/i digital computer. The data processing equipment is packaged in a single cabinet. The computer has been programmed so that the directional information is printed out by the typewriter as well as being presented on the NIXIE display.

The electromechanical switch rotor is driven by an eighth horsepower synchronous motor through a multiple gear reduction assembly. The multiple gear reduction unit provides choices of switching speeds that range from 1000 to 1 rpm in 10 steps. The RF switch itself consists of a capacitive coupling for the switching ports and rotary joint.

3.2 Analytical Analysis

The data processing technique chosen to be used with the A-EDF system required several successive vector additions of the data. Analytical analyses

have been made to determine the effect of the following system parameters:

1) antenna pattern,
2) number of receiving antennas,
3) antenna location, and
4) the measurement errors particular to the system.

3.2.1 Data Requirements for the DF Data Processing System

The analytical studies showed that the system accuracy was strongly dependent upon the antenna pattern characteristics and less dependent on the geometrical location of the antennas. Further, there are inherent limitations associated with the three-dimensional system that are not found in the conventional two-dimensional system, e.g., the Watson-Watt DF system employing four antennas, (Jasik, 1961). To gain familiarity with the vector addition concept an analysis was first made of a simplified two-dimensional model employing a ring of n antennas, separated by equal angles of θ as shown in Fig. 3-4.

Table 3-1 notes the expressions from which the relative amplitude levels for each antenna may be calculated (assuming the direction of the unknown signal is arriving from an angle θ).

TABLE 3-1

Antenna Responses

1) $\cos(\theta - 2\beta)$
2) $\cos(\theta - \beta)$
3) $\cos\theta$
4) $\cos(\theta + \beta)$
5) $\cos(\theta + 2\beta)$

To illustrate one of the limitations of this system, it is assumed that the unknown signal is arriving from an arbitrary angle θ and that only three antennas receive data. Further, it is assumed that the antennas are located at $\beta = 0^{\circ}$ and $\pm 45^{\circ}$. These angular locations were chosen to simplify the equations, however,

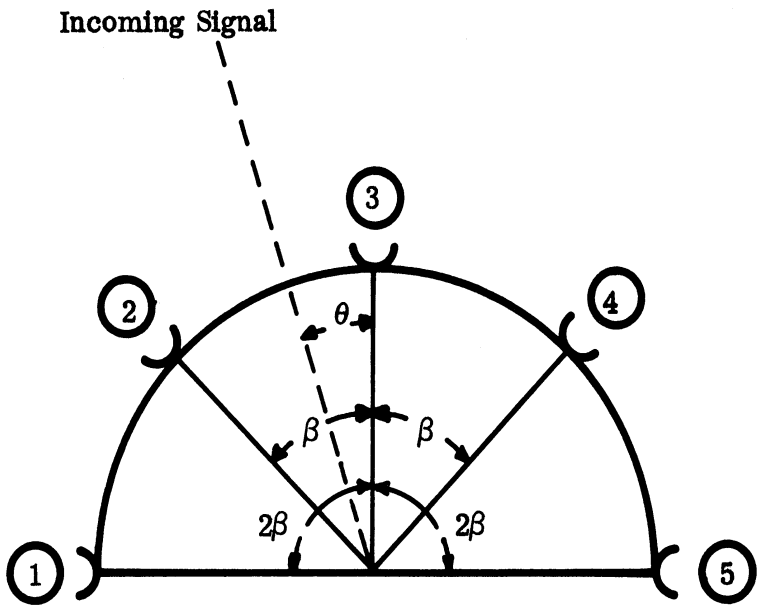

FIG. 3-4: TWO-DIMENSIONAL DIRECTION FINDING WITH SOME NUMBER "N" OF EQUALLY SPACED ANTENNAS.

if one were to employ a more general analysis, the results would be similar to those obtained from this analysis. Here it will be shown that unless one considers all antennas over a $\beta = 180^{o}$ sector, there will be an inherent discrepancy in the calculation of the predicted angle of arrival of the unknown signal. Table 3-2 provides the expression for the vertical and horizontal components of three of the antennas noted above.

TABLE 3-2

Vertical Component

2) $\cos(\theta - \beta)\cos\beta$

3) $\cos(\theta)\cos 0^{o}$

4) $\cos(\theta + \beta)\cos\beta$

Horizontal Component

2) $\cos(\theta - \beta)\sin\beta$

3) $\cos\theta \sin 0^{o}$

4) $-\cos(\theta + \beta)\sin\beta$

The vertical and horizontal components are combined in a ratio to attain $\tan\theta$ of equation (3.6).

$$\tan\theta = \frac{\text{hor. comp.}}{\text{vert. comp.}} = \frac{\cos(\theta - \beta)\sin\beta - \cos(\theta + \beta)\sin\beta}{\cos(\theta - \beta)\cos\beta + \cos\theta + \cos(\theta + \beta)\cos\beta} \qquad (3.6)$$

Expanding the sum and difference trigonometric expressions, equation (3.7) is obtained, which reduces to a more simple form involving $\tan\theta$ multiplied by a trigonometric ratio which is dependent on the angular position of the antennas. It is the multiplication factor which causes the discrepancy between the calculated and actual angle of arrival (θ).

$$\frac{(\cos\theta\cos\beta + \sin\theta\sin\beta)\sin\beta - \left[\cos\theta\cos\beta - \sin\theta\sin\beta\right]\sin\beta}{\left[\cos\theta\cos\beta + \sin\theta\sin\beta\right]\cos\beta + \cos\theta + \left[\cos\theta\cos\beta - \sin\theta\sin\beta\right]\cos\beta} =$$

$$\frac{\sin\theta}{\cos\theta}\left(\frac{2\sin^{2}\beta}{1 + 2\cos^{2}\beta}\right) = \tan\theta\ \frac{2\sin^{2}\beta}{1 + 2\cos^{2}\beta} \qquad (3.7)$$

Consider now using antennas that are within a $\beta = 180^{o}$ sector ($\pm 90^{o}$) with respect to the angular position of the unknown signal. For the purposes of this analysis we will assume five antennas, (however, one need not be limited to five). Table 3-3 lists the expression for the vertical and horizontal components that would be associated with each of the five antennas.

Table 3-3

Vertical Component

1) $\cos(\theta - 2\beta) \cos 2\beta$

2) $\cos(\theta - \beta) \cos \beta$

3) $\cos \theta \cos 0^{o}$

4) $\cos(\theta + \beta) \cos \beta$

5) does not receive signal as $\theta + 2\beta > 90^{o}$

Horizontal Component

1) $\cos(\theta - 2\beta) \sin 2\beta$

2) $\cos(\theta - \beta) \sin \beta$

3) $\cos \theta \sin 0^{o}$

4) $\cos(\theta + \beta) \sin \beta$

5) does not receive signal as $\theta + 2\beta > 90^{o}$

Through the use of equation (3.8), $\tan \theta$ for the unknown signal is obtained employing all antennas within the 180^{o} sector.

$$\tan \theta = \frac{\text{horizontal comp.}}{\text{vertical comp.}} =$$

$$\frac{\cos(\theta - 2\beta) \sin 2\beta + \cos(\theta - \beta) \sin \beta - \cos(\theta + \beta) \sin \beta}{\cos(\theta - 2\beta) \cos 2\beta + \cos(\theta - \beta) \cos \beta + \cos \theta + \cos(\theta + \beta) \cos \beta} \qquad (3.8)$$

Equation (3.9) is the trigonometric expansion of this and equation (3.10) has been simplified to a form which gives a trigonometric ratio times the tangent of θ.

It may be shown that the trigonometric ratio is equivalent to unity for the case of five antennas that are equally spaced ($\beta = 45^{o}$). However, had there been more antennas and again equally spaced, the trigonometric ratio would have been more complex, but it can be shown that it would be equivalent to unity as in the case for five antennas. Therefore, the predicted angle of arrival is equal to the actual angle of arrival only when all of the sampling antennas are located within a 180^{o} sector and these outputs are employed in the data processing. Intuitively, one might reason that this is to be expected since for the purposes of this simplified analysis, it has been assumed that the radiation patterns of each of the antennas fits a cosine distribution in the range of $\beta = \pm 90^{o}$.

$$\tan \theta = \frac{\gamma \sin 2\beta + \psi \sin \beta - \zeta \sin \beta}{\gamma \cos 2\beta + \psi \cos \beta - \zeta \sin \beta} \tag{3.9}$$

where

$\gamma = \cos \theta \cos 2\beta + \sin \theta \sin 2\beta$

$\psi = \cos \theta \cos \beta + \sin \theta \sin \beta$

$\zeta = \cos \theta \cos \beta - \sin \theta \sin \beta$

Note: $\beta = 45^{o}$, and $\cos 2\beta = 0$ $\sin 2\beta = 1$

$$\tan \theta = \frac{\sin \theta \,(1 + 2 \sin^{2} \beta)}{\cos \theta \,(1 + 2 \cos^{2} \beta)} \tag{3.10}$$

From this analysis it is shown that if antennas are not located over a 180^{o} sector, there will be an inherent error in the calculation of the angular position of the received signal. However, the error is predictable and therefore can be corrected as necessary. A more rigorous analysis of this technique is presented by Ferris, et al (1967) for a three-dimensional DF system.

3.2.2 Analytical Results for a Three-Dimensional DF System

Several computer programs have been employed to evaluate the three-dimensional DF system using antennas mounted on a hemispherical surface. Data from these programs have shown that there will be an error in the calculated angle for both elevation and azimuth similar to that noted above. The error in elevation has been greater because of the non-symmetry of the antennas (antennas are located on a hemisphere of 2π steradians) which was expected

from the previous discussion for the two-dimensional system. The azimuth errors were found to be minimal provided the element patterns were well behaved and therefore required no correction factor.

The first calculated data assumed the 17 antennas were equally spaced over 2π steradians (at θ and ϕ increments of 45^{o}, as shown in Fig. 3-5) of the hemisphere and that each antenna had a cosine pattern which is symmetrical about its axis. Calculated data is shown in Fig. 3-6 which illustrates the errors of the calculated angle as compared to the true elevation angle. It will be noted there are two sets of data points which represent the maximum and minimum error of the calculated elevation angle as a function of the azimuth angle. The large variations associated with the calculated angle for elevation is corrected for, within the computer, prior to the data being shown by the display system.

Figure 3-7 illustrates typical element radiation (voltage) patterns and are referred to as cosine, linear 90^{o}, 80^{o}, and 70^{o}. Figures 3-8, 3-9, and 3-10 are respectively the calculated elevation angles for linear 90^{o}, 80^{o}, and 70^{o} patterns. It is interesting to note there is very little difference between the data for the cosine patterns (Fig. 3-6) and the linear 90^{o} pattern (Fig. 3-8). However, the error for the linear 70^{o} and 80^{o} (with respect to the cosine data) are appreciably larger. Typical far-field radiation patterns that have been measured for spiral antennas have shown that they exhibit patterns that may be closely approximated by an analytical expression similar to that for the 90^{o} distribution.

Many spiral patterns have their maximums skewed from the axis of the antenna surface. In an attempt to determine the effects of a skewed pattern on the calculated elevation angle versus the actual angle of arrival, a computer program was employed assuming the main beam skewed 10^{o} off axis for a linear 90^{o} pattern. The program also assumed the patterns were randomly oriented over the hemispherical surface such that the skewing would not all point in the same direction. Figure 3-11 is a plot of the calculated elevation angles as a function of the actual angle employing the skewed patterns. The variation in the predicted angle exhibits a random variation which would be difficult to correct to obtain the actual angle of arrival. Therefore, it has been concluded that the individual element patterns must be well behaved (have a minimum of skewing $<< 5^{o}$) both as a function of antenna orientation as well as a function of frequency, i.e., the main lobe must be symmetrical about the axis of the antenna as a function of antenna orientation and frequency.

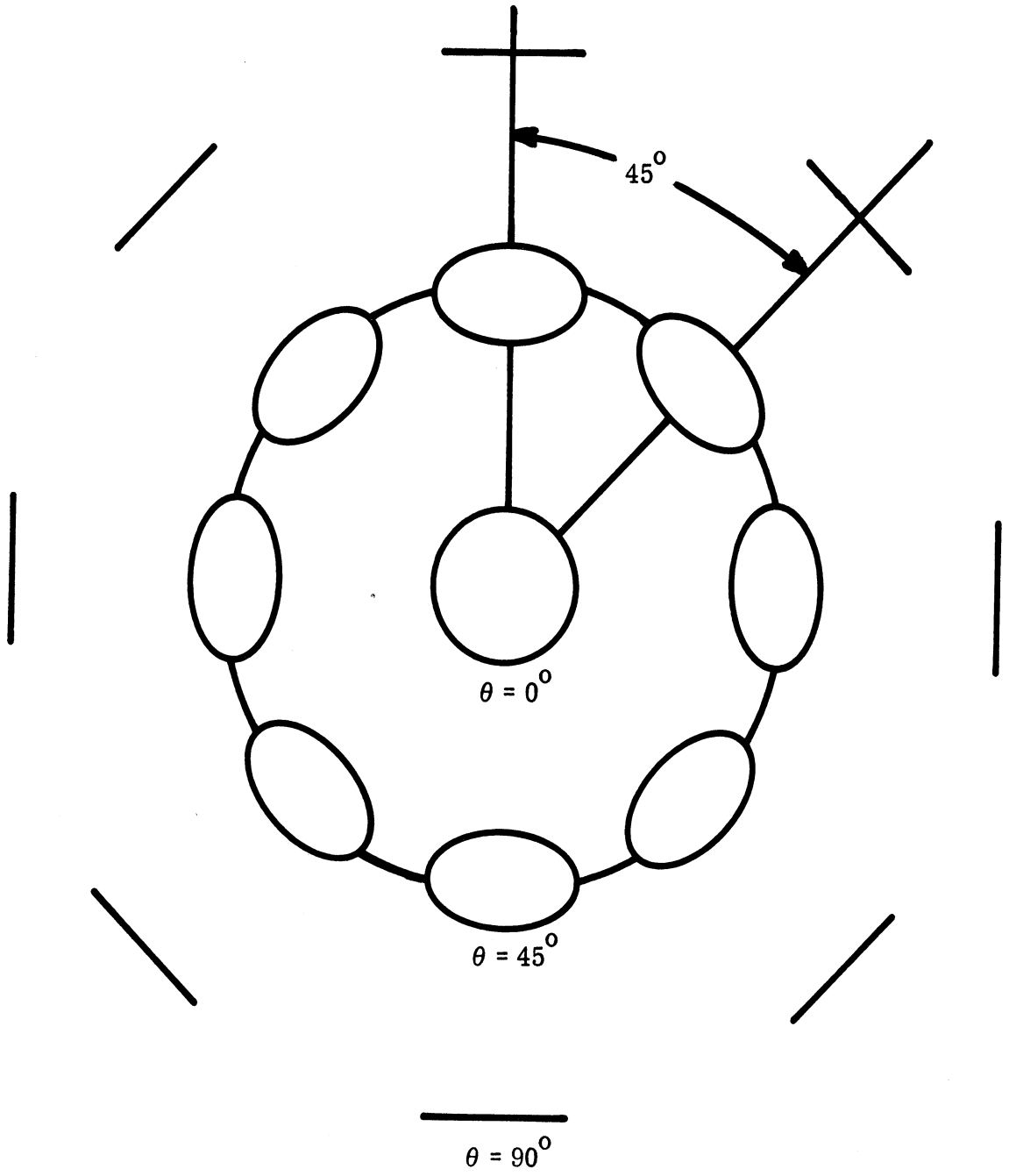

FIG. 3-5: GEOMETRY OF AZIMUTH-ELEVATION DIRECTION FINDER WITH SEVENTEEN ANTENNAS. NOTE ANTENNAS ALIGN ON RINGS IN ELEVATION PLANE.

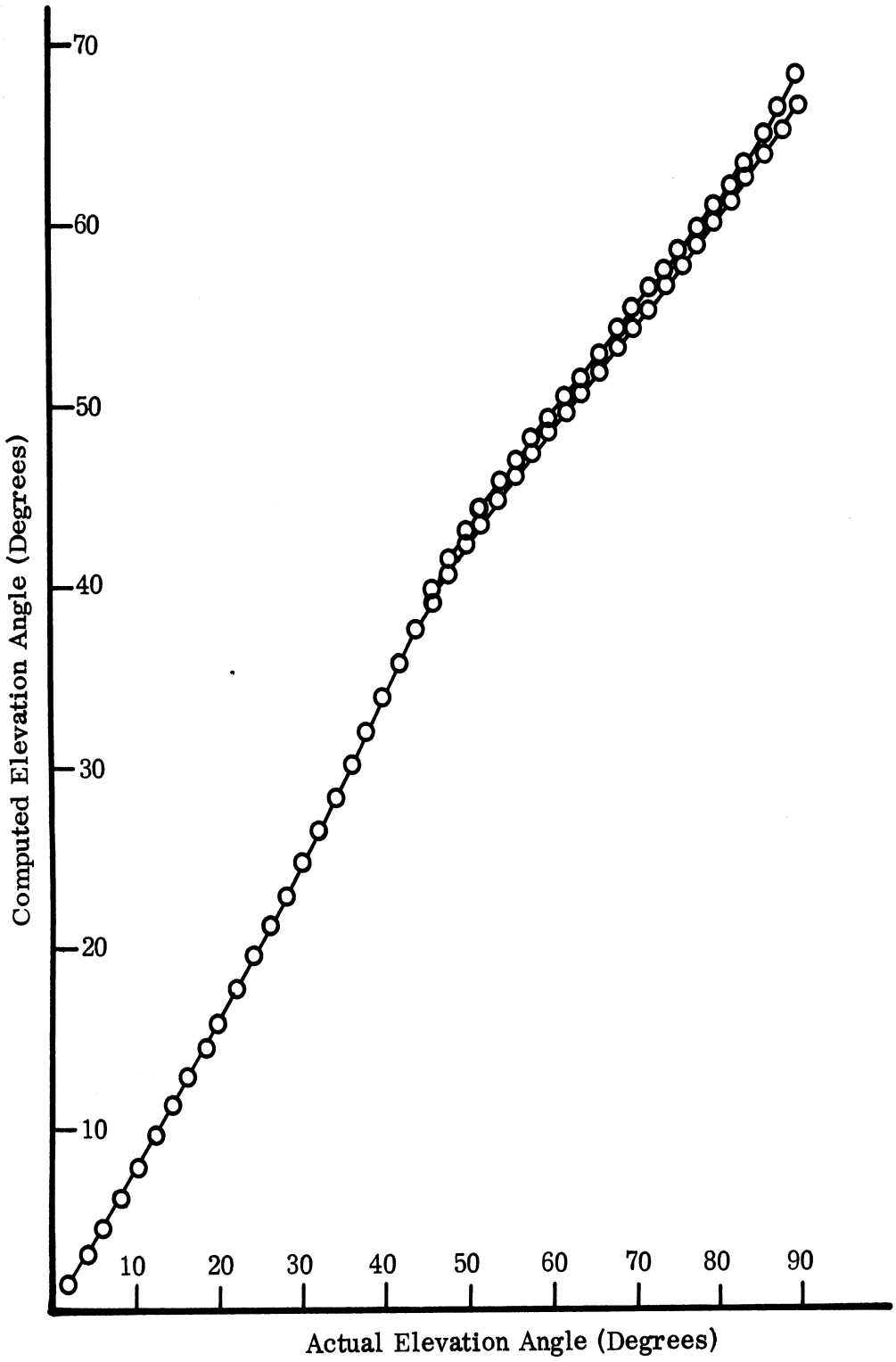

FIG. 3-6: COMPUTED ELEVATION ANGLE versus ACTUAL ELEVATION ANGLE FOR COSINE ANTENNA PATTERN; SEVENTEEN ANTENNAS.

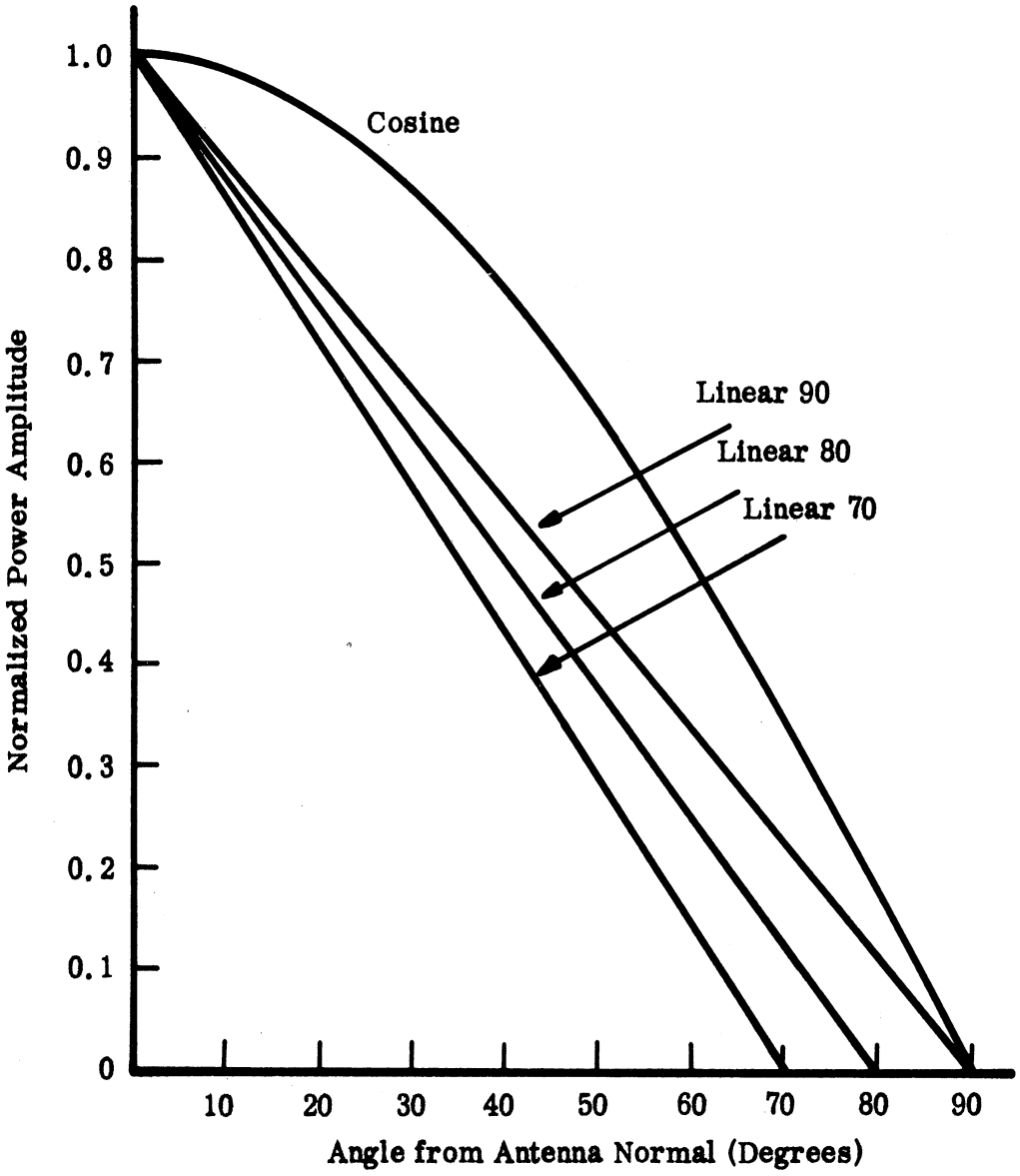

FIG. 3-7: VARIOUS TYPES OF FAR FIELD ANTENNA PATTERNS CONSIDERED IN COMPUTER PROGRAMS.

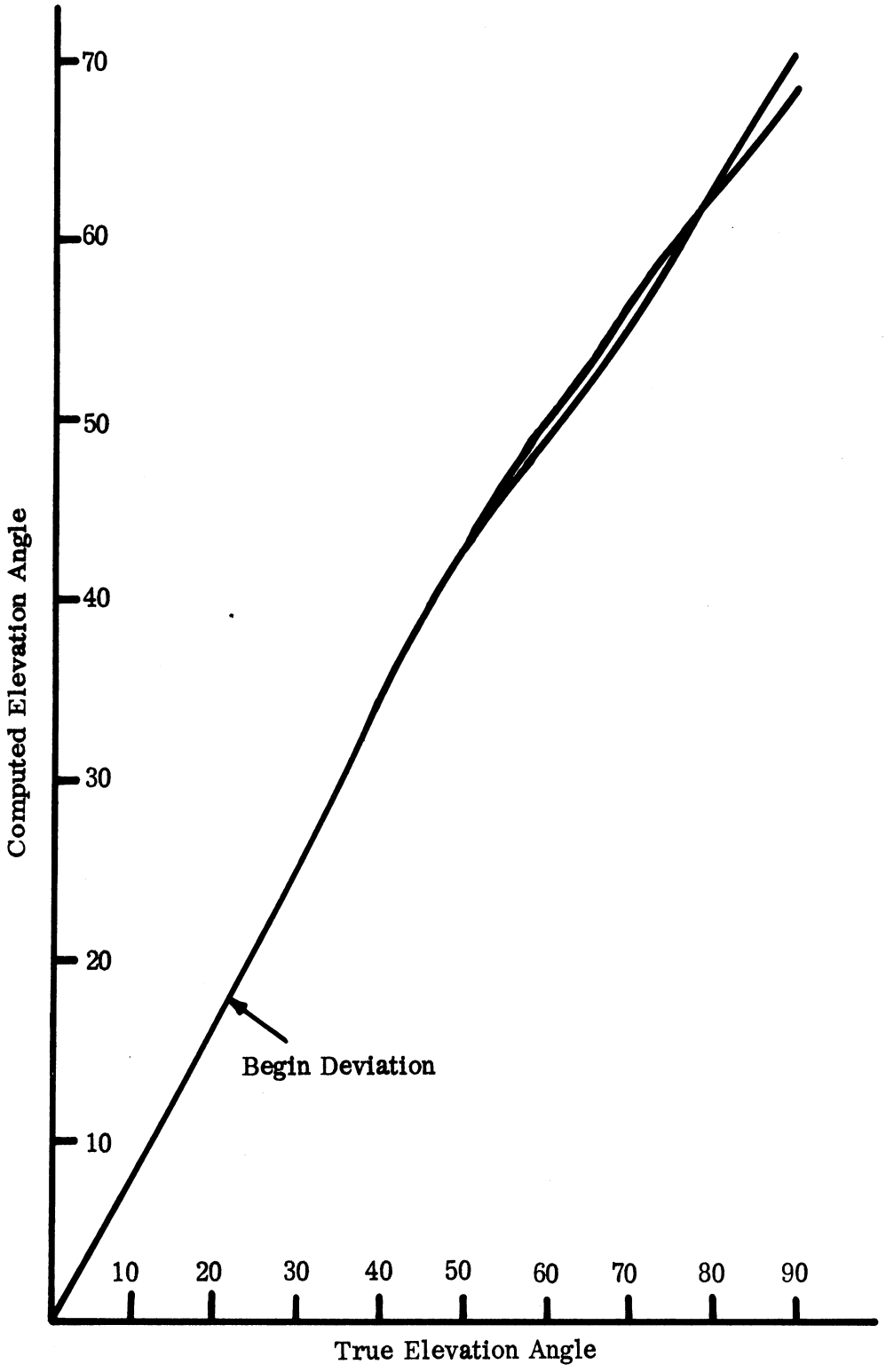

FIG. 3-8: COMPUTED ELEVATION ANGLE versus ACTUAL ELEVATION ANGLE FOR LINEAR 90 ANTENNA PATTERN, SEVENTEEN ANTENNAS.

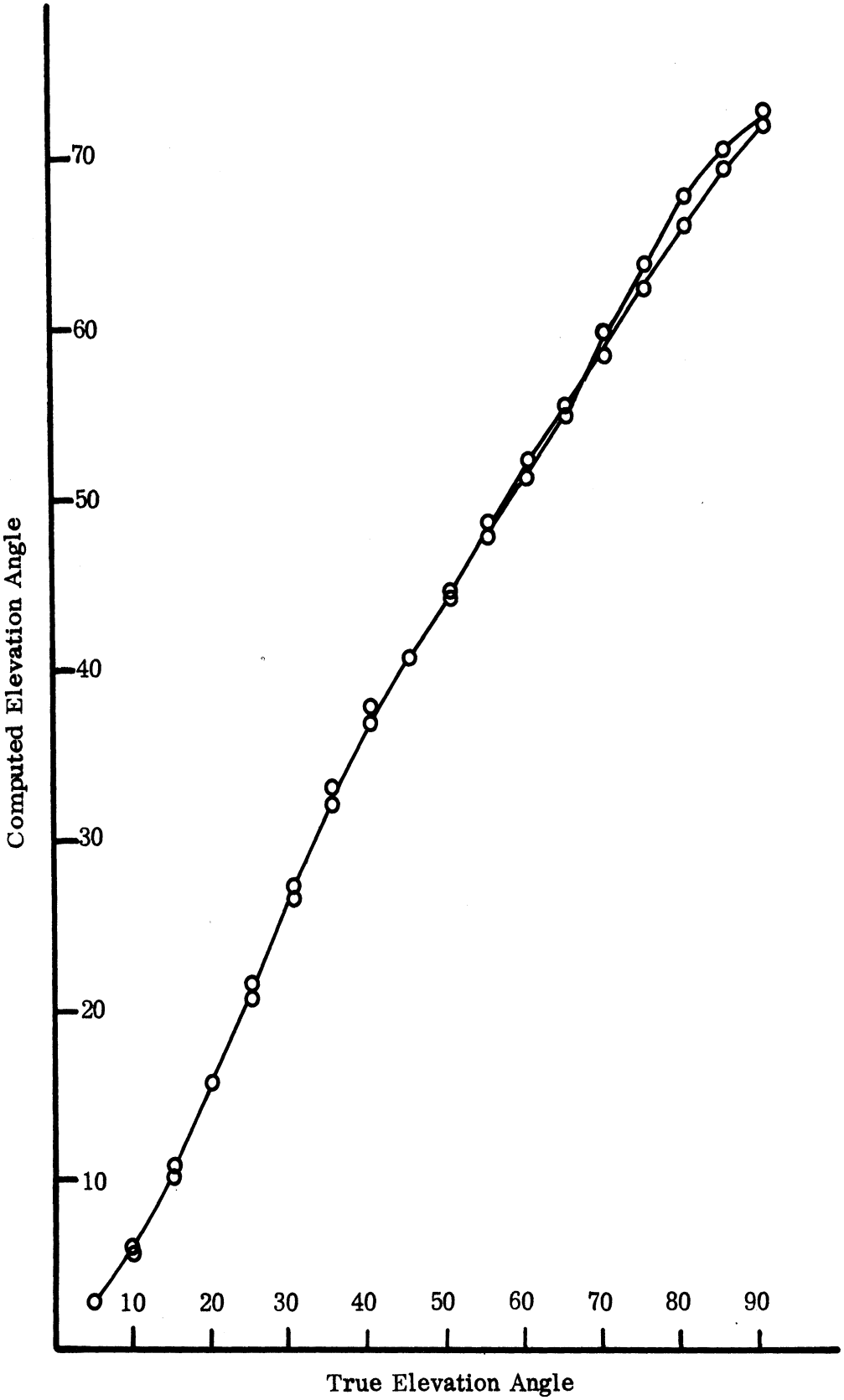

FIG. 3-9: COMPUTED ELEVATION ANGLE versus ACTUAL ELEVATION ANGLE FOR LINEAR 80 PATTERN, SEVENTEEN ANTENNAS.

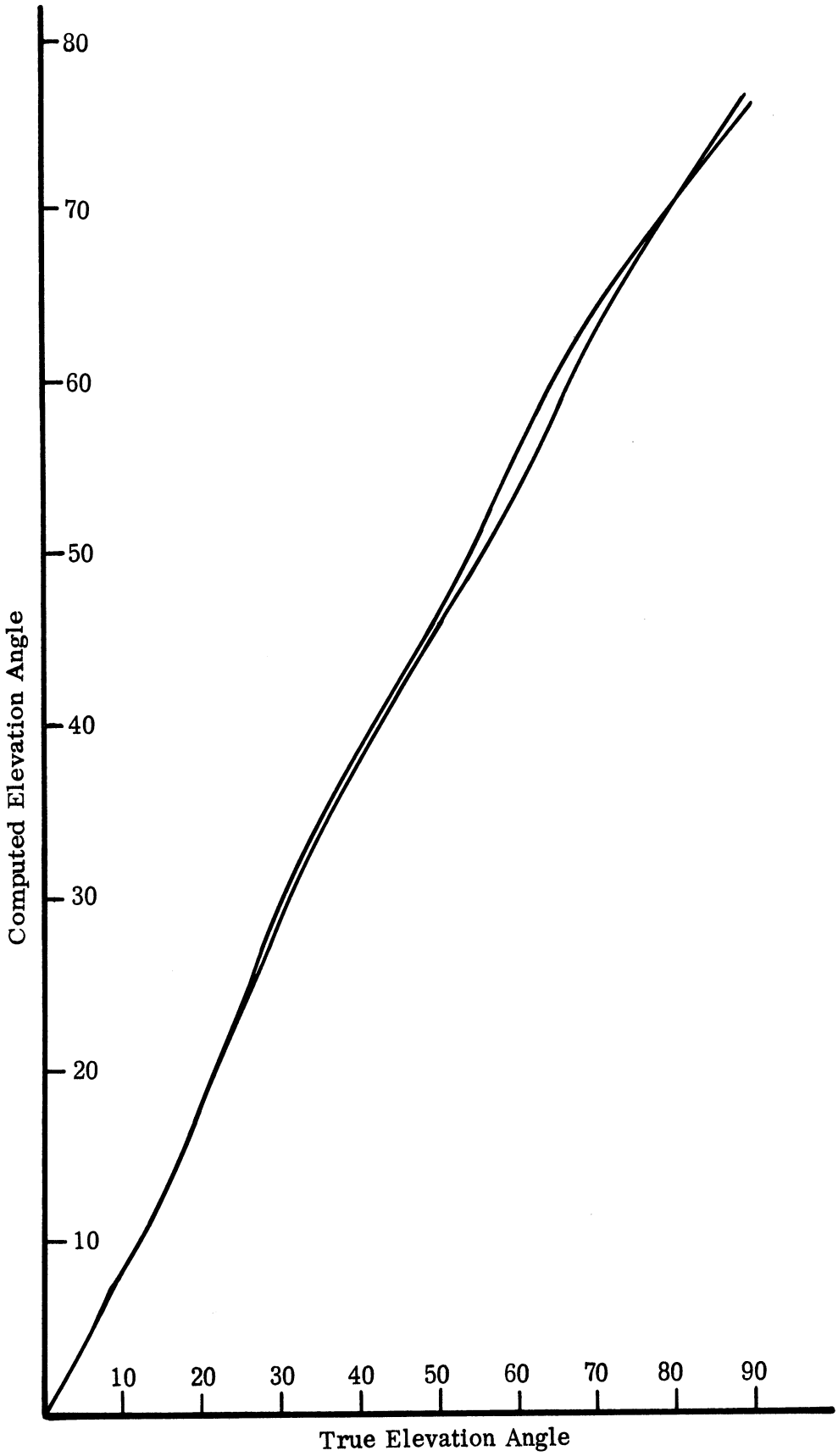

FIG. 3-10: COMPUTED ELEVATION ANGLE versus ACTUAL ELEVATION ANGLE FOR LINEAR 70 ANTENNA PATTERN, SEVENTEEN ANTENNAS.

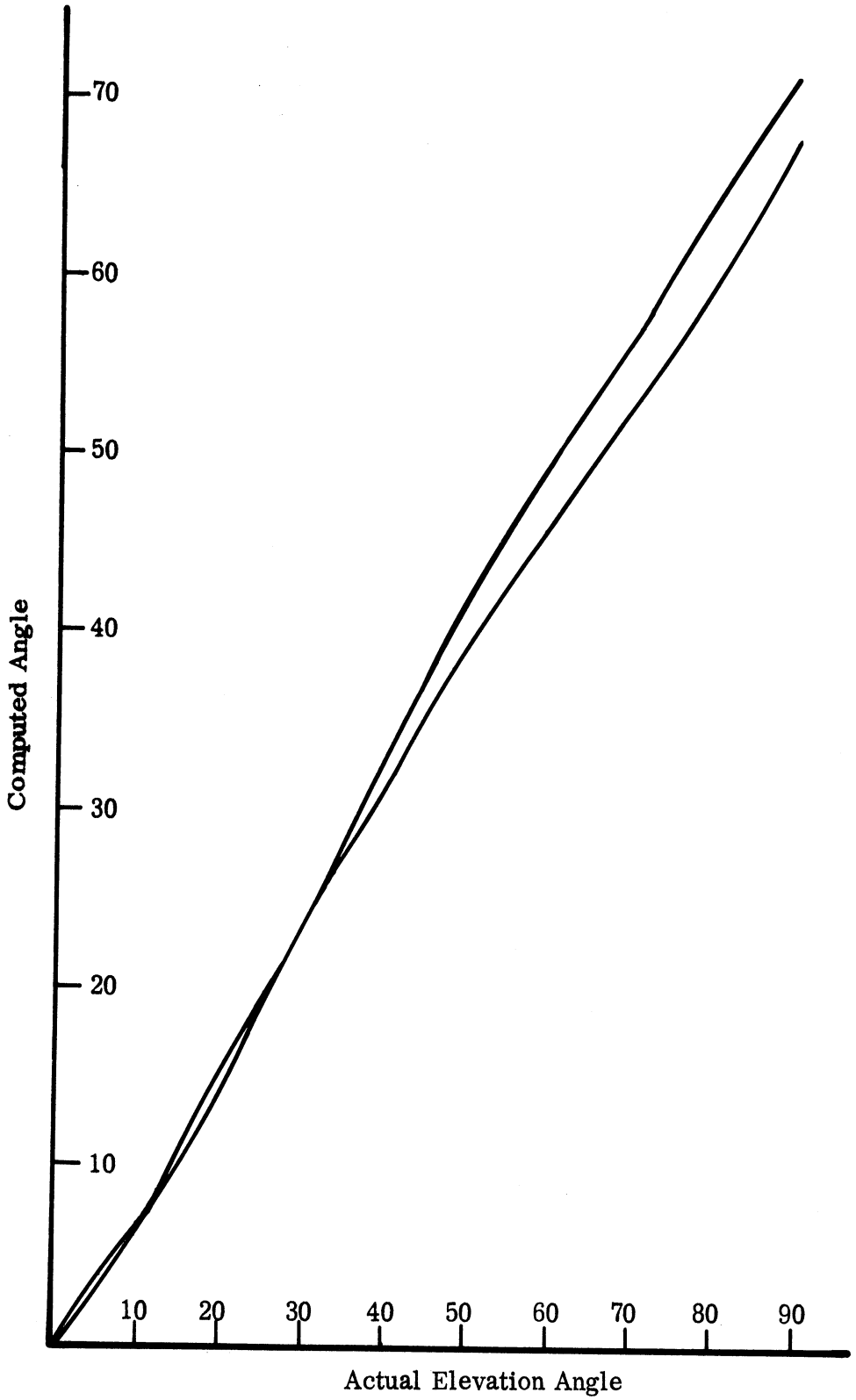

FIG. 3-11: COMPUTED ELEVATION ANGLE versus ACTUAL ELEVATION ANGLE FOR COSINE PATTERNS SKEWED 10^{o} OFF NORMAL, SEVENTEEN ANTENNAS.

Because of the absence of antennas below $\theta = 90^{o}$, there will be errors in the azimuth calculation as will be shown below. Figure 3-12 is a plot of the maximum azimuth error as a function of the elevation angle (assuming the element patterns satisfy a cosine distribution). It is interesting to note that from $\theta = 0^{o}$ to 45^{o}, there is no azimuthal discrepancy. However, from $\theta = 45^{o}$ to 90^{o}, there is an error which is a periodic function with the maximum error occurring at $\theta = 80^{o}$. Since the error is periodic, it is amenable to correct within the computer as was the case for the elevation error. However, because of the relatively small magnitude of the error, a correction factor for it is not used in the present A-EDF system.

In the discussion of the elevation angles, consideration was given to the use of antennas whose patterns may be skewed. A similar analysis was made as a part of the azimuth study. Figure 3-13 is a plot of the calculated angle in azimuth as a function of the elevation angle. Note that the deviation of the calculated angle from the actual angle is greatest near $\theta = 0^{o}$, (top of the hemisphere), where it approaches 10^{o} or more. However, when data is collected near the horizon, the discrepancy decreases to approximately 3^{o}. Although the discrepancy has decreased, it is larger than is acceptable. Therefore, it was concluded that the use of elements with skewed patterns for the A-EDF would be unacceptable because of the large discrepancies incurred both in azimuth and elevation.

3.2.3 Consideration of Antenna Number and Location

The above calculations employed 17 antennas equally distributed over the surface of the hemisphere. A second distribution consisted of 26 antennas located on a icosahedron as shown in Fig. 3-14 and discussed by Sengupta, et al (1966). The icosahedron distribution has the advantage of achieving a uniform coverage of antennas over the surface of the hemisphere. Data from a 26 element icosahedron distribution exhibited little advantage over the 17 element design. Figure 3-15 is a plot of the azimuth error as a function of the elevation angle for the icosahedron distribution. The data shown in Fig. 3-15 was calculated in increments of 5^{o} for the azimuth angle. A later set of data was collected at 1^{o} increments and when compared with the 17 element data it exhibited little improvement in system operation.

The maximum error for the 17 element system with cosine pattern distribution occurs at $\theta = 80^{o}$ and midway between elements in the ϕ plane. A plot of the discrepancy as a function of ϕ for $\theta = 80^{o}$ is shown in Fig. 3-16. The maximum discrepancy here is 0.86^{o}. It may be shown that the discrepancy can either be increased or decreased by respectively decreasing or increasing the

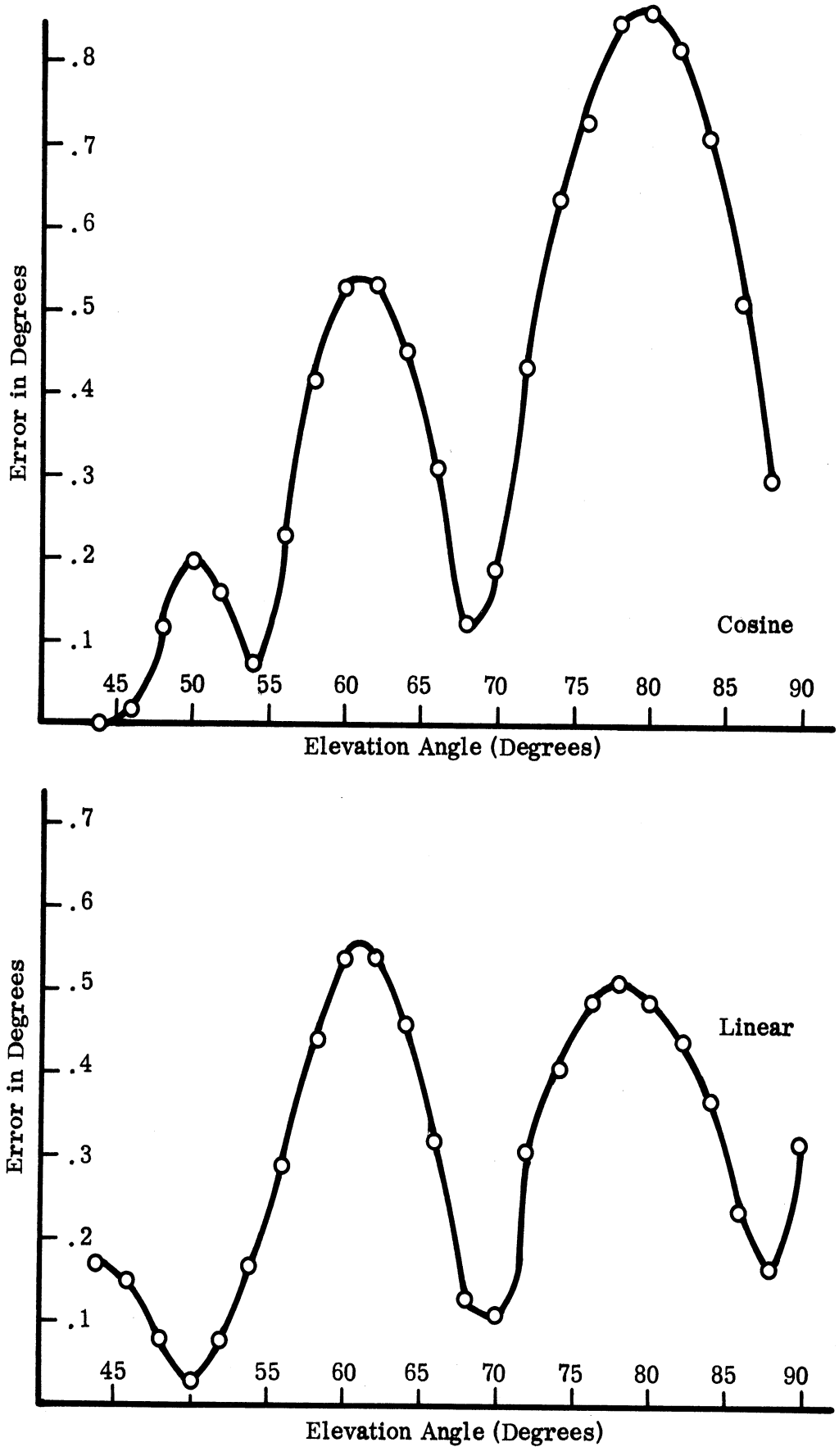

FIG. 3-12: MAXIMUM ERROR IN AZIMUTH versus ELEVATION ANGLE θ FOR COSINE PATTERN, SEVENTEEN ANTENNAS.

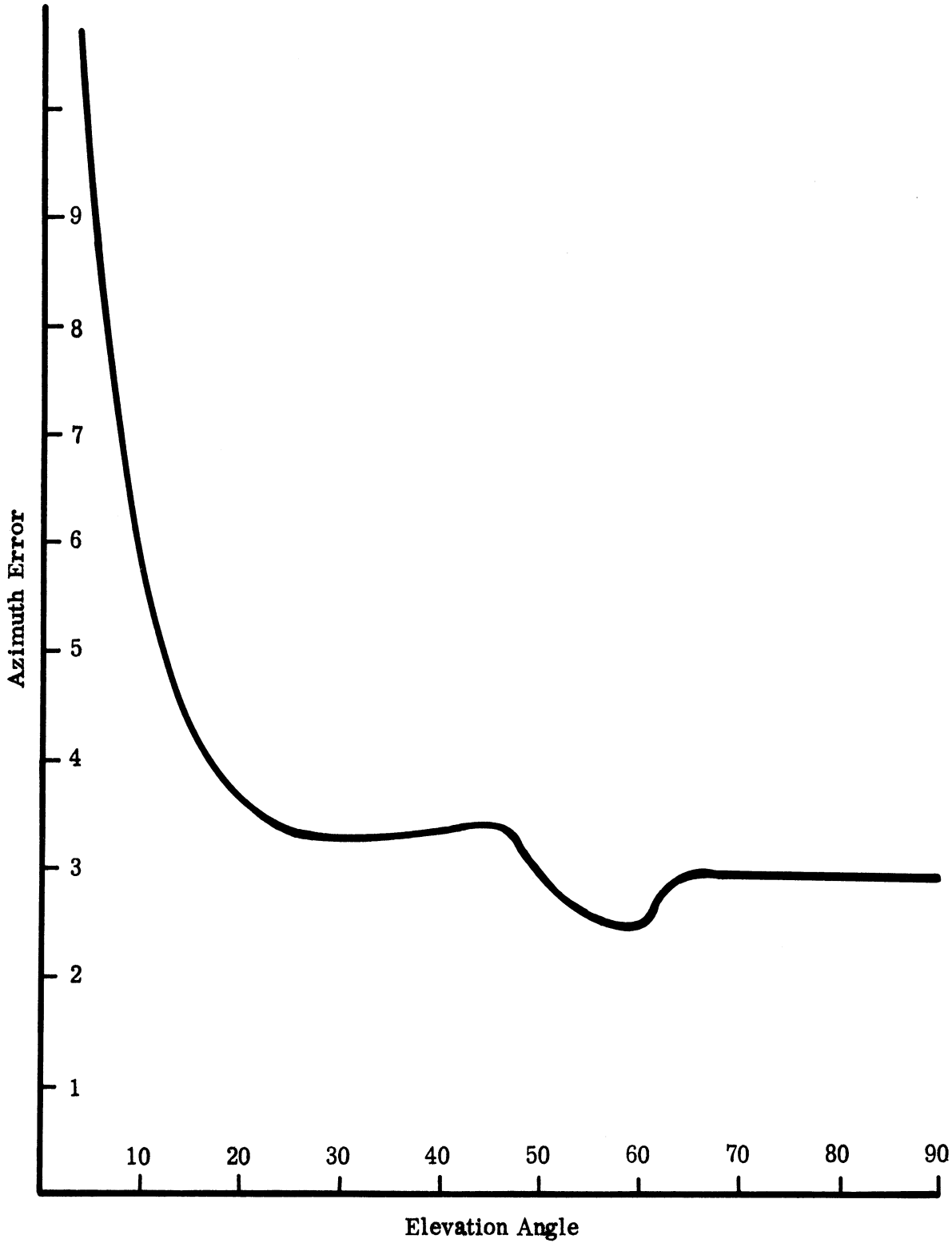

FIG. 3-13: MAXIMUM AZIMUTH ERROR versus ELEVATION ANGLE FOR COSINE PATTERN SKEWED 10^{o}, SEVENTEEN ANTENNAS.

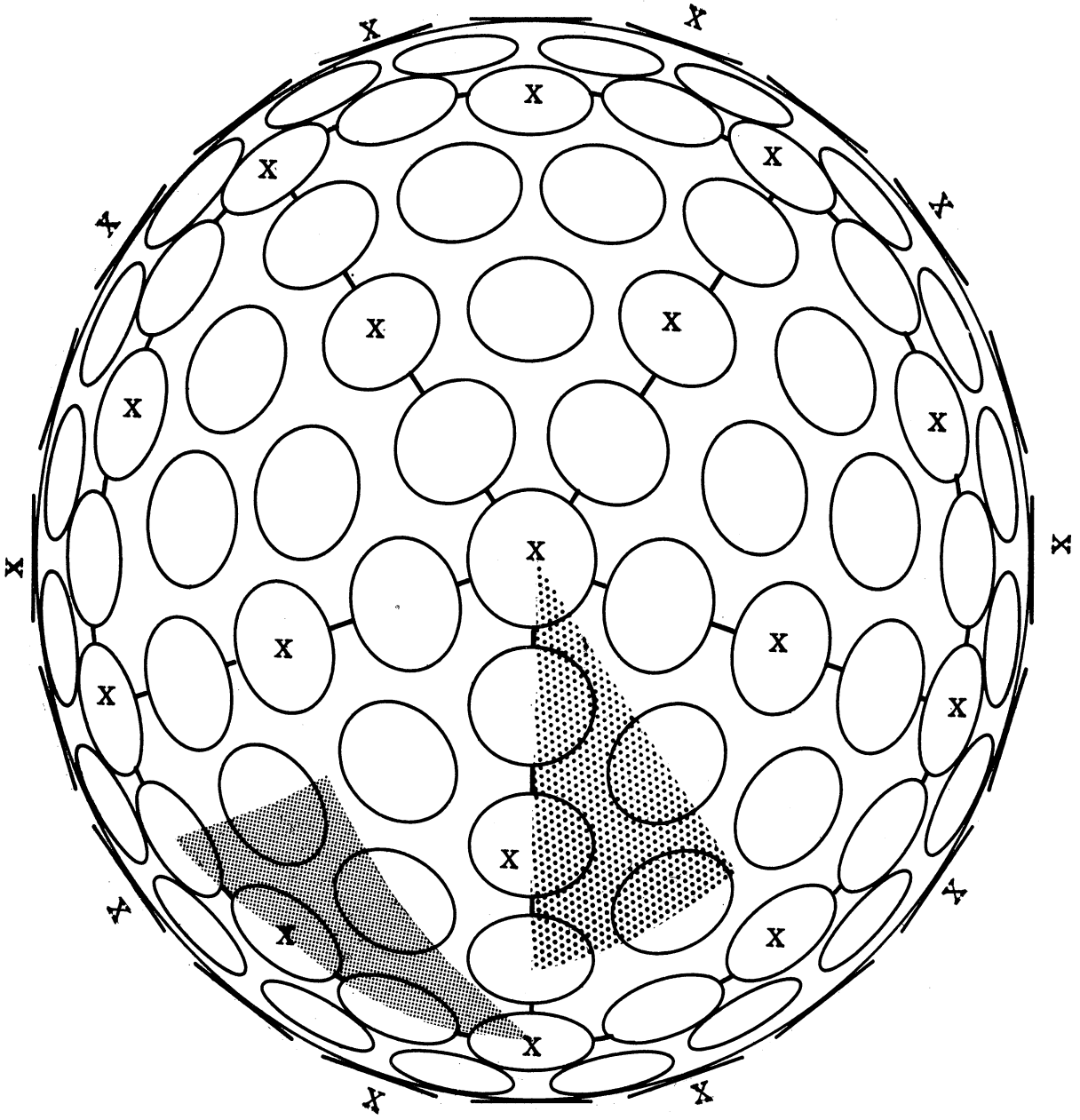

FIG. 3-14: SPHERICAL ARRAY. X's MARK ELEMENTS UTILIZED FOR ICOSAHEDRON DIRECTION FINDING CALCULATIONS

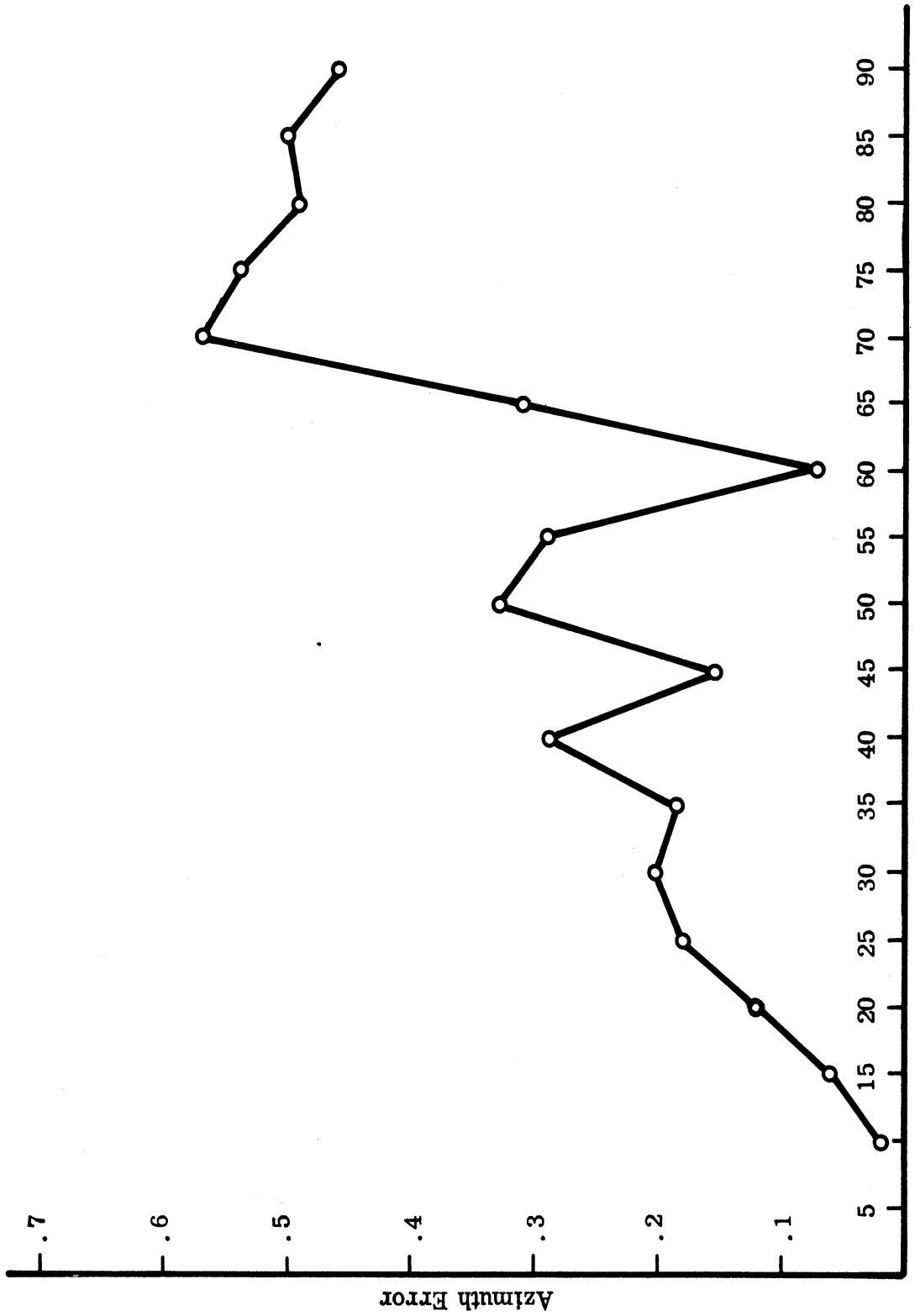

FIG. 3-15: MAXIMUM AZIMUTH ERROR VERSUS ELEVATION ANGLE FOR ICOSAHEDRON GEOMETRY WITH COSINE PATTERNS.

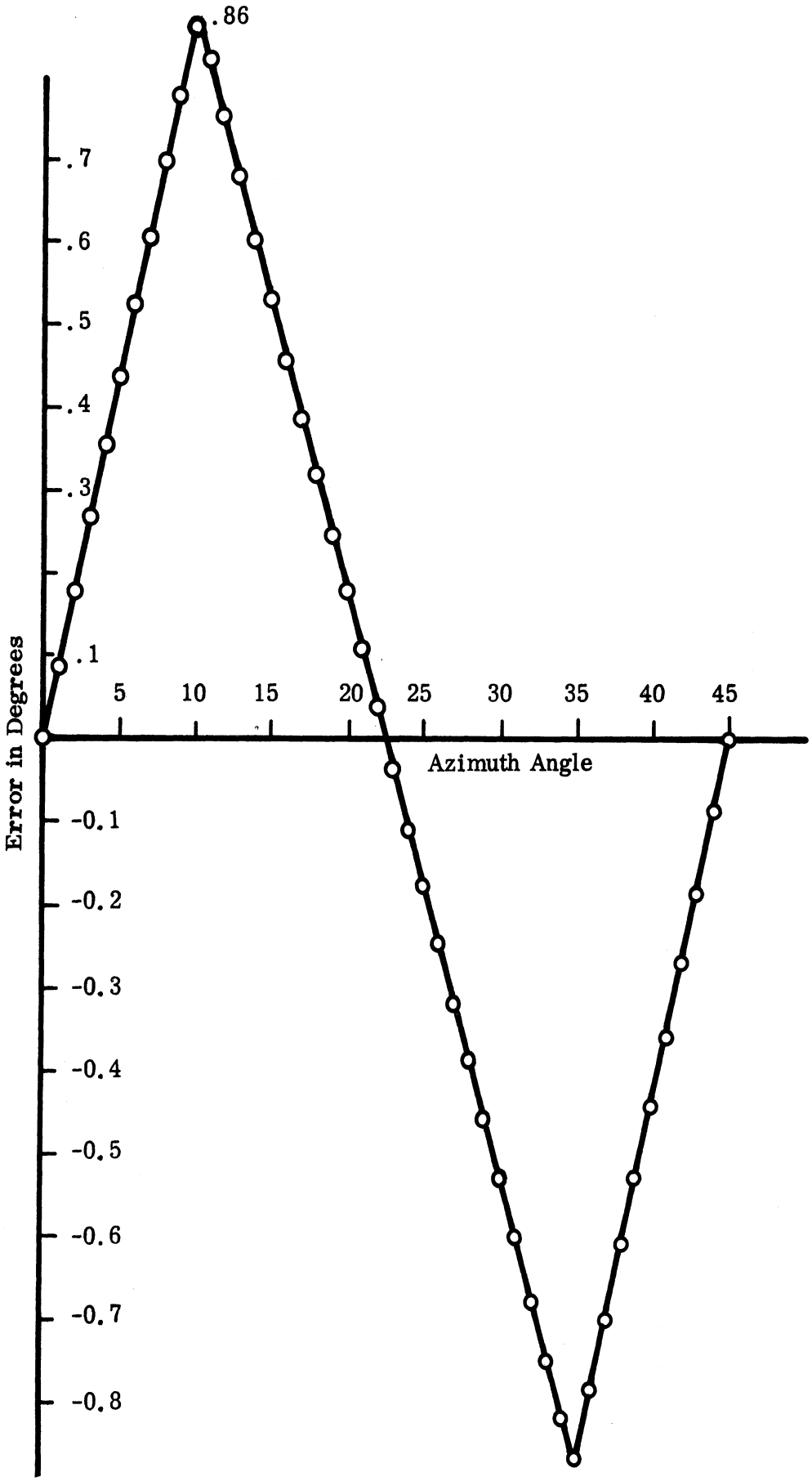

FIG. 3-16: ERROR IN AZIMUTH versus AZIMUTH ANGLE ϕ for $\theta = 80^{\circ}$, SEVENTEEN ELEMENTS WITH COSINE PATTERN.

number of elements. Increasing the number of elements would improve both the accuracy and sensitivity but would further complicate the data processing requirement (computer and associated hardware) thus increasing the costs. For these reasons, the 17 element system was employed for the exploratory A-EDF model.

3.3 Typical Results Obtained From the Feasibility Azimuth - Elevation System Model

A brief description of the free space data collected from the A-EDF is presented below along with a description and the results of the fly-by tests.

3.3.1 Free Space Test Data

Free space data for the A-EDF system was collected with the antenna oriented such that constant azimuth angle ($\phi = 90^{o}$ or 270^{o}) calculations were made as the elevation angle was varied through 180^{o}. The coordinate system of Fig. 3-2 has been employed. A typical set of azimuth data is shown graphically in Fig. 3-17. This graph shows the system calculated azimuth information on the vertical axis as a function of elevation angle (of the horizontal axis) at a frequency of 1.6 GHz. Ideally the azimuth data should read either 90^{o} or 270^{o} depending upon which side of the hemisphere (east or west) data is being collected. It will be observed that the data near the pole position of the hemisphere (i.e., data looking straight above the hemisphere, $\theta = 0^{o}$) is of least accuracy. However, since the elevation data is accurate to within $\pm 5^{o}$, the ambiguity in the polar region is less than 0.5 percent of a steradian. A cause for the errors near the polar region ($\theta = 0^{o}$) is imperfections associated with radiation patterns of the antenna.

One will also observe that there is an increase in the error near the horizon (at elevation angles of $\pm 90^{o}$). This error is caused because of the inaccuracy in the positioning of the antenna system with respect to the illuminating antenna. The cause for the error in the elevation data is due to the non-symmetry in the location of antennas in the θ plane of the antenna system, i.e, antenna elements are only employed in the upper hemisphere of a spherical surface. Therefore, since the data employed to calculate the elevation angle are from a non-symmetrical system, the errors noted above are expected as noted in 3.2.1.

For the purposes of comparison the theoretically computed elevation angle versus the actual elevation angle assuming a cosine antenna pattern for the individual elements is shown in Fig. 3-18. Referring to Fig. 3-18,

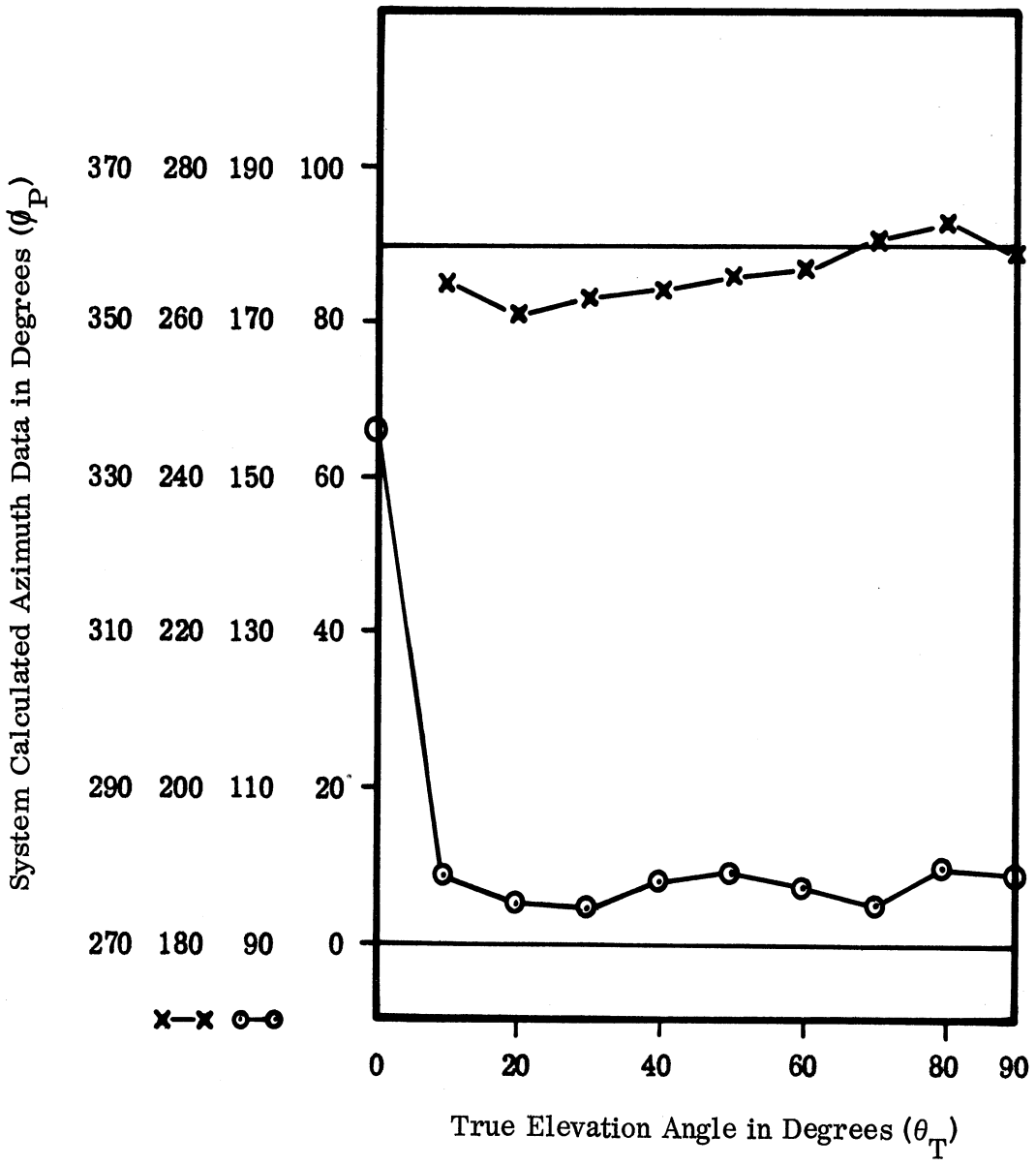

FIG. 3-17: AZIMUTH ANGLE AS GENERATED BY THE DF SYSTEM AS A FUNCTION OF THE TRUE ELEVATION ANGLE FOR $\phi = 90^o$ ⊙—⊙ AND $\phi = 270^o$ ✕—✕ .

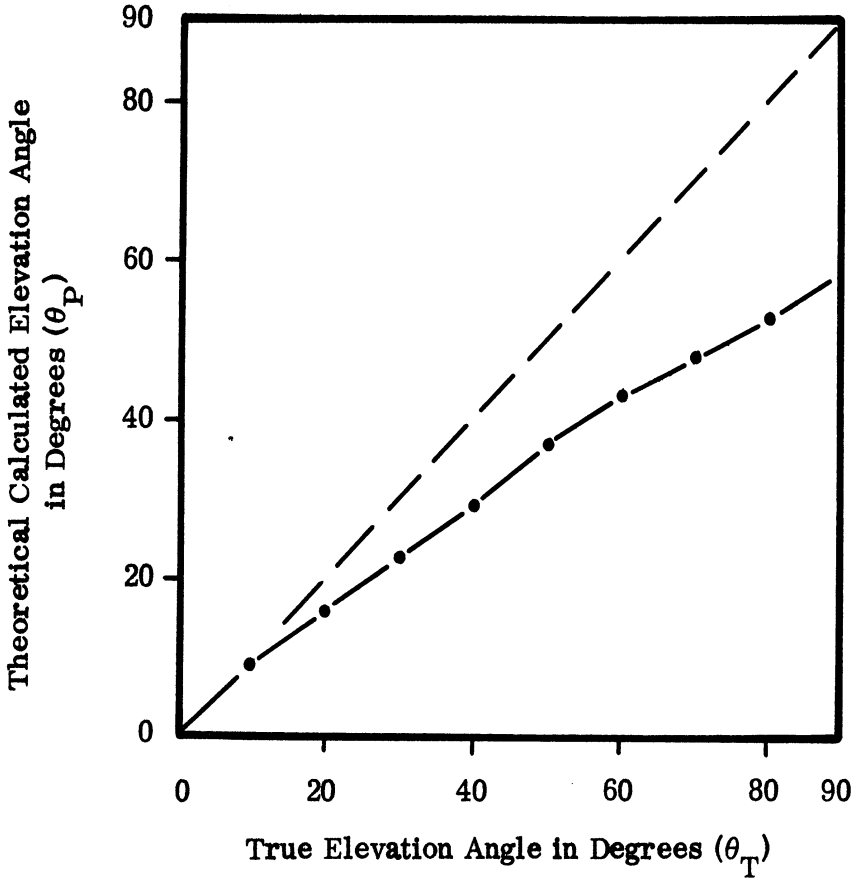

FIG. 3-18: THEORETICAL CALCULATED ELEVATION ANGLE versus TRUE ELEVATION ANGLE (Assuming a Cosine Element Pattern with Elements Placed at $\theta = 40^{\circ}$ and 80°).

it is to be noted that the data varies in a piecewise linear fashion such that the correction factor to be inserted in the computer is relatively simple. Referring now to the elevation data in Figs. 3-19 through 3-22, it will be observed that the system generated data agrees well with the theoretical data of Fig. 3-18.

To gain some insight as to the performance of the A-EDF system as a function of frequency, the orientation of the illuminating antenna was held fixed (with respect to the azimuth - elevation system) and the data of Fig. 3-23 and 3-24 was collected. The cause for the errors apparent in Figs. 3-23 and 3-24 are related to the symmetry associated with the antenna element patterns both as a function of frequency and orientation.

The above data has been collected employing a CW source. In addition, tests have been made employing pulse data. In these tests a pulse width of approximately 4 microseconds duration and a repetition rate of 1000 pulses per second was used. This data agreed well with the CW data presented above.

3.3.2 Fly-By Test Results

The fly-by series of tests were designed to evaluate the effect of ground reflections on the A-EDF system performance under dynamic environmental conditions. To conduct these tests, the A-EDF system was installed at the University of Michigan's NIKE-AJAX radar site. A photograph of the radar site and sketch of the A-EDF system installation appear in Figs. 3-25 and 3-26 respectively.

A 1.6 KHz CW source was installed in a DC-3 aircraft, and the aircraft tracked simultaneously by the A-EDF system and the NIKE-AJAX radar. The aircraft maneuvered in a random fashion around the vicinity of the test site at an altitude of approximately 10,000 feet and ranges from two to ten miles. The NIKE-AJAX radar coordinates were correlated with the A-EDF system by the use of a data multiplex switch which read the radar coordinates into the A-EDF system computer. This data was then printed out on the A-EDF system teletype. The data multiplex switch and voltage scaling networks are described in the Appendix.

The results of the fly-by tests appear in Table 3-4. For the 60 data samples collected, the average azimuth error and standard deviations were respectively 1.55 and 5.9^{o}. If the error distribution were normal (Gaussian), the average error would be zero. Assuming the distribution is normal, one would expect the error on 68 per cent of the data points to lie within the standard deviation. Of the data collected, 77 per cent of the points were within $\pm 6^{o}$, suggesting that the assumption of a Gaussian distribution is acceptable and

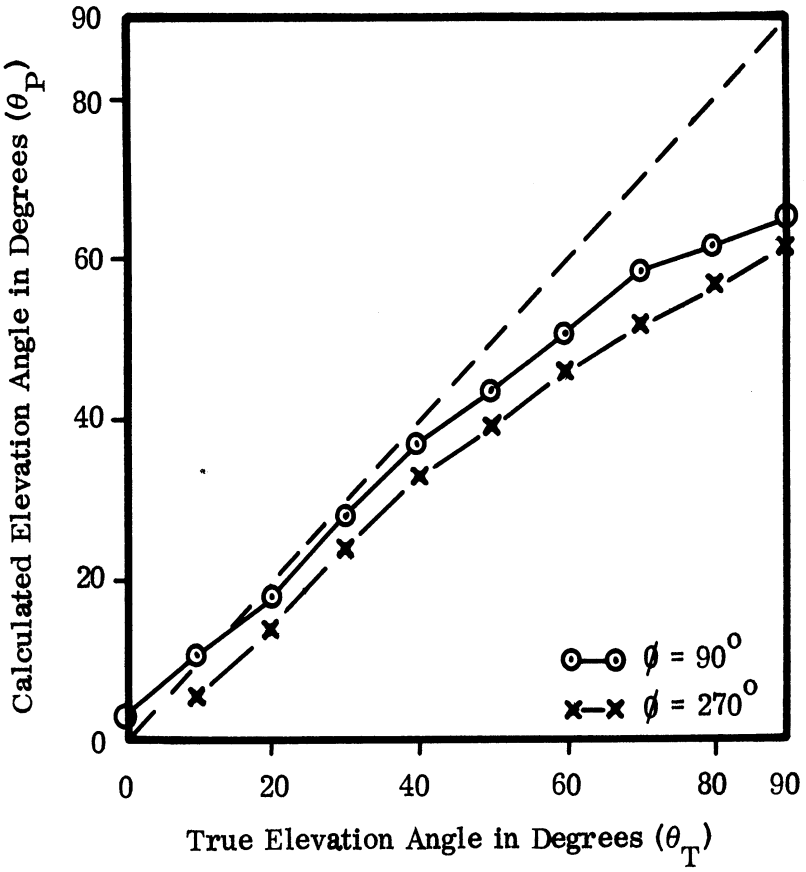

FIG. 3-19: SYSTEM GENERATED ELEVATION ANGLE versus TRUE ELEVATION ANGLE (Frequency = 1.6 GHz).

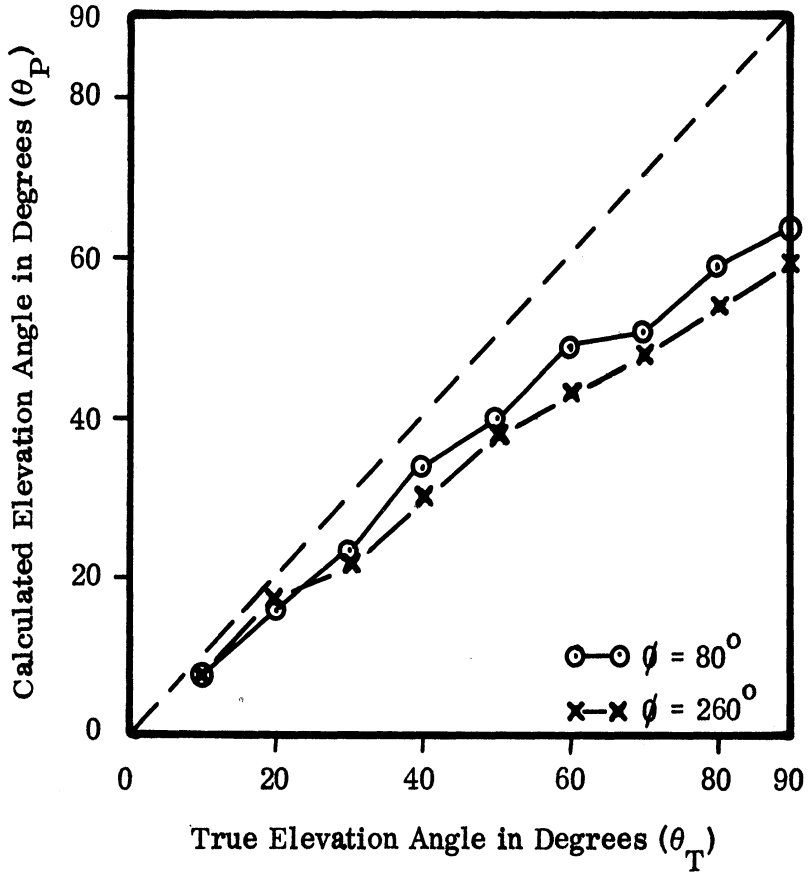

FIG. 3-20: SYSTEM GENERATED ELEVATION ANGLE versus TRUE ELEVATION ANGLE (Frequency = 1.6 GHz).

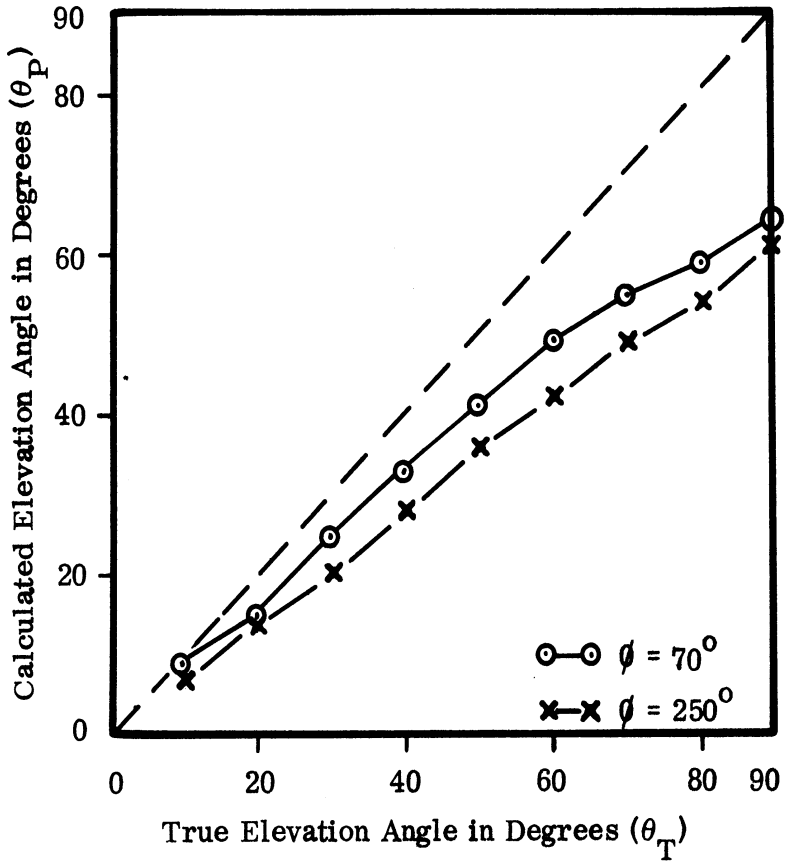

FIG. 3-21: SYSTEM GENERATED ELEVATION ANGLE versus TRUE ELEVATION ANGLE (Frequency = 1.6 GHz).

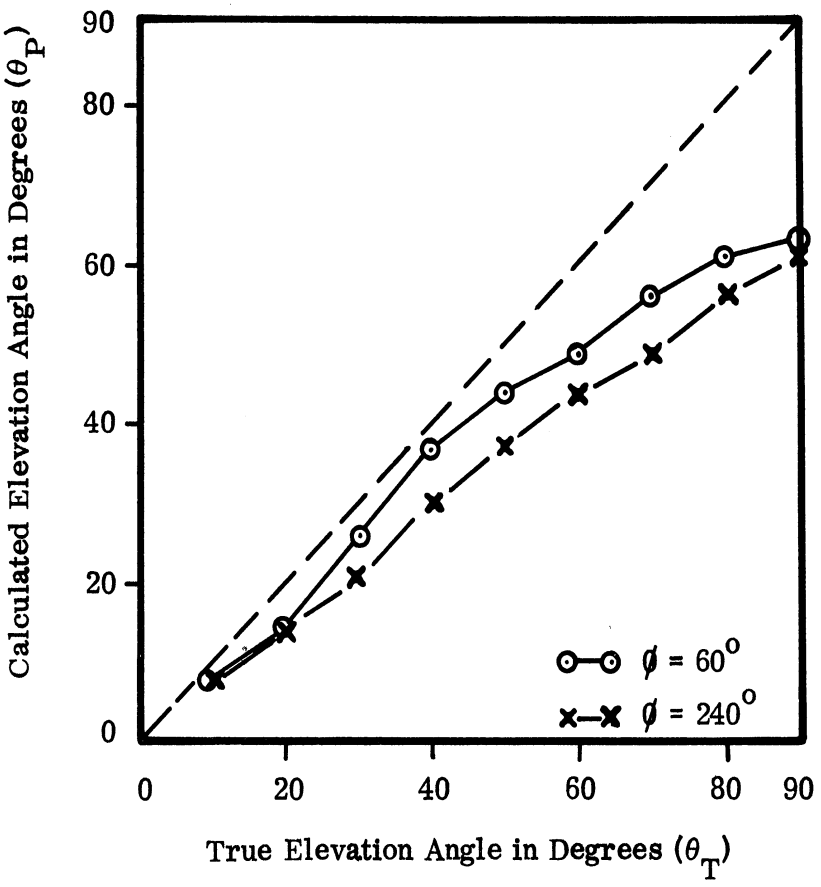

FIG. 3-22: SYSTEM GENERATED ELEVATION ANGLE versus TRUE ELEVATION ANGLE (Frequency = 1.6 GHz).

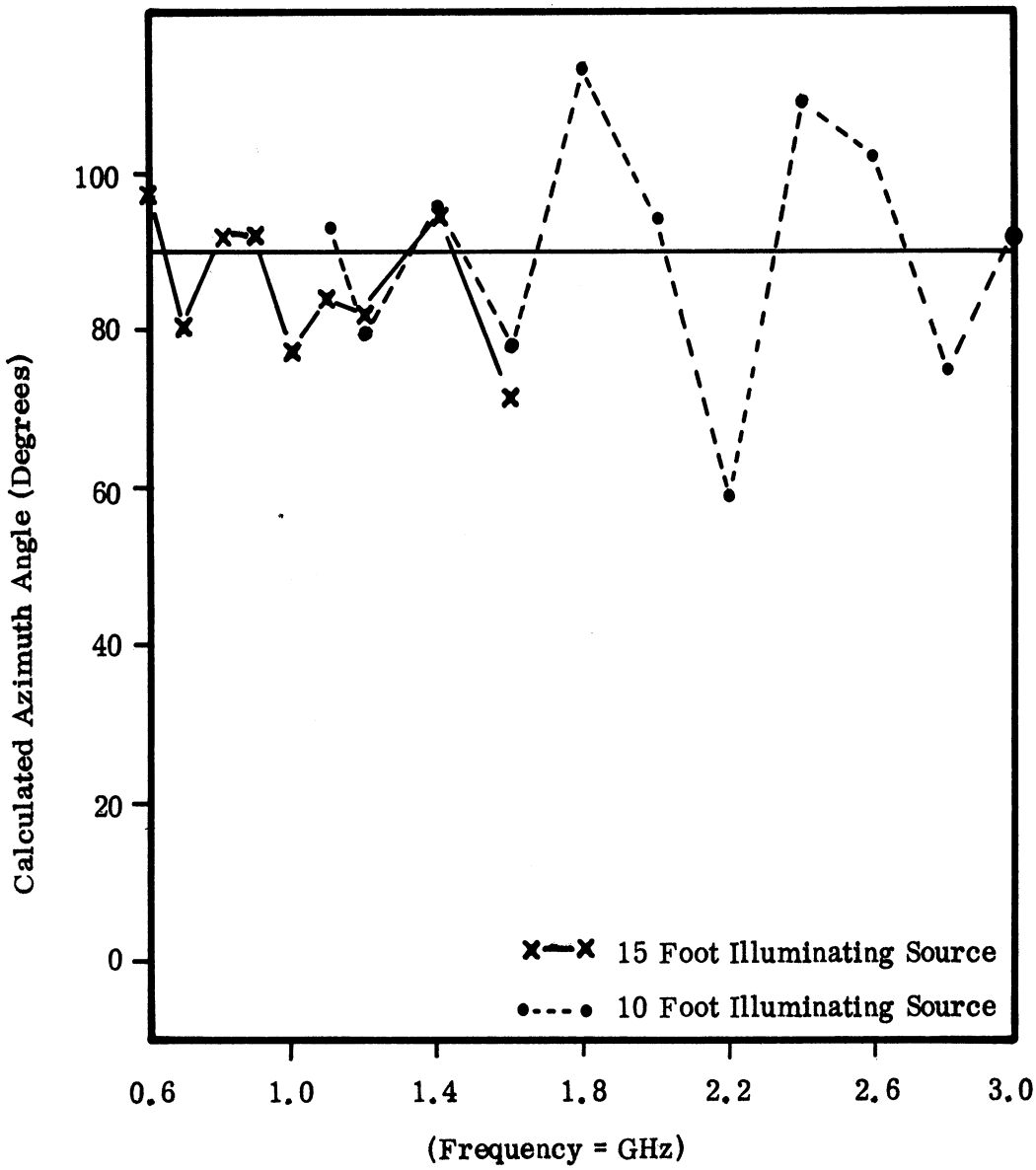

FIG. 3-23: SYSTEM GENERATED AZIMUTH ANGLE versus FREQUENCY FOR A FIXED AZIMUTH AND ELEVATION OF ILLUMINATING SOURCE ($\theta = 90^{o}$, $\phi = 30^{o}$).

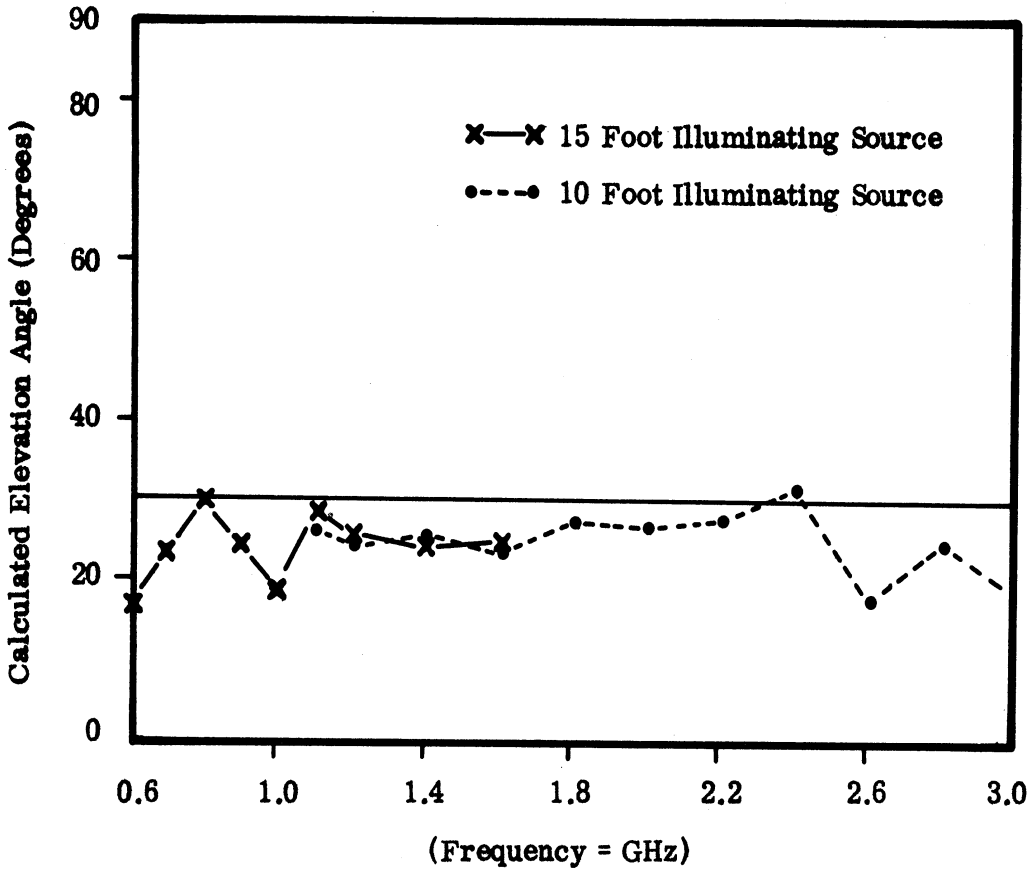

FIG. 3-24: SYSTEM GENERATED ELEVATION ANGLE versus FREQUENCY FOR A FIXED AZIMUTH AND ELEVATION OF ILLUMINATING SOURCE ($\theta = 90^{o}$, $\phi = 30^{o}$).

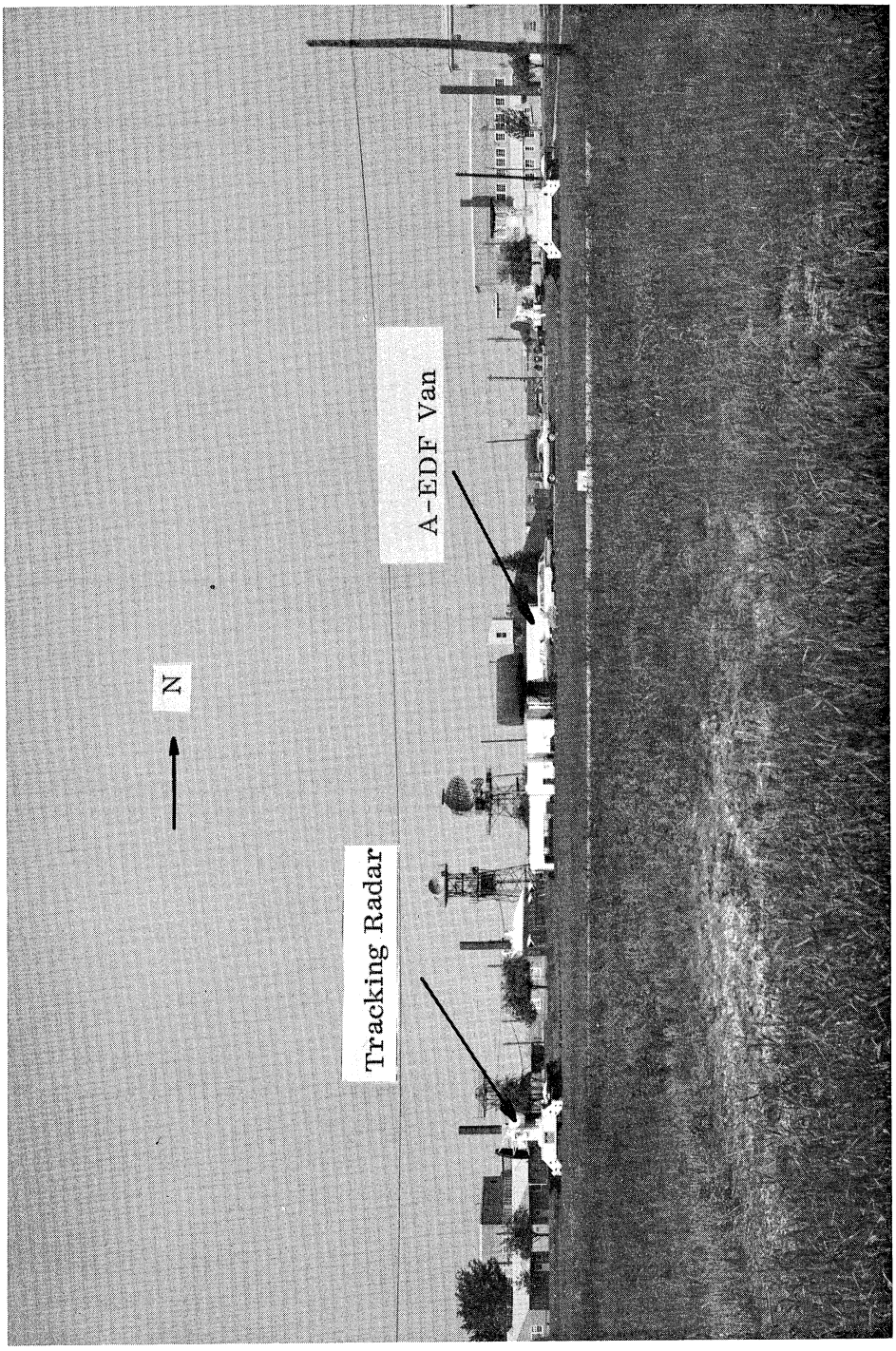

FIG. 3-25: NIKE AJAX TEST SITE.

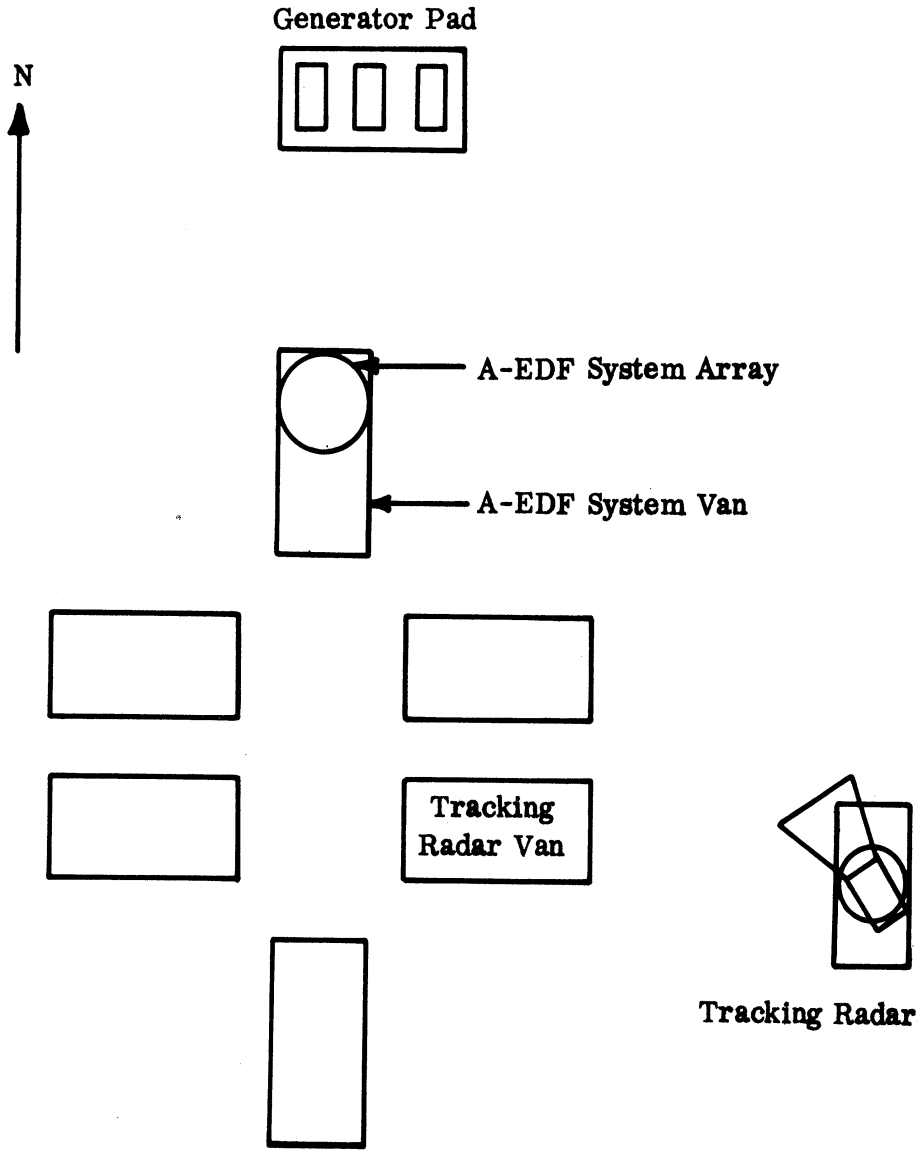

FIG. 3-26: SKETCH OF A-EDF SYSTEM NIKE RADAR SITE DURING FLY-BY TESTS (not to scale).

TABLE 3-4 (a)

Results of Fly-By Tests

Sample	A-EDF	Radar	Δ^{o}_{A}	A-EDF	Radar	Δ^{o}_{E}
	Azimuth (degrees)			Elevation (degrees)		
1	204	208	-4	51	65	-14
2	269	267	+2	21	31	-10
3	172	173	-1	69	61	+8
4	32	40	-6	30	21	+9
5	173	172	+1	54	61	-7
6	289	287	+2	40	44	-4
7	164	159	+5	40	29	+11
8	195	195	0	57	64	-7
9	274	282	-8	46	61	-15
10	307	316	-9	36	37	-1
11	198	201	-3	59	58	+1
12	329	319	+10	31	30	+1
13	331	325	+6	42	38	+4
14	16	10	+6	42	30	+12
15	12	8	+4	42	27	+15
16	18	23	-5	15	17	-2
17	50	46	+4	22	11	+11
18	276	278	-2	25	24	+1
19	285	284	+1	18	23	-5
20	353	347	+6	28	30	-2
21	16	7	+9	40	29	+11
22	14	7	+7	33	34	-1
23	218	228	-10	33	31	+2
24	318	329	-11	40	38	+2
25	338	331	+7	49	50	-1
26	325	329	-2	40	49	-9
27	352	349	+3	52	65	-13
28	352	351	+1	57	63	-6
29	41	35	-6	54	66	-8
30	43	38	+5	62	66	-4

continued

TABLE 3-4 (a)

Results of Fly-By Tests

Sample	A-EDF	Radar	Δ^{o}_{A}	A-EDF	Radar	Δ^{o}_{E}
	Azimuth (degrees)			Elevation (degrees)		
31	58	60	-2	55	56	-1
32	71	65	+6	54	58	+4
33	75	72	+3	62	58	+4
34	106	107	-1	62	58	+4
35	144	144	0	64	68	-4
36	198	188	+10	55	54	+1
37	266	266	0	21	26	-5
38	344	335	+9	15	19	-4
39	67	68	-1	1	2	-1
40	151	141	+10	7	8	-1
41	200	191	+9	31	33	-2
42	5	16	-11	34	24	+10
43	84	77	+7	51	36	+15
44	154	154	0	43	44	-1
45	14	17	-3	39	24	+15
46	25	22	+3	43	30	+13
47	15	10	+5	45	49	-4
48	14	23	-9	37	30	+7
49	322	317	+5	18	10	+8
50	317	310	+7	19	23	-4
51	325	315	+10	31	31	0
52	333	325	+8	36	37	-1
53	331	327	+4	36	40	-4
54	325	331	-6	40	43	-3
55	7	11	-4	52	61	-9
56	35	31	+4	31	17	+15
57	176	175	+1	60	59	+1
58	183	181	+2	69	63	+6
59	194	197	-3	66	71	-5
60	196	197	-1	71	72	-1

TABLE 3-4 (b)

Summary of Statistical Results

Average Azimuth Error

$$\overline{\Delta}_A = \frac{\sum_{n=1}^{N} \Delta A_n}{N} = +1.55^o$$

Azimuth Standard Deviation

$$\sigma_A = \left[\frac{\sum_{n=1}^{N} \left(\Delta A_n\right)^2}{N-1} \right]^{1/2} = 5.9^o$$

Average Elevation Error

$$\overline{\Delta}_E = \frac{\sum_{n=1}^{N} \Delta E_n}{N} = +.53^o$$

Elevation Standard Deviation

$$\sigma_E = \left[\frac{\sum_{n=1}^{N} \left(\Delta E_n\right)^2}{N-1} \right]^{1/2} = 7.5^o$$

conservative. The average elevation error and standard deviations were respectively 0.53^{o} and 7.5^{o}. Seventy-two percent of the elevation data points collected had an error of less or equal to 8^{o}. The error distribution is slightly skewed from the normal, but conforms well to the results predicted by assuming a normal distribution. It should also be noted that the radar data presented in Table 3-4 has associated with it a random uncertainty of $\pm 1^{o}$ due to the processing of the data through the multiplexer and scaling amplifier.

Referring to Figs. 3-25 and 3-26 one can easily see that the possibility of multiple signal paths is high. An example is diagrammed in Fig. 3-27. Due to the irregular nature of the positions and geometries of the reflecting objects and the irregular flight paths of the aircraft, little correlation exists between a specific azimuth or elevation angle and the error experienced at that angle. It is highly improbable that the contribution of the reflections to the A-EDF system output can be quantiatively evaluated from these tests.

A second known source of uncertainty is the low signal to noise ratio of the signals received during these tests. Knowing the output power of the airborne source, the transmitting and receiving antenna gains, and the signal path attenuation, one can calculate the magnitude of the received signal. With the aid of the path length versus attenuation graph in Fig. 3-28, the computations indicated above are performed in Table 3-5. The results of the computations, which are graphed in Fig. 3-29, indicate that for a range of two miles, the signal power into the receiver is a maximum of -65dBm. Previous experience with the A-EDF system has indicated that a minimum signal power of -70dBm into the receiver (Micro-Tel) is necessary for a 6dB signal to noise ratio into the memory voltmeter, which is the very minimum signal to noise ratio for meaningful system operation. An input signal of -55dBm is the minimum desirable input level. The signals received during these tests were seldom more than the absolute minimum required for system operation, and could at times be observed receding into the noise. It should also be noted that the signal levels in Fig. 3-29 are somewhat optimistic since the airborne antenna was a monopole, vertically polarized with respect to the wings of the aircraft and exhibited somewhat less than 0dB gain at elevation angles near the zenith. As a result of these tests, the computer program has been modified to reject data below a minimum signal to noise ratio selected by the operator.

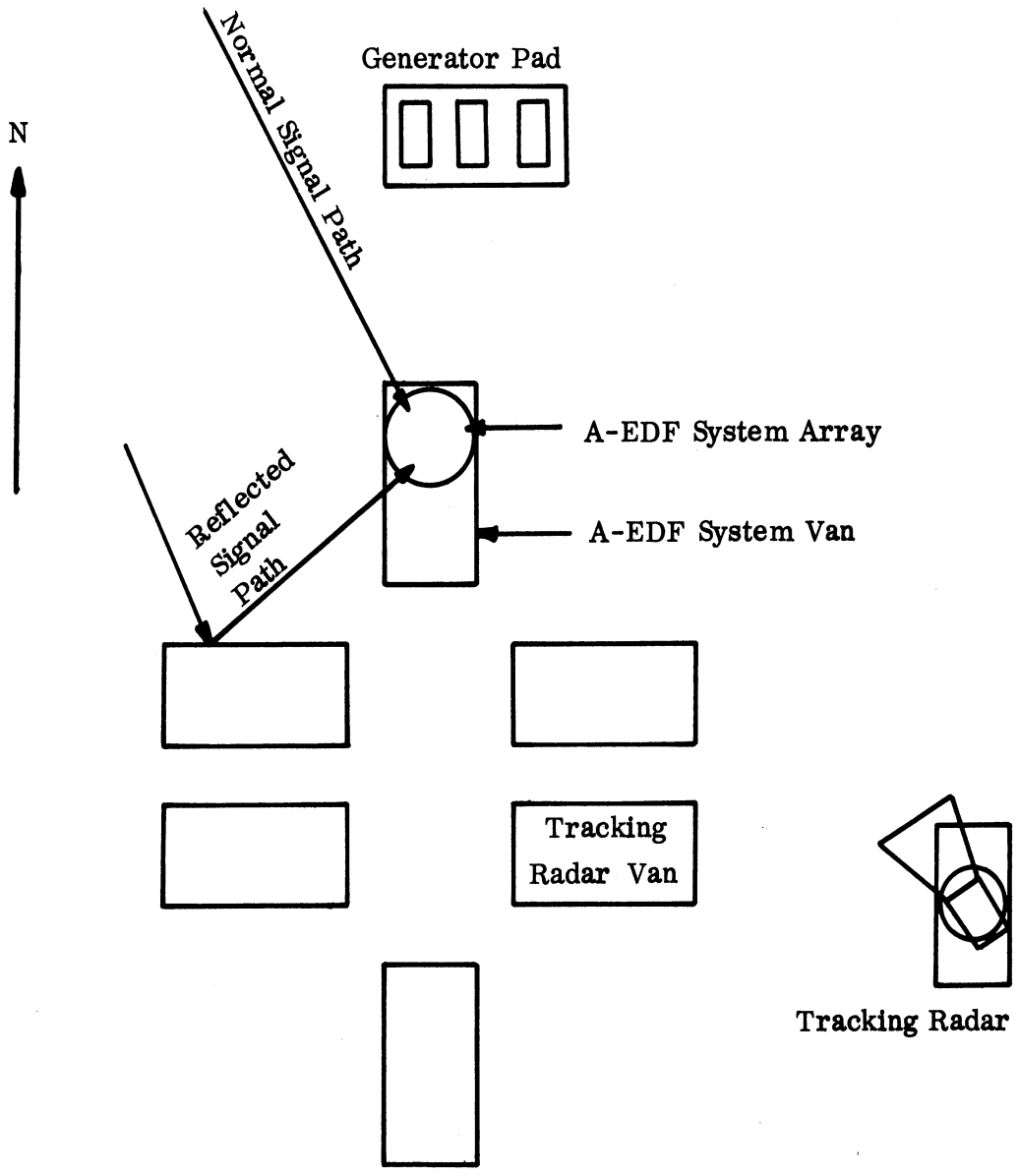

FIG. 3-27: EXAMPLE OF MULTIPLE PATH REFLECTION.

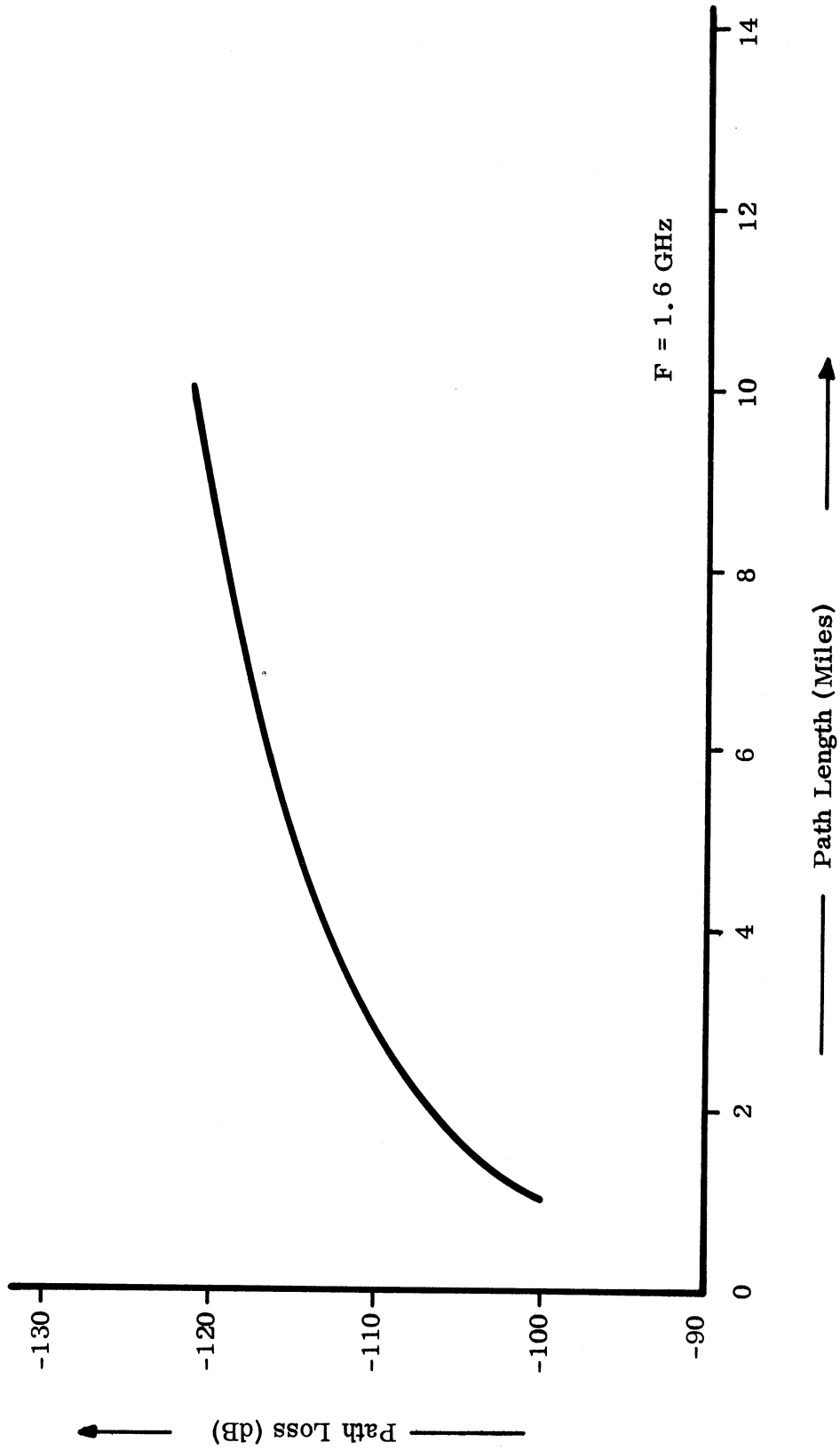

FIG. 3-28: PATH LOSS versus PATH LENGTH.

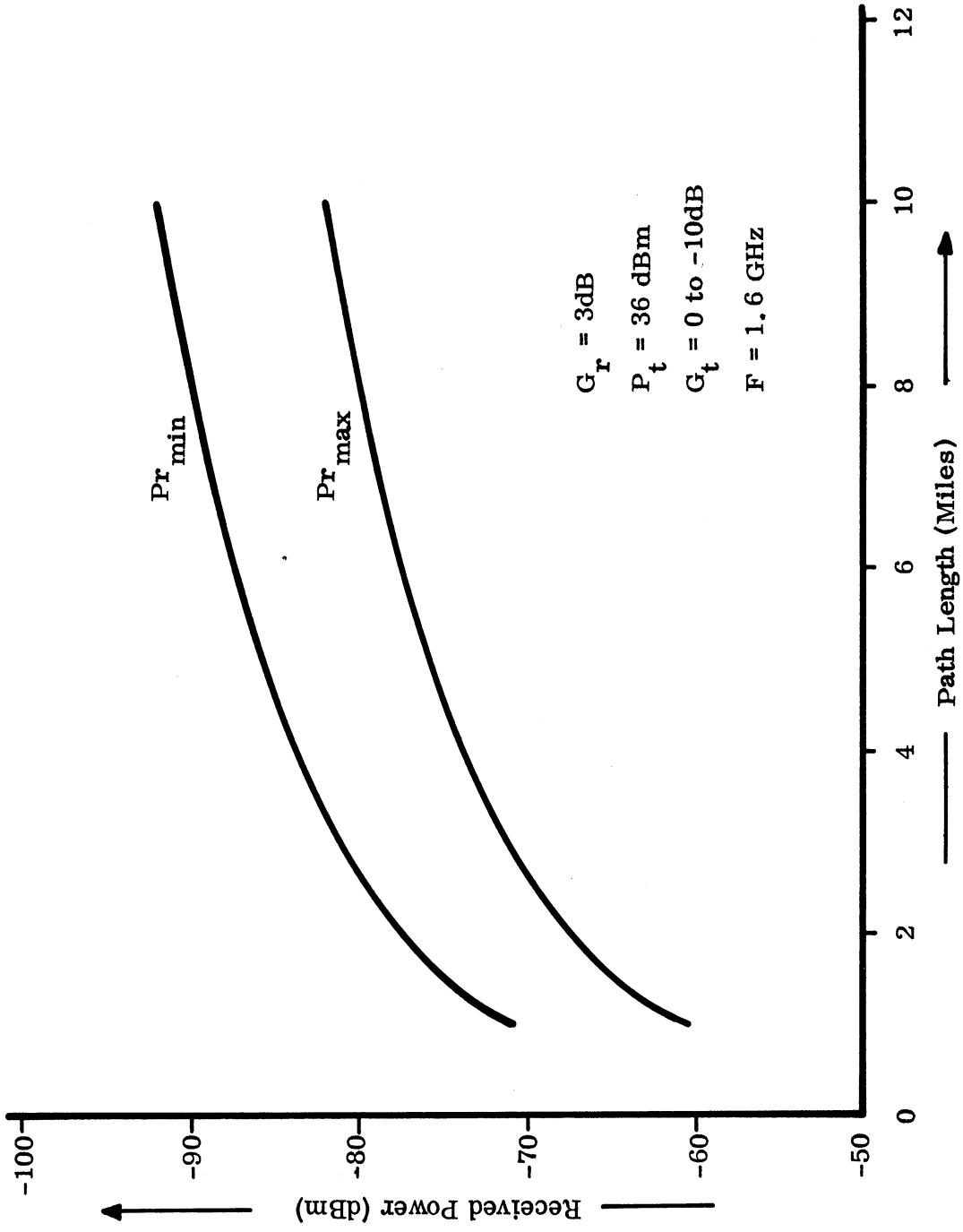

FIG. 3-29: RECEIVED POWER versus PATH LENGTH.

TABLE 3-5

Computations for Received Power

$P_r = P_t + G_t + G_r + N_r$

where

P_r = Received Power (dBm)

P_t = Transmitted Power (dBm) $\cong$ + 36dBm (4 watts)

N_r = Path Loss (dB)

G_r = Receiving Antenna Gain (dB) = +3dB above a linearly polarized isotrope

G_t = Transmitting Antenna Gain (dB) = +0 to -10dB above a linearly polarized isotrope

such that

$P_r = 39\text{dBm} + N_r$.

IV

SYSTEM ERROR ANALYSIS

Previous chapters of this report have described the performance of the A-EDF system. In this chapter we will examine the system to determine the limiting factors that may be associated with the system bearing accuracy. This analysis will indicate those components which require further work for an improvement in system accuracy.

4.1 A-EDF Errors

The limitations on the determination of any physical phenomena are the degree with which the phenomena can be described in terms of measurable quantities and the precision with which the necessary measurements can be made. In this instance, the energy distribution that should appear across the A-EDF system array from a far-field source in a free space environment can be accurately predicted from electromagnetic theory. However, there are limitations to the precision with which the amplitude distribution over the hemispherical surface can be measured. The following investigation will assume that the amplitude distribution can be predicted to any desired degree of precision and concentrate on the system performance degradation due to measurement inaccuracies. The justification for the previous assumption is that an approximate free space environment can be obtained by employing a carefully designed antenna range as in the first set of system measurements described in the preceding chapter.

This investigation has been performed by synthesizing a mathematical model of the system components (e.g., receiver, amplifier, etc). This model has also been used to predict the precision with which the free space amplitude distribution is represented at the computer input terminals.

A real receiver's output can be closely approximated by an ideal receiver in series with a noise voltage source. Since this model is to be used for predicting the rms signal variation into the computer, the deviations in receiver linearity will be included as system noise, although, strictly speaking, it is not. Similarly, the broadband amplifier and memory voltmeter are modeled as ideal elements with equivalent noise voltage sources.

The entire system including equivalent noise sources is diagrammed in Fig. 4-1. Linearity specifications are normally written by specifying the maximum deviation over the entire operating range while equipment noise is specified in rms volts. To make these two specifications compatible for this

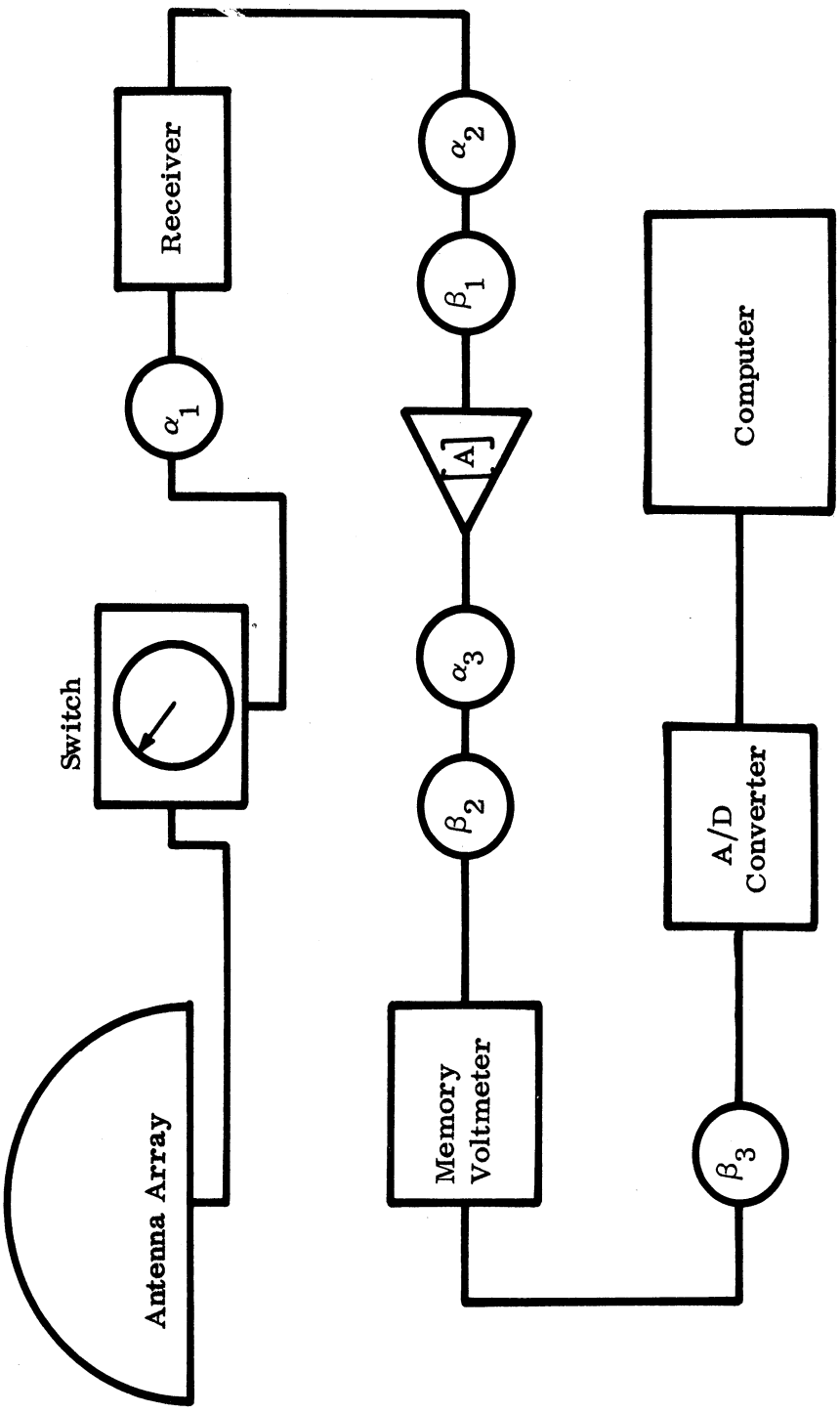

FIG. 4-1: SYSTEM DIAGRAM INCLUDING NOISE SOURCES.

analysis, the linearity deviations are assumed to exhibit a Gaussian distribution about the truly linear behavior, and the maximum deviation is chosen as twice the standard deviation. The rms variation is then set equal to the standard deviation (Beers, 1957). While this method of converting may seem somewhat arbitrary, it does simplify the error analysis and provides a first order approximation to the system performance. The generators labeled α represent gain variations (i.e., linearity) and are controlled sources, while the β generators are constant noise voltages.

S_o is the noiseless input level required by the amplifier to produce a 10v output assuming the amplifier is a noiselss device, i.e, it generates no noise. When a signal is incident on the antennas, the output to the A/D converter may be expressed as

$$V_{A/D} = A\left\{\eta S_o (1 \pm \alpha_1)(1 \pm \alpha_2) + \beta_1\right\}(1 \pm \alpha_3) \pm \beta_2 \pm \beta_3 \qquad (4.1)$$

where $\eta = \frac{S}{S_o}$, $0 \leq \eta \leq 1$ is that fraction of the maximum useable signal which is actually present.

Representative error values for the equipment used in the A-EDF system are given in Table 4-1. Substituting these values into (4.1),

$$V_{A/D} \cong 10\,\eta\, S_o (1 \pm .2) \pm .403 \quad (A = 20dB) \qquad (4.2)$$

$$V_{A/D} \cong 100\,\eta\, S_o (1 \pm .2) \pm 1.65 \quad (A = 40dB) \qquad (4.3)$$

Notice from (4.2) and (4.3) that in each case there is a minimum error of 20 percent due to equipment non-linearities. Of this 20 percent, 16 percent is produced by the antennas and switch. That is, the largest contribution to the system non-linearity is the sum of the α_1, α_2, and α_3 terms. Of this sum, the contribution from the antenna and switch alone is 1.5dB or 0.16 v/v out of a total of 0.20 v/v. A second error contribution that becomes large as the input signal diminishes is random noise. Two major noise sources are: 1) receiver noise, which is amplified by the video amplifier and becomes the limiting factor at low signal levels, and 2) memory voltmeter which contributes over one-third of the total noise when the video amplifier is adjusted for 20dB gain. The error predicted by (4.2) and (4.3) is plotted in Fig. 4-2, for video

TABLE 4-1

Equipment Noise Performance

Equipment	Manufacturers Specification	Equivalent Noise
Antennas and Switch		α_1 = 1.5dB*
Receiver	± .25dB Linearity	α_2 = .1dB*
	4dB NF at 75 MHz	β_1 = 25 mv
Amplifier	± .5dB Linearity	α_3 = .25dB
	2.5 mv Noise (20dB gain)	β_2 = 2.5 mv (20dB gain)
	4.0 mv Noise (40dB gain)	β_2 = 4.0 mv (40dB gain)
Voltmeter	± 3 percent full scale	β_3 = 150 mv
A/D Converter	.015 percent full scale	Ideal
Computer		Ideal

* Based on test results.

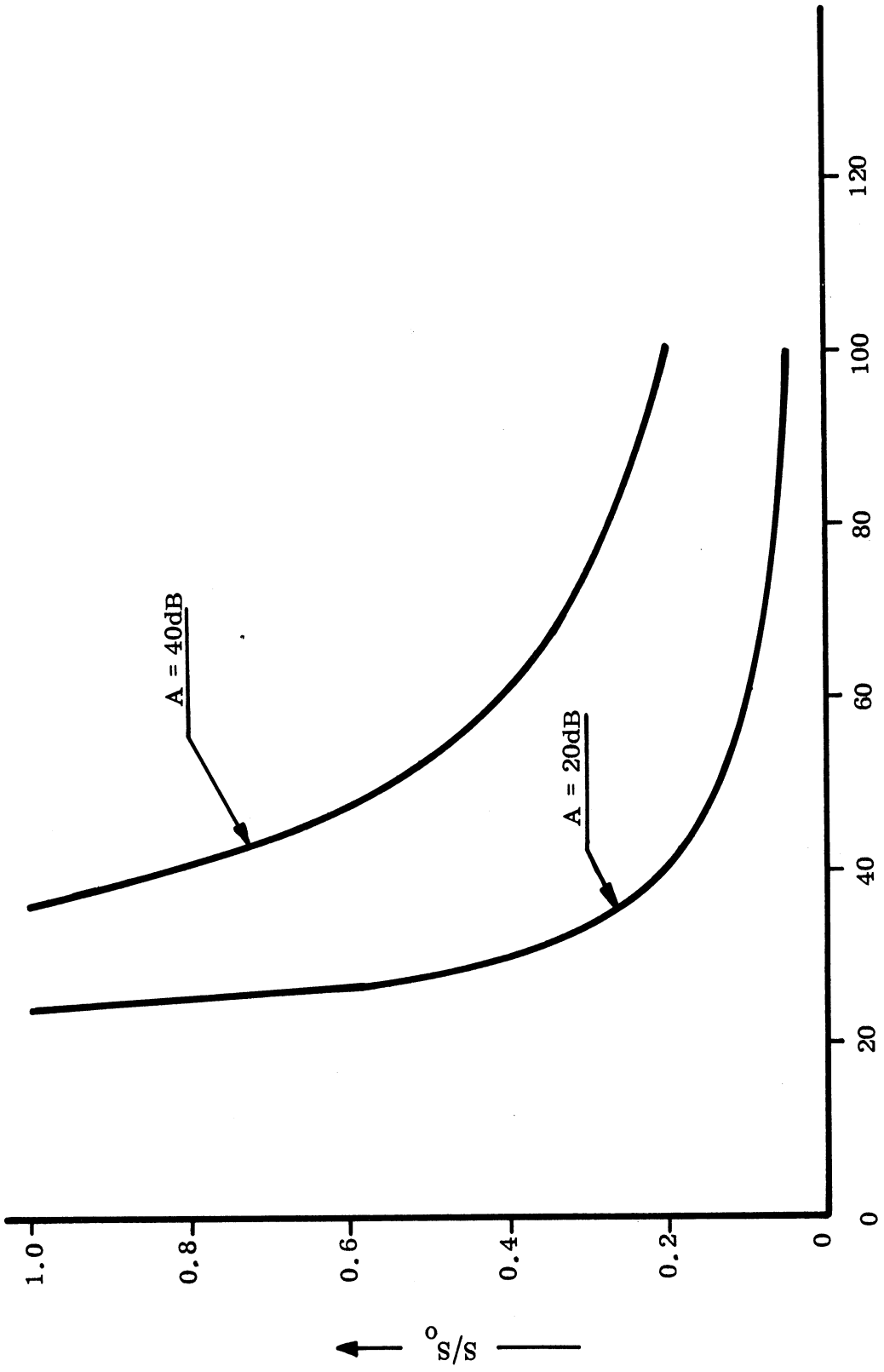

FIG. 4-2: CALCULATED SYSTEM rms ERROR.

amplifier gains of 20dB and 40dB. The ordinate, S/S_0, is the fraction of the maximum useable voltage that is present at the amplifier input terminals. The abscissa is the ratio of the rms deviation to the nominal signal level. Thus the actual deviation at any one instant in time will be within the rms deviation predicted approximately 70 percent of the time.

We have also attempted to relate the rms signal deviation at the computer input to the variations in bearing angle predicted by the computer. The computations performed by the computer are not simple. S/S_0 will in general differ for each antenna and bearing determination. Also, the illumination distribution is a unique function of the bearing angle, suggesting that for a given maximum S/S_0 the error will be different for different bearing angles.

To obtain an estimate for the magnitudes of the deviations that can be expected, a computer program was written to generate the exact voltages that would be obtained from each antenna for a given bearing angle. These voltages were then allowed to vary up to 10 percent from the calculated values, and a new bearing angle, which included the effect of the variations, was calculated. Figure 4-3 shows the maximum azimuthal variations encountered for five azimuthal samples at elevation angles of 30^o and 60^o respectively. The maximum elevation variations for the full azimuth coverage are also indicated. For the 100 points calculated, only 3 have a deviation exceeding 3^o from the nominal value. It is well to note that the maximum elevation deviation is less than 2^o. These data suggest that the accuracy of the system can be substantially improved if the computer input voltage variations can be more rigidly constrained. Voltage variations of less than 10 percent necessarily require that the antenna element gains be matched to within 1dB. It is recognized that the $\pm$ 10 percent voltage variations allowed in this analysis may not be realistic for the antennas at low illumination levels. However, if one antenna is receiving sufficient energy the low signal antennas will contribute little to the bearing determination and greater deviations can be tolerated without adversely affecting the bearing error.

4.2 System Specifications

There are a variety of methods for describing the bearing accuracy of an A-EDF system. One approach (the description given in the specifications section of this contract) is to specify that the calculated bearing be accurate to $\pm \phi'$ degrees in azimuth and $\pm \theta'$ degrees in elevation. For the purposes of this study ϕ' degrees is $\pm 2^o$ and $\theta' \pm 5^o$.

The ϕ' and θ' values may also be used to provide a measure of system resolution. System-resolution is defined as the precision with which an RF source may be located within the confines of a hemisphere (2π steradians).

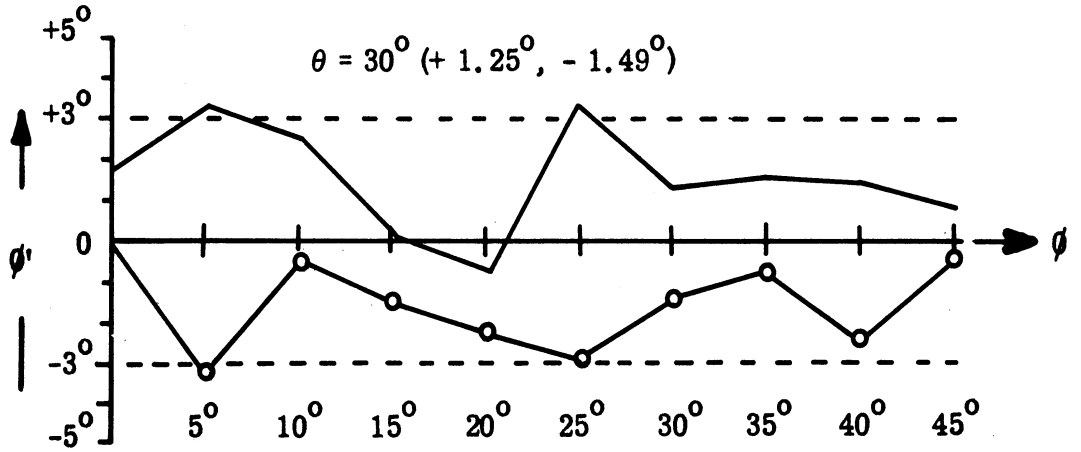

FIG. 4-3: RESULTS OF ERROR ANALYSIS FOR $V_{in} = V_{in} \pm 10$ percent at $\theta = 30^{\circ}$, 60°.

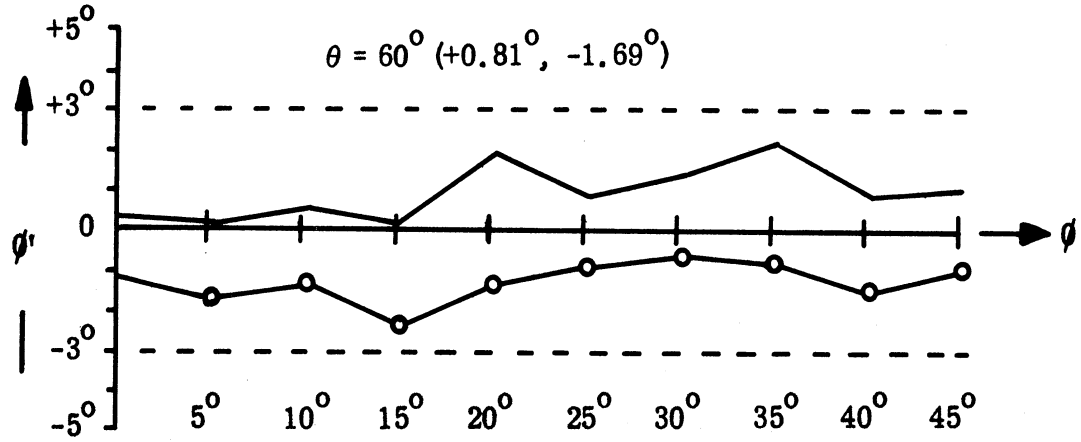

We will further define system-resolution in percentile as

$$\Delta \text{ percent} = 100 \frac{\psi'}{2\pi}$$

where ψ' = solid angle of uncertainty

or $$\psi' = \int_{\theta_1}^{\theta_2} \int_{\phi_1}^{\phi_2} \text{Sin } \theta \, d\theta \, d\phi$$

where $$\theta_2 - \theta_1 = 2 \left|\theta'\right|, \quad \phi_2 - \phi_1 = 2 \left|\phi'\right|$$

Employing this definition it can be shown that the A-EDF system resolution is poorest (Δ' = 0.2 percent) at the horizon ($\theta = 90^{\circ}$) and best (Δ' = .01 percent) at the zenith ($\theta = 0^{\circ}$). Therefore, it is apparent that the system-resolution varies as a function of elevation angle. A plot of the variation, for the A-EDF system is shown in Fig. 4-4. From the system-error analysis discussed above it may be concluded that a variable system-resolution may be unrealistic and in place of it a constant system-resolution would be more desirable.

A system-resolution of 0.2 percent appears to be within the present state-of-the-art of the equipment used in the A-EDF system. Assuming a system-resolution (Δ') of 0.2 percent and a constant elevation ambiguity (θ') of $\pm 5^{\circ}$, the azimuth ambiguity as a function of elevation angle is shown in Fig. 4-5. It is to be noted that maintaining a constant system-resolution is equivalent to ensuring that the solid angle ψ' of ambiguity associated with the A-EDF system also remains constant as is the case for precision gun laying radars.

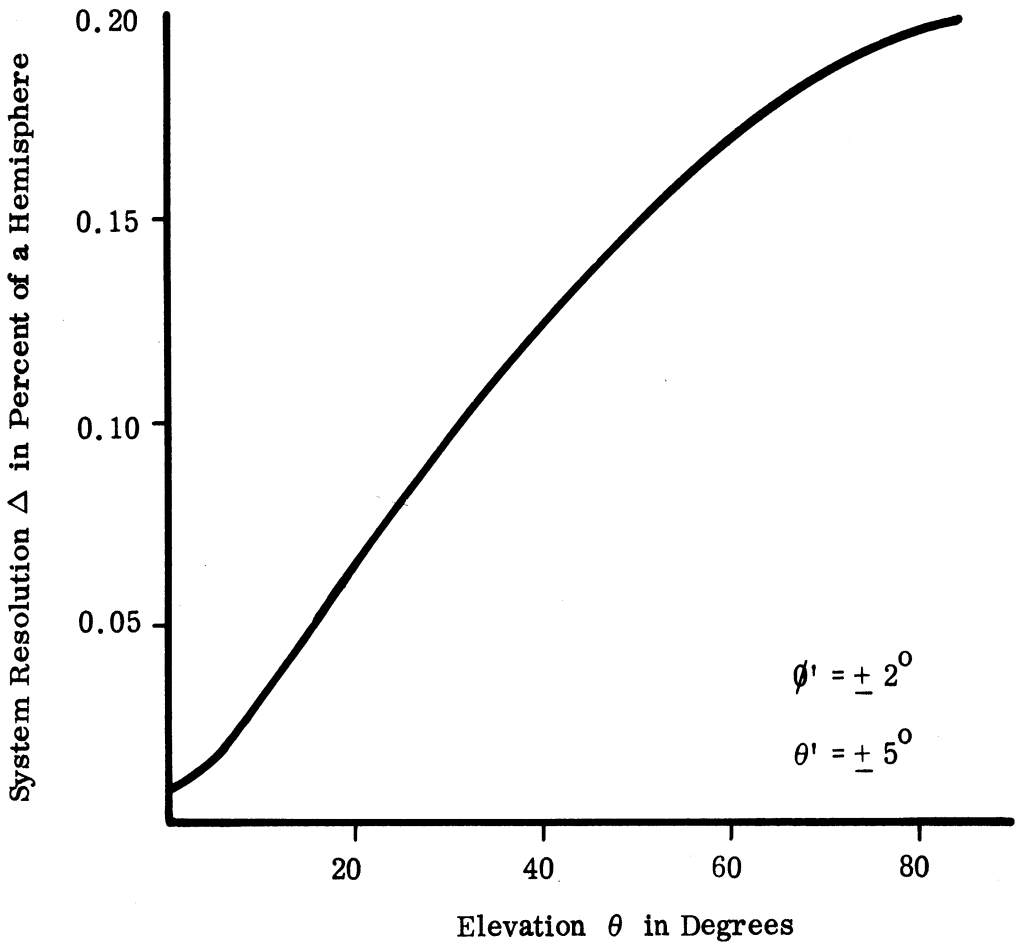

FIG. 4-4: SYSTEM RESOLUTION AS A FUNCTION OF ELEVATION ANGLE.

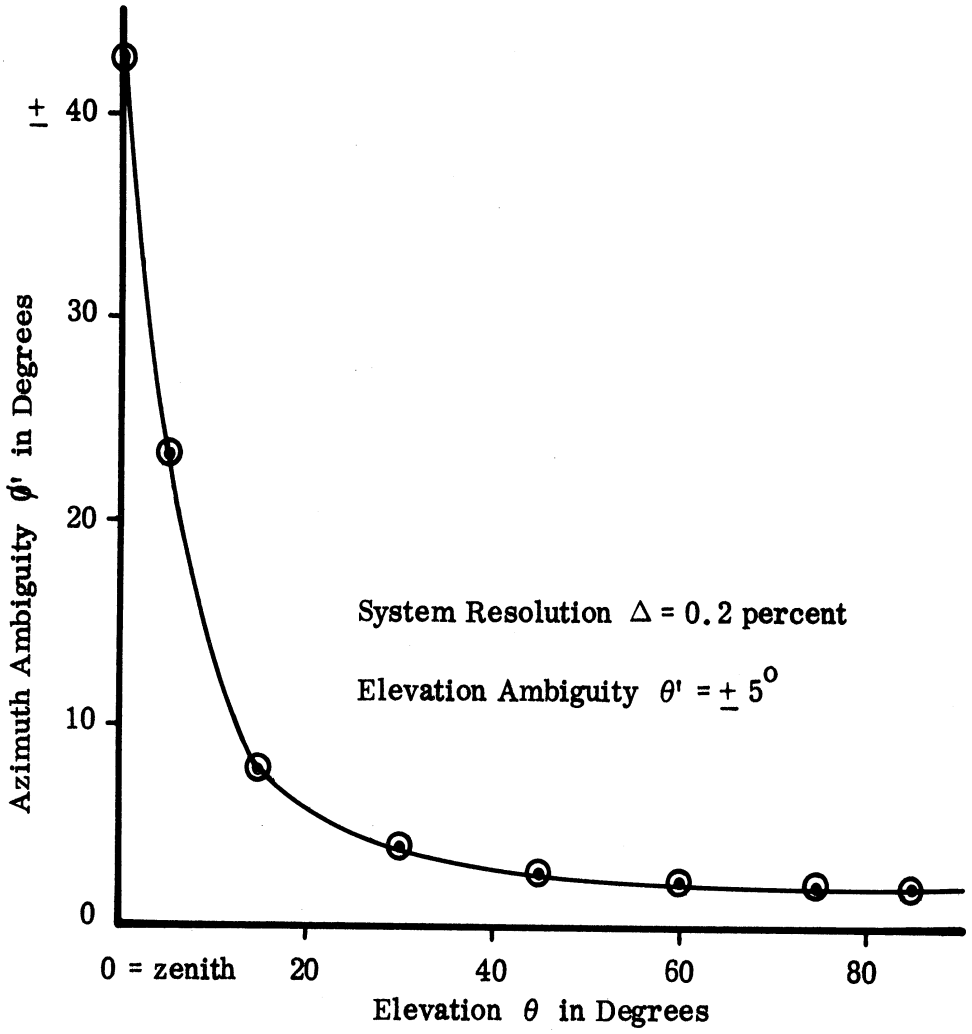

FIG. 4-5: AZIMUTH AMBIGUITY versus ELEVATION ANGLE.

V

CONCLUSIONS AND RECOMMENDATIONS

The Azimuth and Elevation Direction Finding system constructed as part of the present study demonstrates successfully the feasibility of employing the vector summation process for azimuth and elevation direction finding. Although the data presented in Chapter III does not exhibit the accuracy specified in the contract, the error analysis in Chapter IV and the results obtained from the free space measurements shows that the system has the capability of meeting the specifications. Improved performance will require improved components, e.g., the antenna elements and the memory voltmeter.

The fabrication of the quadrafilar balun network was completed and the phase data was not as well controlled as desired. However, it is felt that with some additional effort, the balun may be optimized to operate in accordance with the design criteria. It is recommended that this effort (optimization of the balun network) be continued, so as to obtain the proper amplitude and phase characteristics required for the quadrafilar spiral.

As noted in Chapter II, some preliminary radiation patterns recorded for the quadrafilar spiral were unsatisfactory. The cause for the poor pattern characteristics is the improper phase distribution associated with the balun, and the wrap angle of the spiral and perhaps irregularities in the winding of the spiral elements. The present quadrafilar spiral was hand-made and errors undoubtedly exist because of the manner in which the elements were wound. Therefore, it is recommended that the study of the quadrafilar spiral configuration be continued so as to also optimize the element design, thus enhancing accuracy of the direction finder system. As a part of the optimization of the elements, consideration should be given to the cone angle and material, element conductor and wrap angles. Although several investigators are working with the multifilar spiral configuration, no satisfactory antennas are available commercially at this time.

Future studies associated with the vector summation technique should give consideration to the following areas: 1) frequency bandwidth, 2) antenna elements, 3) high-gain antenna elements, and 4) memory voltmeter replacement.

In future systems the bandwidth requirement must be carefully evaluated. It is questionable whether or not it is feasible to construct an operational system for field use covering a bandwidth of 5:1 similar to that attempted with the exploratory model. The chief difficulty in designing for such a wide bandwidth is the employment of antenna elements that satisfy the criteria of uniform radiation patterns as a function of frequency and antenna orientation. During this program a study was conducted to determine the feasibility of constructing a quadrafilar spiral which might better fit the needs of the A-EDF system. This

proved to be a difficult problem because of the tight tolerance involved in the construction of the quadrafilar balun and antenna elements. For the immediate future, it is felt that azimuth-elevation systems should be limited to an octave bandwidth (2:1 frequency band). It is recommended that a system operating over an octave bandwidth and employing circularly polarized horn antennas be considered for a developmental model.

The error analysis of Chapter IV showed that the antenna elements were one of the chief limiting factors associated with the exploratory model. Through the use of the horn antenna one should be able to achieve higher gain elements, thus improving the operating characteristics of the system. The use of higher gain elements will require that the computer be reprogrammed to incorporate the new pattern characteristics. Further, it will be necessary to increase the memory capacity of the present system to store the high gain element patterns.

During future follow-on work consideration must be given to replacing the memory voltmeter presently employed in the exploratory azimuth-elevation model. From Chapter IV it can be seen that the memory voltmeter is the second major source of error in the system. At the present time the memory voltmeter lacks the ability to convert the analog data into the 12 bit accuracy the A/D converter is capable of receiving.

A further enhancement can be achieved by operating the system over a ($< 2:1$) narrower frequency band. With such a bandwidth one could replace the electromechanical switch presently used with a diode switch which would permit high speed (nanosecond) electronic switching. This should be an advantage when interrogating ground-based radar systems. After development, the diode switch should be more rugged and less costly.

In summary, the two principal limiting factors in the present system are the antenna elements because of their poor pattern characteristics and the memory voltmeter due to its lack of ability to convert the analog data into the required 12 bit format of the A/D converter. It is felt the sponsor will gain appreciation for the system as he works with it. Further, the vector summation concept is not limited to azimuth and elevation direction finders but also is applicable to present direction finders, e.g., Wullenweber arrays now in operation.

APPENDIX

Soon after the development of the A-EDF system, it was deemed desirable to determine the system's applicability to airborne targets. This initiated a series of experiments in which a radio frequency source was installed in an airplane, and the source tracked by the direction finding system while the aircraft was simultaneously skin tracked by radar. The two tracking systems were interfaced by a unit which allowed the teletype printer associated with the direction finding system to print out the target coordinates as determined by the radar as well as the DF information. This provided an excellent correlation in time between the two data sets, and greatly simplified the evaluation of the data. This Appendix is a description of the interface equipment.

The design objectives were to create a switching arrangement which would interrupt the DF's normal operation at judiciously chosen intervals just long enough to read the target coordinates from the radar into the DF system computer, and then resume normal operation. The time between samples of the radar information should not be so frequent so as to provide an abundance of redundant data nor interfere with the normal DF function, but should be frequent enough to allow the target's path to be accurately plotted and provide adequate comparison between the results of the two systems. Since the target was slow moving and the A-EDF system required only about 60 ms per sample, a rate of one radar sample per 65 data samples was adequate.

Figure A-1 is a simplified diagram of the multiplex switch. Referring to Fig. A-1 input data samples are counted until the count reaches 64. At this time the counter enables a gate which switches clock pulses into a stepping switch. The switch is arranged so that the normal signal channel is normally closed. When the clock pulses arrive, the target coordinates from the radar are sequentially switched to the output, after which the system is reset. The clock also provides an interrupt to the computer to interrupt the normal mode of operation.

The entire switch is shown schematically in Fig. A-2. The 1 PPR and 17PPR inputs are pulses generated by a pulse generator associated with the A-EDF system array. The switch operation is as follows: Each time a pulse is received on the 1PPR channel, it is amplified by Q_1, used to operate the normal computer interrupt channel via Q_2, and counted. Similarly, pulses on the 17PPR channel are amplified by Q_4 and pass through G_1, which is normally conducting, to Q_3, which operates a second normal interrupt channel. Once 64 pulses have been received on the 1PPR channel, the counter output disables G_1 and the 17PPR pulses are rerouted through G_2 to the stepping switch and Q_5. The pulses cause FF_8 and FF_9 to change state gating on, in sequence, G_4, G_5, and G_6. This switches the multiplex switch from the normal signal input to the target X, Y,

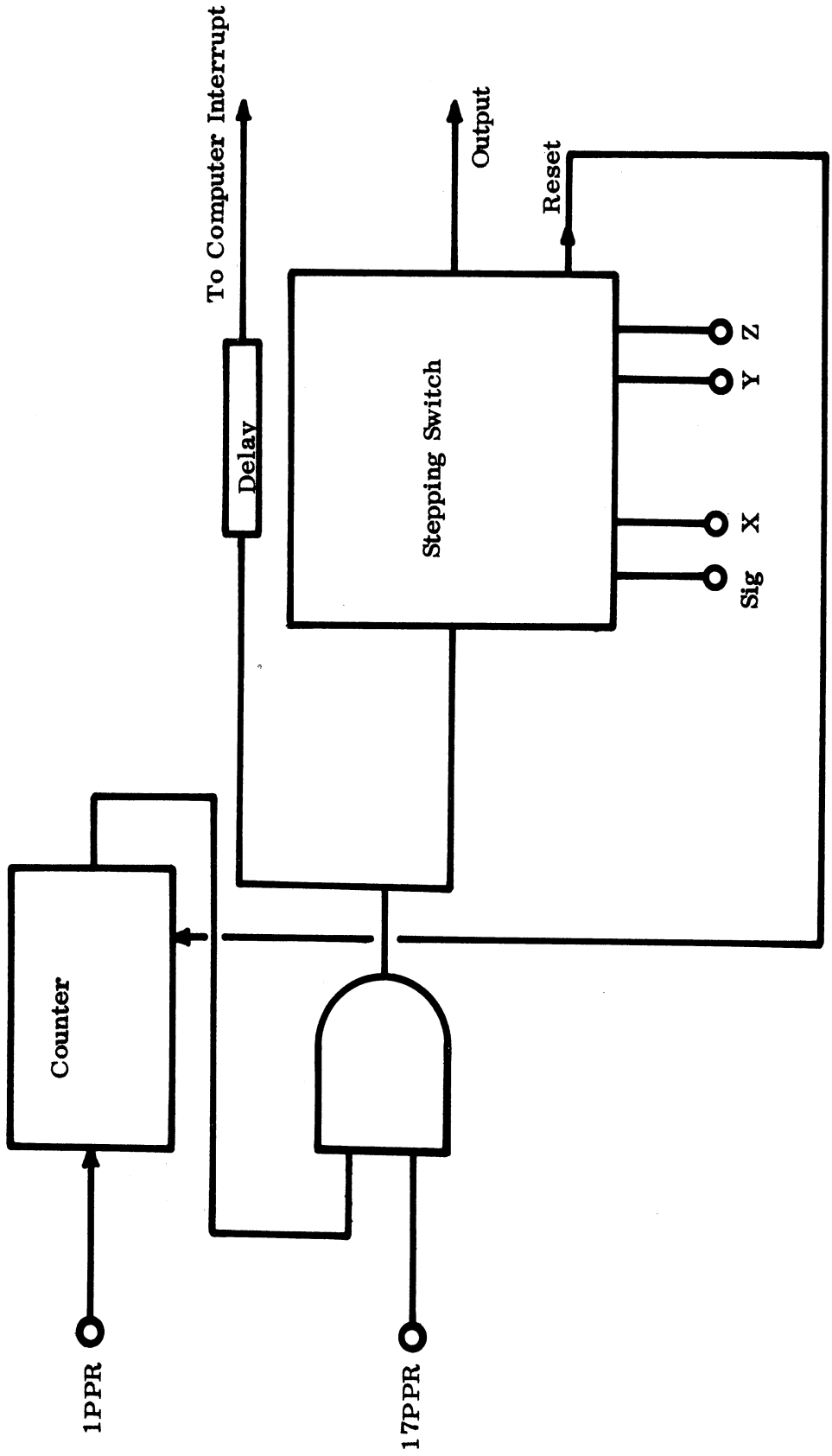

FIG. A-1: SIMPLIFIED BLOCK DIAGRAM OF MULTIPLEX SWITCH.

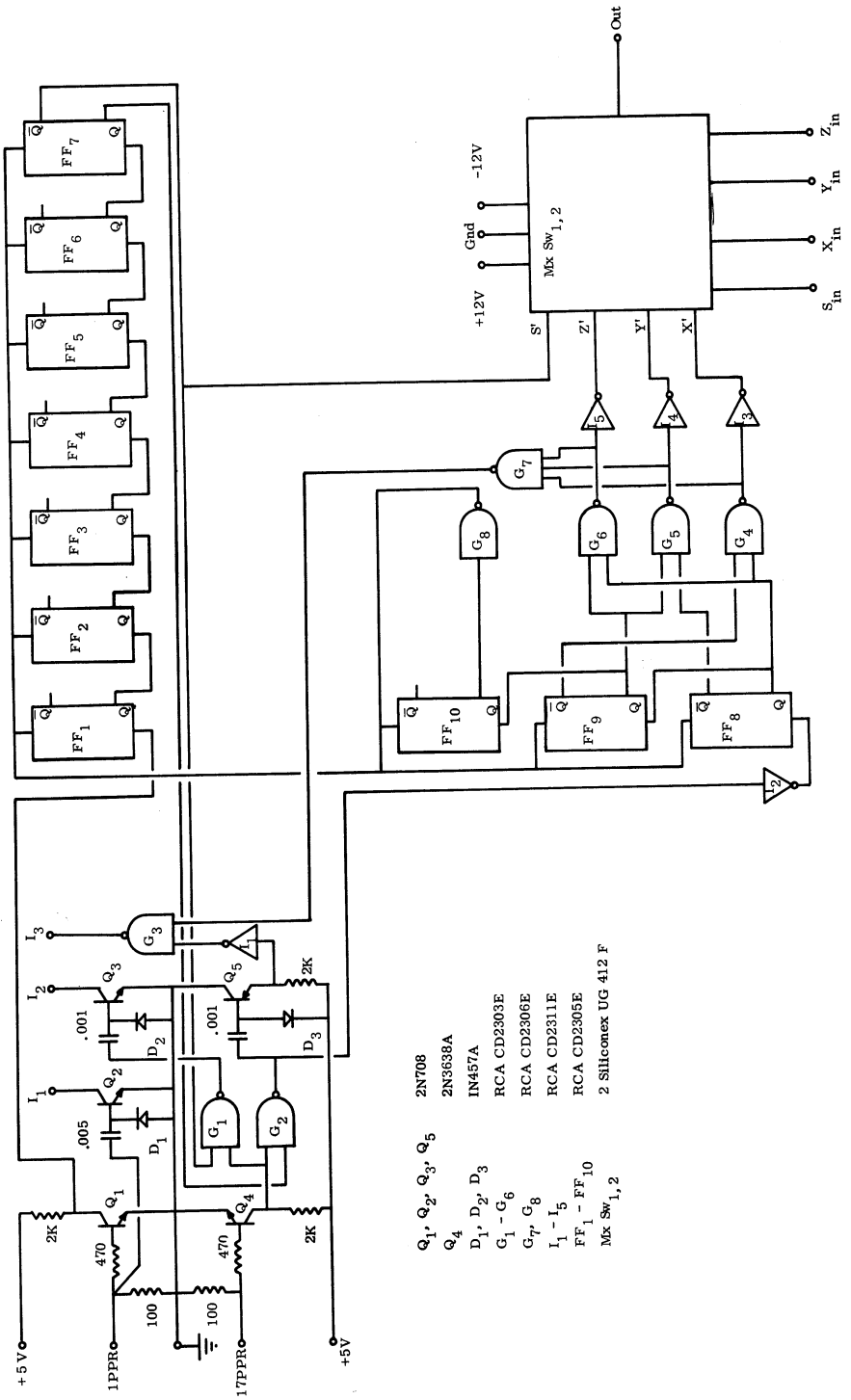

FIG. A-2: SCHEMATIC OF MULTIPLEX SWITCH.

and Z coordinates from the radar. Q_5 acts as a delay, providing a delay of one pulse width from the time the switching sequence is initiated to the time a data channel is sampled by the computer. G_7 insures one of the radar coordinates is indeed being inputed before the special computer interrupt, I_3, is signaled. Finally, after the Z coordinate information has been sampled, $\overline{FF}_{10}$ enables a high fan out gate, G_8, to reset the entire system.

The construction techniques were straightforward. The multiplexer was divided into three sections: pulse receiver, counter, and stepping switch. Printed circuit boards were fabricated for the sections, and the interconnections were made by conventional wiring. A .001 capacitor was shunted across the $\overline{Q}$ output of FF_8 to ground at the point marked by an X on the schematic to delay the leading edge of the pulse into G_5. Once the switch was made to operate successfully, no further adjustments were necessary during the tests.

This completes the multiplex description. The other equipment necessary to support its operation include a 5 volt supply for the logic elements and plus and minus 12 volt supplies for the multiplex switch itself. Also, since the radar outputs were not directly compatible with the A-EDF system inputs, scaling networks were required to interface the two systems.

The outputs from the radar are voltages which are directly proportional to the targets X, Y, and Z coordinates. These voltages range in value from -100 to +100v. Since the maximum voltage accepted by the A-EDF system memory voltmeter is +10v, linear voltage scaling is necessary to interface the two units. To minimize the load on the radar's high impedance source, active scaling networks were chosen. Figure A-3 is a schematic of the network employed for the X and Y coordinate channels. The active device is an integrated circuit operational amplifier, in this case an RCA CA3033. The external feedback capacitors are chosen to limit the closed loop gain bandwidth product to the few Hertz. The DC closed loop gain is nominally .2.

The network is calibrated by adjusting R_b for Ov output with no input. Gain adjustment is provided by R_g. The Z coordinate network is identical except that the feedback resistance R_p is 9.1M and the input resistor, R_{in}, is 3.6M, providing a nominal gain of 2.

Care was taken to insure the unit was shielded from excess electrical and thermal gradients and electronically regulated supplies were employed.

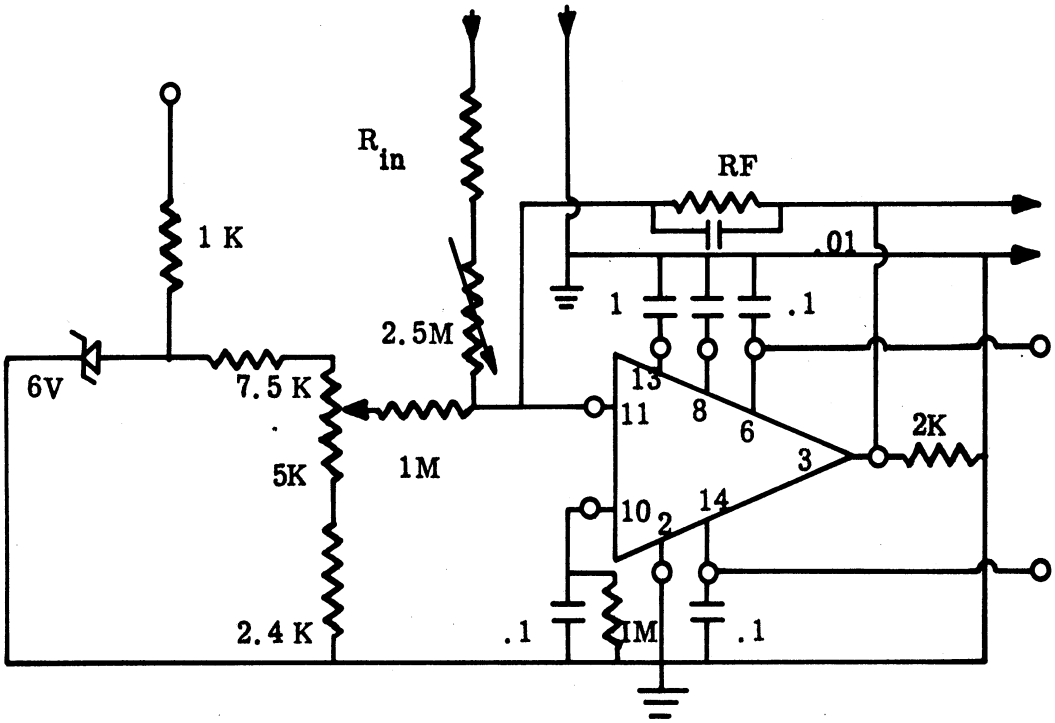

A = RCA CA 3033

$Rf_x = Rf_y = 2.2M$

$Rf_z = 9.1M$

$Rin_x = Rin_y = 8.2M$

$Rin_z = 3.6M$

FIG. A-3: RADAR COORDINATE SCALING NETWORK.

REFERENCES

Beers, Yardley, Theory of Error, Addison-Wesley Publishing Company, Inc. Reading, Massachusetts, 1967.

Jasik, H. Antenna Engineering Handbook, McGraw-Hill Book Company, New York, p. 28-24, 1961.

Ferris, J.E., B.L.J.Rao, and W.E.Zimmerman, "Azimuth and Elevation Direction Finder Techniques", Quarterly Report No. 1, ECOM-00547-1, The University of Michigan Radiation Laboratory Report 1084-1-Q, October, 1967.

Sengupta, D.L., J.E.Ferris, R.W.Larson, G.Hok, and T.M.Smith, "Azimuth and Elevation Direction Finder Study", Final Report, ECOM-01499-4, The University of Michigan Radiation Laboratory Report 7577-1-F, 1966.

DISTRIBUTION LIST FOR REPORTS UNDER DAAB07-67-C0547 U of M Project 01084

Destination	Number of Copies
Technical Library, Rm. 3E-1039, Pentagon Dir., Defense, Research and Engineering Washington, DC 20301	1
Defense Intelligence Agency ATTN: DIARD Washington, DC 20301	1
Director, National Security Agency ATTN: C31 Ft. George G. Meade, MD 20755	20
Naval Ships Systems Command ATTN: Technical Library 20526 Main Navy Bldg., Rm. 1528 Washington, DC 20325	1
Dir., U.S. Naval Research Laboratory ATTN: Code 2027 Washington, DC 20390	1
Rome Air Development Center ATTN: EMTLD, Documents Library Griffiss AFB, New York 13440	1
Electronic Systems Division, ESTI L. G. Hanscom Field Bedford, Mass. 07130	2
Hq., AFSC ATTN: SCTSE Bolling, AFB, DC 20332	1
CG, U.S. Army Materiel Command ATTN: R and D Directorate Washington, DC 20315	1
Redstone Scientific Information Center Attn: Chief, Document Section U. S. Army Missile Command Redstone Arsenal, Ala. 35809	1
CO, USASA, Test and Evaluation Attn: IAOTR Ft. Huachuca, Ariz. 85613	1

U of M Project 01084 Distribution List (continued)

CO, Aberdeen Proving Ground
Technical Library, Bldg. 313
Aberdeen Proving Ground, MD 21005 1

CG, U. S. Army Combat Developments Command
CDCMR-E
Ft. Belvoir, Va. 22060 1

CO, U. S. Army Combat Developments Command
Communications-Electronics Agency
Ft. Monmouth, N.J. 07703 1

CO, U. S. Army Security Agency Combat Developments Activity
Arlington Hall Station
Arlington, Va. 22212 1

U. S. Army Security Agency
OAC of IS, DEV (IARD-EW)
Arlington Hall Station
Arlington, Va. 22212 3

U. S. Army Security Agency Processing Center
IAVAPC- R and D
Vint Hill Farms Station
Warrenton, Va. 22186 1

CO, U. S. Army Nuclear Defense Laboratory
Attn: Library
Edgewood Arsenal, MD 21010 1

Harry Diamond Laboratories
Attn: Library
Connecticut Ave. and Van Ness St.
Washington, DC 20438 1

CG, U. S. Army Electronic Proving Ground
Attn: Technical Information Center
Ft. Huachuca, Arizona 95613 1

Assistant Secretary of the Army R and D
Department of The Army
Attn: Deputy Assistant for Army R and D
Washington, DC 20315 1

U of M Project 01084 Distribution List (continued)

CO, U. S. Army Limited War Laboratory
Aberdeen Proving Ground, MD 21005 1

CO, U. S. Foreign Science and Technology Center
Attn: AMXST-RD-R, Munitions Bldg.
Washington, DC 20315 1

Office, AC of S for Intelligence
Department of the Army
ATTN. ACSI-DSRS
Washington, DC 20310 1

CG, U. S. Army Electronics Command
Attn: AMSEL-MR
225 South 18th Street
Philadelphia, Pa. 19103 1

Director, Electronic Defense Laboratories
Sylvania Electronic Products, Inc.
ATTN: Documents Acquisition Librarian
P. O. Box 205
Mountain View, California 94040 1

Chief, Intelligence Materiel Development Office
Electronic Warfare Lab., USAECOM
Ft. Holabird, Md. 21219 1

Chief, Missile Electronic Warfare Tech Area
EW Lab., USAECOM
White Sands Missile Range, NM 88002 1

HQ, U. S. Army Combat Developments Command
Attn: CDCLN-EL
Ft. Belvoir, Va. 22060 1

USAECOM Liaison Officer
Aeronautical Systems, ASDL-9
Wright-Patterson AFB, Ohio 45433 1

USAECOM Liaison Office
U. S. Army Electronic Proving Ground
Ft. Huachuca, Arizona 85613 1

U of M Project 01084 Distribution List (continued)

CG, U.S. Army Electronics Command Ft. Monmouth, N.J. 07703	
ATTN: AMSEL-EW	1
AMSEL-IO-T	1
AMSEL-RD-MAT	1
AMSEL-RD-LNA	1
AMSEL-RD-LNJ	1
AMSEL-XL-D	1
AMSEL-NL-D	1
AMSEL-HL-CT-D	2
AMSEL-WL-S	6
NASA Scientific and Technical Info. Facility Attn: Acquisitions Branch S-AK/DL P. O. Box 33 College Park, Md. 20740	2
Battelle-Defender Info. Center Battelle Memorial Institute 505 King Avenue Columbus, Ohio 43201	1
Remote Area Conflict Info. Center Battelle Memorial Institute 505 King Avenue Columbus, Ohio 43201	1
TOTAL	72

Security Classification

DOCUMENT CONTROL DATA - R&D

(Security classification of title, body of abstract and indexing annotation must be entered when the overall report is classified)

1. ORIGINATING ACTIVITY *(Corporate author)* The University of Michigan, Radiation Laboratory Department of Electrical Engineering, 201 Catherine St. Ann Arbor, Michigan 48108	2a. REPORT SECURITY CLASSIFICATION UNCLASSIFIED 2b. GROUP NA

3. REPORT TITLE

AZIMUTH AND ELEVATION DIRECTION FINDER TECHNIQUES

4. DESCRIPTIVE NOTES *(Type of report and inclusive dates)*

Final Report 1 July 1967 through 31 December 1968

5. AUTHOR(S) *(Last name, first name, initial)*

Ferris, Joseph E., Henry, William B., Wilcox, Peter H., and Zimmerman, Wiley E.

6. REPORT DATE	7a. TOTAL NO. OF PAGES	7b. NO. OF REFS
April 1969	77	4

8a. CONTRACT OR GRANT NO. DA AB 0767C-0547 b. PROJECT NO. 5A6 79191 D902 0511 c. d.	9a. ORIGINATOR'S REPORT NUMBER(S) 1084-1-F 9b. OTHER REPORT NO(S) *(Any other numbers that may be assigned this report)* ECOM-0547-F

10. AVAILABILITY/LIMITATION NOTICES

Each transmittal of this document outside the Department of Defense must have prior approval of CG, US Army Electronics Command, Fort Monmouth, New Jersey, 07703 ATTN: AMSEL-WL-S

11. SUPPLEMENTARY NOTES	12. SPONSORING MILITARY ACTIVITY
	US Army Electronics Command AMSEL-WL-S Ft. Monmouth, N.J. 07703

13. ABSTRACT

During the period covered by the final report the Radiation Laboratory of the University of Michigan has designed, developed and tested an Azimuth - Elevation Direction Finding system. The tests are not felt to be conclusive, however, they do demonstrate the capability of this system to perform azimuth and elevation direction finding of detected RF sources. The system has been tested in both the free space environment (employing an antenna range) and in a cluttered RF environment employing an aircraft from which azimuth and elevation data has been collected. The result of the free space tests suggest that the system has an accuracy of $\pm 5^{o}$, in both azimuth and elevation. However, it is difficult to assign an accuracy figure to the system on the basis of the fly-by tests due to the hostile environment in which the system was operated. This report presents a review of the system from its conception to its final testing phases with suggested recommendations for improvements.

DD FORM 1 JAN 64 1473

Security Classification

14. KEY WORDS	LINK A		LINK B		LINK C	
	ROLE	WT	ROLE	WT	ROLE	WT
Azimuth - Elevation Direction Finder Cavity Backed Spiral Memory Voltmeter System Resolution Data Processing Vector Summation						

INSTRUCTIONS

1. ORIGINATING ACTIVITY: Enter the name and address of the contractor, subcontractor, grantee, Department of Defense activity or other organization *(corporate author)* issuing the report.

2a. REPORT SECURITY CLASSIFICATION: Enter the overall security classification of the report. Indicate whether "Restricted Data" is included. Marking is to be in accordance with appropriate security regulations.

2b. GROUP: Automatic downgrading is specified in DoD Directive 5200.10 and Armed Forces Industrial Manual. Enter the group number. Also, when applicable, show that optional markings have been used for Group 3 and Group 4 as authorized.

3. REPORT TITLE: Enter the complete report title in all capital letters. Titles in all cases should be unclassified. If a meaningful title cannot be selected without classification, show title classification in all capitals in parenthesis immediately following the title.

4. DESCRIPTIVE NOTES: If appropriate, enter the type of report, e.g., interim, progress, summary, annual, or final. Give the inclusive dates when a specific reporting period is covered.

5. AUTHOR(S): Enter the name(s) of author(s) as shown on or in the report. Enter last name, first name, middle initial. If military, show rank and branch of service. The name of the principal author is an absolute minimum requirement.

6. REPORT DATE: Enter the date of the report as day, month, year; or month, year. If more than one date appears on the report, use date of publication.

7a. TOTAL NUMBER OF PAGES: The total page count should follow normal pagination procedures, i.e., enter the number of pages containing information.

7b. NUMBER OF REFERENCES: Enter the total number of references cited in the report.

8a. CONTRACT OR GRANT NUMBER: If appropriate, enter the applicable number of the contract or grant under which the report was written.

8b, 8c, & 8d. PROJECT NUMBER: Enter the appropriate military department identification, such as project number, subproject number, system numbers, task number, etc.

9a. ORIGINATOR'S REPORT NUMBER(S): Enter the official report number by which the document will be identified and controlled by the originating activity. This number must be unique to this report.

9b. OTHER REPORT NUMBER(S): If the report has been assigned any other report numbers *(either by the originator or by the sponsor)*, also enter this number(s).

10. AVAILABILITY/LIMITATION NOTICES: Enter any limitations on further dissemination of the report, other than those imposed by security classification, using standard statements such as:

(1) "Qualified requesters may obtain copies of this report from DDC."

(2) "Foreign announcement and dissemination of this report by DDC is not authorized."

(3) "U. S. Government agencies may obtain copies of this report directly from DDC. Other qualified DDC users shall request through _____."

(4) "U. S. military agencies may obtain copies of this report directly from DDC. Other qualified users shall request through _____."

(5) "All distribution of this report is controlled. Qualified DDC users shall request through _____."

If the report has been furnished to the Office of Technical Services, Department of Commerce, for sale to the public, indicate this fact and enter the price, if known.

11. SUPPLEMENTARY NOTES: Use for additional explanatory notes.

12. SPONSORING MILITARY ACTIVITY: Enter the name of the departmental project office or laboratory sponsoring *(paying for)* the research and development. Include address.

13. ABSTRACT: Enter an abstract giving a brief and factual summary of the document indicative of the report, even though it may also appear elsewhere in the body of the technical report. If additional space is required, a continuation sheet shall be attached.

It is highly desirable that the abstract of classified reports be unclassified. Each paragraph of the abstract shall end with an indication of the military security classification of the information in the paragraph, represented as *(TS), (S), (C), or (U)*.

There is no limitation on the length of the abstract. However, the suggested length is from 150 to 225 words.

14. KEY WORDS: Key words are technically meaningful terms or short phrases that characterize a report and may be used as index entries for cataloging the report. Key words must be selected so that no security classification is required. Identifiers, such as equipment model designation, trade name, military project code name, geographic location, may be used as key words but will be followed by an indication of technical context. The assignment of links, rules, and weights is optional.